2018

Wnt5a Signaling Induced Phosphorylation Increases Acyl Protein Thioesterase Activity And Promotes Melanoma Metastatic Behavior

Rochelle Shirin Sadeghi
University of Pennsylvania, RSadeghi@pennmedicine.upenn.edu

Wnt5a Signaling Induced Phosphorylation Increases Acyl Protein Thioesterase Activity And Promotes Melanoma Metastatic Behavior

Abstract
Wnt5a has been implicated in melanoma progression and metastasis, although the exact downstream signaling events that contribute to melanoma metastasis are poorly understood. Wnt5a signaling results in acyl protein thioesterase 1 (APT1) mediated depalmitoylation of pro-metastatic cell adhesion molecules CD44 and MCAM, resulting in increased melanoma invasion. The mechanistic details that underlie Wnt5a-mediated regulation of APT1 activity and cellular function remains unknown. Here, we show Wnt5a signaling regulates APT1 activity through induction of APT1 phosphorylation and we further investigate the functional role of APT1 phosphorylation on its depalmitoylating activity. We found phosphorylation increased APT1 depalmitoylating activity and reduced APT1 dimerization. We further determined APT1 phosphorylation increases melanoma invasion in vitro and is also correlated with increased tumor grade and metastasis. Our results further establish APT1 as an important regulator of melanoma invasion and metastatic behavior. Inhibition of APT1 may represent a novel way to treat Wnt5a driven cancers.

Degree Type
Dissertation

Degree Name
Doctor of Philosophy (PhD)

Graduate Group
Cell & Molecular Biology

First Advisor
Eric S. Witze

Keywords
APT1, cancer biology, melanoma, metastasis, Wnt5a, Wnt signaling

Subject Categories
Cell Biology | Molecular Biology | Oncology

WNT5A SIGNALING INDUCED PHOSPHORYLATION INCREASES ACYL PROTEIN THIOESTERASE 1 ACTIVITY AND PROMOTES MELANOMA METASTATIC BEHAVIOR

Rochelle Shirin Sadeghi

A DISSERTATION

in

Cell and Molecular Biology

Presented to the Faculties of the University of Pennsylvania

in

Partial Fulfillment of the Requirements for the

Degree of Doctor of Philosophy

2018

Supervisor of Dissertation

_____

Eric S. Witze, Ph.D.

Assistant Professor of Cancer Biology

Graduate Group Chairperson

_____

Daniel S. Kessler, Ph.D.

Associate Professor of Cell and Developmental Biology

Dissertation Committee

Constantinos Koumenis, Ph.D., Richard H. Chamberlain Professor of Research Oncology

Donita C. Brady, Ph.D., Presidential Professor of Cancer Biology

Luca Busino, Ph.D., Assistant Professor of Cancer Biology

Ellen Puré, Ph.D., Professor of Pharmacology

This thesis is dedicated to Gladys Esther Martinez.

ACKNOWLEDGMENTS

I would first like to thank my advisor Eric S. Witze for his guidance throughout the research project, giving me the freedom to explore my own interests, and supporting this research project and my ideas. Thank you to my lab mates for always answering my many questions and for being there for me through the difficult times.

Many thanks to my thesis committee, Costas Koumenis, Luca Busino, Donita Brady, and Ellen Puré. I sincerely appreciate all of their critical feedback, compelling ideas, and encouragement. They provided insightful suggestions and constructive criticism that helped strengthen my research and build my confidence as a scientist.

I'm extremely grateful for the small group of close friends in the program and department that have been there for me through it all: Rizwan Saffie, Dahmane Ouazia, Claudia Lanauze, Akriti Kharbanda, and Chris Natale. Their support and friendship helped me get through the toughest moments in this journey.

Endless gratitude for my parents, Jessica and Khosrow Sadeghi, for their constant, unwavering, love and support. They have encouraged me to pursue my dreams my entire life and none of this would be possible without them. Their many sacrifices and endless love does not go unnoticed or unappreciated. Their profound belief in my abilities and myself is one of the things that drives me still to be the best that I can be. Many thanks to my brother, Amir Sadeghi, for always being there for me. His enthusiasm and support about my research has been extremely important to me. I am so grateful for my two best friends, Anna Frias and Maria Frias, for their valuable advice and invaluable friendship of many, many years. I can't imagine not having them as part of my support system during graduate school.

I cannot begin to express my deepest gratitude to my fiancé, Michael Joseph Holland. I am so fortunate to have Mike always by my side and to have his love, support, patience, and encouragement throughout this process.

ABSTRACT

WNT5A SIGNALING INDUCED PHOSPHORYLATION INCREASES ACYL PROTEIN THIOESTERASE 1 ACTIVITY AND PROMOTES MELANOMA METASTATIC BEHAVIOR

Rochelle Shirin Sadeghi

Dr. Eric S. Witze

Wnt5a has been implicated in melanoma progression and metastasis, although the exact downstream signaling events that contribute to melanoma metastasis are poorly understood. Wnt5a signaling results in acyl protein thioesterase 1 (APT1) mediated depalmitoylation of pro-metastatic cell adhesion molecules CD44 and MCAM, resulting in increased melanoma invasion. The mechanistic details that underlie Wnt5a-mediated regulation of APT1 activity and cellular function remains unknown. Here, we show Wnt5a signaling regulates APT1 activity through induction of APT1 phosphorylation and we further investigate the functional role of APT1 phosphorylation on its depalmitoylating activity. We found phosphorylation increased APT1 depalmitoylating activity and reduced APT1 dimerization. We further determined APT1 phosphorylation increases melanoma invasion *in vitro* and is also correlated with increased tumor grade and metastasis. Our results further establish APT1 as an important regulator of melanoma invasion and metastatic behavior. Inhibition of APT1 may represent a novel way to treat Wnt5a driven cancers.

TABLE OF CONTENTS

ACKNOWLEDGMENTS III

ABSTRACT IIV

LIST OF ILLUSTRATIONS VII

CHAPTER 1: MELANOMA AND THE ROLE OF WNT5A SIGNALING 1

OVERVIEW 1

MELANOMA 1

WNT5A SIGNALING 3

APT1-MEDIATED DEPALMITOYLATION 5

WNT5A SIGNALING IN CANCER 7

THESIS OBJECTIVES 12

CHAPTER 2: CHARACTERIZATION OF APT1'S ENZYMATIC ACTIVITY 13

OVERVIEW 13

INTRODUCTION 14

RESULTS 14

FIGURES 18

DISCUSSION 20

METHODS 20

CHAPTER 3: WNT5A SIGNALING INDUCED PHOSPHORYLATION INCREASES APT1 ACTIVITY AND PROMOTES MELANOMA METASTATIC BEHAVIOR 24

OVERVIEW 24

INTRODUCTION 24

RESULTS 27

FIGURES 38

DISCUSSION 52

METHODS 56

CHAPTER 4: IDENTIFYING APT1'S KINASE 65

OVERVIEW 65

INTRODUCTION 65

RESULTS 66

FIGURES 71

DISCUSSION 75

METHODS 77

CHAPTER 5: FUTURE DIRECTIONS 81

OVERVIEW 81

CONFIRMING LOK AS APT1'S KINASE 81

IDENTIFICATION OF OTHER PROTEINS INVOLVED IN THE WNT5A SIGNALING PATHWAY 84

UNDERSTANDING THE ROLE OF APT1 PHOSPHORYLATION IN VIVO 85

INVESTIGATING THE WNT5A/APT1 SIGNALING AXIS IN OTHER CANCERS 86

CONCLUDING REMARKS 89

BIBLIOGRAPHY 91

LIST OF ILLUSTRATIONS

Figure 2.1. *Characterization and optimization of analyzing APT1's depalmitoylating activity.*

Figure 3.1. *Wnt5a signaling induces APT1 phosphorylation on serine's 209 and 210.*

Figure 3.2. *Wnt5a stimulation increases APT1 depalmitoylating activity.*

Figure 3.2 – figure supplement 1. *Activity of APT1 in response to Wnt5a stimulation or the phosphomimetic mutation.*

Table 1. Enzyme kinetics of $APT1^{WT}$ and $APT1^{S209D}$.

Figure 3.3. *APT1 phosphorylation increases APT1 depalmitoylating activity in cells and increases melanoma invasion.*

Figure 3.4. *APT1 phosphorylation impedes dimer formation.*

Figure 3.5. *Increased phospho-APT1 staining correlates with increased tumor grade and metastasis.*

Figure 3.5 – figure supplement 1. *Response of $APT1^{S210L}$ mutant to APT1 inhibitor ML348.*

Figure 4.1. *Inhibition or knockdown of LOK reduces pAPT1 levels and Wnt5a treatment increases LOK-MCAM interactions.*

Figure 4.2. *Inhibition or knockdown of LOK inhibits Wnt5a induced melanoma invasion.*

CHAPTER 1: MELANOMA AND THE ROLE OF WNT5A SIGNALING

OVERVIEW

Melanoma, the deadliest form of skin cancer, is caused by the transformation of melanocytes, or the pigment-producing cells in the skin. With over 90,000 new melanomas being diagnosed this year, and the rates of melanoma rising over the past 30 years, it's clear that this disease is a significant health concern that needs to be addressed (American Cancer Society). With a 5-year survival rate of only 17% for metastatic melanoma patients, it is imperative we fully understand the downstream signaling events that are promoting melanoma metastasis, so we can create more targeted therapies for patients. Several *in vitro* studies and observations of clinical data have suggested a role for Wnt5a signaling in melanoma metastasis. Here, we provide relevant background information important to understand and present other findings that draw a parallel of Wnt5a signaling to melanoma metastasis.

MELANOMA

Melanocytes are specialized pigment-producing cells in the basilar epidermis of the skin. Their main biological function is to provide melanin pigment to their neighboring keratinocytes (Shain, A. and Bastian, B., 2016). Melanocytes are neural crest-derived cells and during development, they colonize throughout the skin, eye, and to a lesser extent, other areas of the body (Mort et al., 2015). Understanding the biology of melanocytes, and the genes and pathways that regulate melanocytes is key to understanding melanoma development.

Melanocytes typically divide infrequently (Jimbow et al., 1975). Melanocyte proliferation and pigment production are itself stimulated by UV-radiation. They then produce and provide melanin to keratinocytes, which provides protection from UV radiation-induced DNA damage (Costin, G-E.E., Hearing, V.J., 2007). UV radiation-induced DNA damage results in secretion of the α-melanocyte stimulating hormone (αMSH), αMSH then binds to the melanocortin 1 receptor (MC1R) expression on melanocytes and induces synthesis of melanin pigment. Melanocytes then deliver the melanin to keratinocytes where it scatters and absorbs UV radiation. In addition, keratinocytes use melanin to protect their nucleus from receiving further UV radiation-induced DNA damage.

Melanocytic naevi are benign proliferations of melanocytes and are also referred to as naevi in the radial growth phase. Nevertheless, naevi in the radial growth phase have a low potential to metastasize and stop proliferation. Many different types of mutations can be responsible for the benign proliferation. Activation of BRAF is among the most frequent in melanoma, specifically the constitutively activated mutant $BRAF^{V600E}$. When a naevus accumulates genetic alterations, through activation mutations of BRAF or NRAS for example, it can result in increased proliferation and benign naevi progressing to a dysplastic naevus. The most recurrent somatic mutations affect genes in key signaling pathways that govern proliferation (BRAF, NRAS), growth and metabolism (PTEN, KIT), resistance to apoptosis (TP53), cell cycle control (CDKN2A), and replication (TERT) (Shain et al., 2016). Through more genetic alterations, such as the ones just mentioned, it can progress to a melanoma that remains localized. Some common mutations responsible for this phase of progression are TERT mutations, deletions of CDKN2A, disabling mutations and deletions of PTEN

or TP53. Through mechanisms not well understood, but generally, by acquiring mutations over time, the melanoma can begin vertical growth phase. This is the phase where the melanoma has now breached the basement membrane and begins to metastasize by entering the bloodstream. We are particularly interested in determining the molecular 'switch' that drives radial growth to vertical growth of melanomas.

With the 5-year survival rate dramatically decreasing as tumor stage increases, investigating the mechanism driving melanoma metastasis is important to better understand the driving forces behind melanoma metastasis (Sandru et al., 2014). Several studies have demonstrated an important role for Wnt5a in cancer. Previously, the elevated expression of Wnt5a in melanoma samples and subsequent *in vitro* studies have suggested a role for Wnt5a in melanoma metastasis. Important findings include: Wnt5a expression correlating with increased melanoma tumor grade and decreased melanoma patient survival, Wnt5a signaling increasing melanoma migration, motility, and invasion, and suggestions of Wnt5a expression to be used as a clinical risk factor (Bittner et al., 2000; Weeratna et al., 2002; Carr et al., 2003; Da Forno et al., 2008). With our research, we aim to provide clarity in understanding the mechanism of how Wnt5a signaling is promoting an aggressive phenotype in melanoma.

WNT5A SIGNALING

Wnt proteins are secreted glycoproteins that regulate multiple signaling pathways. There are 19 Wnt members in mice and humans, with unique expression patterns across tissues and various functions in development. They bind to the 10 members of the transmembrane Frizzled (Fz) family of G-protein-coupled receptors and

co-receptors that include Ror family members. Wnt5a is a secreted ligand responsible for a non-canonical Wnt signaling pathway to regulate cell polarity and cell migration. Upon interaction with its Frizzled receptor, it activates a signal transduction cascade that results in cell migration, invasion, among other changes in cell behavior (Sato et al., 2010). Multiple studies have suggested ROR2 acts as a co-receptor for Wnt5a and deemed it necessary for the events downstream that promote melanoma metastatic behavior (Sato et al., 2009; O'Connell et al., 2009). The initial indication that Wnt5a signaling is able to regulate cell migration came from the observation that Wnt5a signaling is responsible for convergent extension in *Xenopus* embryos (Du et al., 1995). Convergent extension is a developmental process driven by migration of polarized cells leading to narrowing and lengthening during morphogenesis. In $WNT5A^{-/-}$ knockout mice, phenotypes include shortened anterior-posterior body axis, truncation of the proximal skeleton in the limbs, an absence of distal digits, and the loss of polarized movement and directional cell growth (Yamaguchi et al., 1999). Wnt5a can regulate distinct pathways by binding to Frizzled2 (Fzd2). By competing with the canonical Wnt ligand, Wnt3a, for Fzd2 binding, Wnt5a can inhibit the Wnt3a-dependent accumulation of β-catenin and phosphorylation of LRP6 (Sato et al., 2009). Wnt5a signaling controls cell polarity and directional cell movement and Wnt5a treatment can promote the recruitment and reorganization of proteins involved in cell adhesion and cell signaling (Witze et al., 2008, Wang et al., 2015). Recruitment and reorganization of actin, myosin IIB, Frizzled3, and melanoma cell adhesion molecule becomes accumulated asymmetrically at the cell periphery to control cell orientation, polarity, and directional movement in response to Wnt5a gradients (Witze et al., 2008). Additionally, Wnt5a signaling can activate the Wnt/Ca^{2+} pathways. Wnt5a signaling results in elevation of free Ca^{2+} levels to induce Ca^{2+} signaling in a polarized manner (Witze et al., 2013). This calcium flux can result in

the activation of several signaling pathways, such as protein kinase C (PKC), calcium/calmodulin-dependent protein kinase II (CAMKII), and JUN N-terminal kinase (JNK) (Kohn, A. and Moon, R., 2005). In this way, Wnt5a signaling itself can result in regulation of various downstream players.

Dishevelled, also known as Dvl, is a scaffold protein that has been shown to be essential in Wnt signaling, across canonical, non-canonical, and planar cell polarity pathways (Liu, et al., 2001; Willert et al., 2003; Wallingford, J. B., and Habas, R., 2005). It is understood that Dvl functions as a scaffold that brings receptors and downstream targets together. Wnt5a-Ror signaling has been shown to result in phosphorylation of Dvl, and it is suggested that Dvl phosphorylation might be a molecular switch that determines its function for the various downstream targets of these pathways (Ho et al., 2012). Dvl is also able to activate the Wnt-Ca^{2+} pathway, as determined by Ca^{2+} flux, PKC, and CAMKII, making it a component of all reported Fz signaling pathways (Sheldahl et al., 2003).

Wnt5a signaling can also result in APT1 mediated depalmitoylation of cell adhesion molecules MCAM and CD44, resulting in their asymmetric localization and increased melanoma invasion (Wang et al., 2015). With this observation, Wnt5a signaling can result in depalmitoylation of cell adhesion molecules to change cell behavior.

APT1 MEDIATED DEPALMITOYLATION

Palmitoylation, also known as S-acylation, is the reversible addition of a 16-carbon fatty acid to cysteine residues via a thioester bond. Palmitate addition is

mediated by palmitoyltransferases, (PATs) that belong to the DHHC (aspartate-histidine-histidine-cysteine) family. Palmitate removal is mediated by acyl-protein thioesterases (APTs). Dynamic changes in protein S-palmitoylation are required for signal transduction. Proteins can be modified with lipid attachments to regulate membrane localization and function. Not only can palmitoylation allow proteins to become associated with membranes, but palmitoylation can also modulate protein behavior and function, especially in the case of integral membrane proteins.

Although there is a certain degree of redundancy among PAT enzymes, some particular substrates have been shown to be dependent on an individual PAT for their modification (Chamberlain, L. H., and Shipston, M. J., 2015). While humans have 23 PATs, there are only two cytoplasmic APTs have been described in detail: APT1 and APT2 (Duncan et al., 1998; Tomatis et al., 2010; Lin et al., 2015; Zeidman et al., 2009). Although APT1 and APT2 share 64% homology, they are thought to be selective since they have different substrate specificity and since they can be inhibited with isoform-selective inhibitors, ML348 and ML349, respectively (Tomatis et al., 2010; Tian et al., 2012; Rusch et al., 2011; Won et al., 2016). APT1 and APT2 contain a catalytic triad consisting of a serine, a histidine, and an aspartic acid (Wang et al., 1997a; Wang et al., 1997b; Devedjiev et al., 2000; Won et al., 2016).

Other depalmitoylases exist in the cell, such as the newly identified ABDH17 hydrolase responsible for depalmitoylation of N-Ras resulting in re-localization to internal cellular membranes and the lysosomal hydrolase PPT, which removes palmitates from proteins in lysosomes (Lin et al., 2015, Verkruyse, L. and Hofmann, S., 1996). However, we focus our studies on APT1 regulation due to the following findings: Wnt5a signaling results in APT1 mediated depalmitoylation of cell adhesion molecules MCAM and CD44,

APT1 overexpression leads to increased melanoma invasion, and conversely, knockdown of APT1 inhibits melanoma invasion (Wang et al., 2015). Since upregulated Wnt5a expression and activation of Wnt5a signaling is observed in human patient samples and results in increased melanoma migration and invasion, and we can see similar responses when modulating APT1 expression, we focus our attention on how Wnt5a signaling may be regulating APT1 activity and function. With the observation of Wnt5a treatment increasing APT1-mediated depalmitoylation of cell adhesion molecules MCAM and CD44 and promoting an invasive phenotype through APT1, we hypothesized APT1 mediated depalmitoylation is regulated by Wnt5a signaling by a post-translational modification to increase APT1 depalmitoylating activity, and elevated Wnt5a/APT1 signaling is responsible for an aggressive melanoma metastasis phenotype.

WNT5A SIGNALING IN CANCER

Wnt proteins are a family of ligands whose functions are well known in embryonic systems development but are increasingly being recognized as key proteins in cancer. Although, its role in cancer is not well understood. Aberrant Wnt5a expression has been characterized in a wide variety of tumor types (Iozzo et al., 1995). Wnt5a has not only been correlated with increased tumor grade or decreased patient survival in melanoma patients (Bittner et al., 2000; Carr et al., 2003; Da Forno et al., 2008). Not only is Wnt5a's expression pattern correlated with tumor progression, but Wnt5a expression can lead to other events that contribute to invasiveness, such as upregulation of metastasis-associated molecules like CD44, initiation of epithelial to mesenchymal transition (EMT), and downregulation of metastasis suppressors (Dissanayake et al., 2007).

Wnt5a has been proposed as a metastatic melanoma mediator, and further evidence has been uncovered to support that proposal. One of its co-receptors, the transmembrane tyrosine kinase receptor ROR2, is expressed predominantly in metastatic melanoma samples, correlates with Wnt5a expression, and is regulated by Wnt5a expression (O'Connell et al., 2009). Also proposed in that study is the necessity of ROR2 for Wnt5a-mediated metastasis in melanoma (O'Connell et al., 2009). If this pathway is repressed through inhibition of various points along the pathway and utilizing different tools, such as knockdown of ROR2, or by inhibiting or knockdown of Frizzled receptors, melanoma invasion is reduced. Furthermore, inhibition of Wnt5a signaling with Wnt5a-derived N-butyloxycarbonyl hexapeptide, termed Box5, inhibited migration and invasion of Wnt5a expressing HTB63 melanoma cells by inhibition of Wnt5a-induced protein kinase C and Ca^{2+} signaling, which has been demonstrated to be essential for cell invasion (Jenei et al., 2009).

Wang et al., 2015 defines some of the downstream events that are playing a role in melanoma metastasis that had not been previously described. Notably, as mentioned above, Wnt5a signaling increasing APT1 mediated depalmitoylation of the cell adhesion molecules MCAM and CD44. MCAM, also known as Melanoma Cell Adhesion Molecule or CD146, is an integral membrane protein consisting of an extracellular fragment containing an immunoglobulin-like domain that responds to the extracellular environment, a transmembrane region, and short cytoplasmic tail (Lehmann et al., 1989). Remarkably, MCAM is strongly expressed in metastatic lesions and advanced primary tumors but rarely detected in benign tissue or neighboring untransformed melanocytes (Lehmann et al., 1987). MCAM is also expressed in endothelia of blood vessels penetrating primary and metastatic melanoma and in a variety of carcinomas in

addition to melanoma (Johnson et al., 1996). Subsequent studies have suggested MCAM has a potential marker for tumor diagnosis, prognosis, and treatment (Johnson et al., 1996; Shih, I.M., 1999; Wu, G.J., 2012).

WM239A cells expressing an MCAM palmitoylation mutant, $MCAM^{C590G}$, is sufficient to polarize MCAM localization, similar to what is observed with Wnt5a treatment, suggesting MCAM depalmitoylation is what is allowing MCAM to be asymmetrically localized (Wang et al., 2015). Expression of the MCAM palmitoylation mutant alone is sufficient to promote cell invasion *in vivo*, as determined by a xenograft tumor model (Wang et al., 2015). Moreover, Wnt5a binds to CD146 (MCAM) to regulate cell migration and zebrafish embryonic convergent extension, and it is suggested CD146 can act as a Wnt5a receptor in regulating cell migration (Ye et al., 2013).

CD44 is an important cell adhesion molecule and is a major receptor for the extracellular matrix component hyaluronan, can act as co-receptor for growth factors, and can reorganize the cytoskeleton through interaction with cytoplasmic linker proteins (Orian-Rousseau et al., 2002; Ponta et al., 2003). CD44 is a class I transmembrane glycoprotein that mediates the response to the environment. The cytoplasmic-tail region can interact with ankyrin to mediate hyaluronan-dependent cell adhesion, and ERM proteins (ezrin, radixin, and moesin) to crosslink the actin cytoskeleton to CD44 (Ponta et al., 2003). CD44 has been implicated in progression for a wide variety of cancers. CD44 is a key regulator of migration and is enriched in cholesterol-enriched membrane microdomains, termed lipid rafts. Lipid raft affiliation of CD44, through palmitoylation, negatively regulates interactions with its migratory binding partner ezrin (Babina et al., 2014). Mutation of CD44 palmitoylation sites, Cys286 and Cys295, also has a similar effect to what is observed with MCAM palmitoylation mutants. CD44 palmitoylation

mutants reduced lipid raft affiliation in invasive MDA-MB-231 breast cancer cells, increased CD44-ezrin co-precipitation, and enhanced cell migration (Babina et al., 2014). This inhibition of CD44 palmitoylation was sufficient to induce the phenotypic appearance of epithelial-to-mesenchymal transition (EMT) and increase cell motility (Babina et al., 2014). Notably, levels of palmitoylated CD44 were lower in primary cultures from invasive ductal carcinomas relative to the non-invasive tissue, providing the clinical data that in combination with the in vitro observations, suggests a role for CD44 palmitoylation and cancer progression. These results suggest both MCAM and CD44 depalmitoylation plays a role in promoting invasive behavior and metastasis.

Previously, it has been proposed that Wnt5a could be a potential therapeutic target for BRAFi-resistant melanoma (Prasat et al., 2015). Patients who develop resistance to standard of care BRAF inhibitors stand to be in dire need of another therapeutic option. Wnt5a inhibition may be a novel way to treat BRAFi resistant tumors and can be an option for other melanoma patients who have elevated Wnt5a expression. This theory is discussed in greater detail in Chapter 5. Based on my own studies described below, APT1 presents itself as an alternative treatment option. In subsequent chapters, we outline the studies and evidence behind that proposal.

Many other studies have begun to investigate Wnt5a's role in other cancer types. Wnt5a expression was investigated in a large cohort of epithelial ovarian cancer patient samples and found to be upregulated in all major subtypes of epithelial ovarian cancer compared to borderline tumors or benign controls (Ford et al., 2014). Integrated transcriptomic and epigenomic analyses uncovered a transcriptional program driving Wnt5a-mediated glioblastoma stem cell (GSC) differentiation into endothelial-like cells, recruitment of endothelial cells to promote satellite lesions, which provided support for

invasive glioma cells away from the primary tumor in a de novo glioblastoma multiforme (GBM) model (Hu et al., 2016). Interestingly, clinical data reveal higher Wnt5a expression in peritumoral and recurrent GBMs relative to primary GBMs. These results suggest a role for Wnt5a-mediated glioblastoma stem cell differentiation and invasive growth in disease recurrence. Additionally, treatment of ovarian surface epithelial cells with Wnt5a decreased cell adhesion and was associated with increased epithelial to mesenchymal transition (EMT) (Ford et al., 2014). Wnt5a and ROR2 expression are also correlated with a poor prognosis in non-small cell lung cancer patients (NSCLC) (Lu et al., 2015). Likewise, ROR2 can regulate migration in osteosarcomas (Dai et al., 2017). Wnt5a overexpression increased clone formation, migration, invasion, and promoted EMT and metastasis in NSCLC (Wang et al., 2017). Since Wnt5a seems to be playing a role in a wide variety of cancer types, by specifically modulating migration, invasion, and metastasis, it is imperative we fully understand the downstream signaling events that are contributing to tumor progression and metastasis.

All of this evidence presented thus far combined suggests that Wnt5a signaling mediates melanoma metastasis among other cancer types besides melanoma. Previous data suggests Wnt5a induced APT1-mediated depalmitoylation of cell adhesion molecules might play a role in driving melanoma metastasis. However, prior to the publication of this thesis work detailed in Chapter 3, the exact details of how APT1 is regulated by Wnt5a signaling remained unknown. Nevertheless, we aim to investigate the mechanism by which Wnt5a signaling is regulating APT1 activity and function, and how activation of this signaling pathway is promoting metastatic behavior.

THESIS OBJECTIVES

Prior to this thesis project, there was a gap in the literature in understanding the how Wnt5a signaling is regulating APT1 activity and function and the downstream events that lead to increased migration, invasion, and promotion of metastasis. The overarching hypothesis of this thesis project was that Wnt5a signaling induces phosphorylation of APT1, thus increasing its depalmitoylating activity. Increased APT1 depalmitoylating activity results in increased depalmitoylation of cell adhesion molecules, driving increased melanoma invasion, and ultimately the promotion of melanoma metastasis. With more details of the Wnt5a signaling pathway uncovered in this research paper, we aim to provide clarity and significance in targeting the Wnt5a pathway as a therapeutic avenue worth pursuing. Below is a picture of the model we are testing.

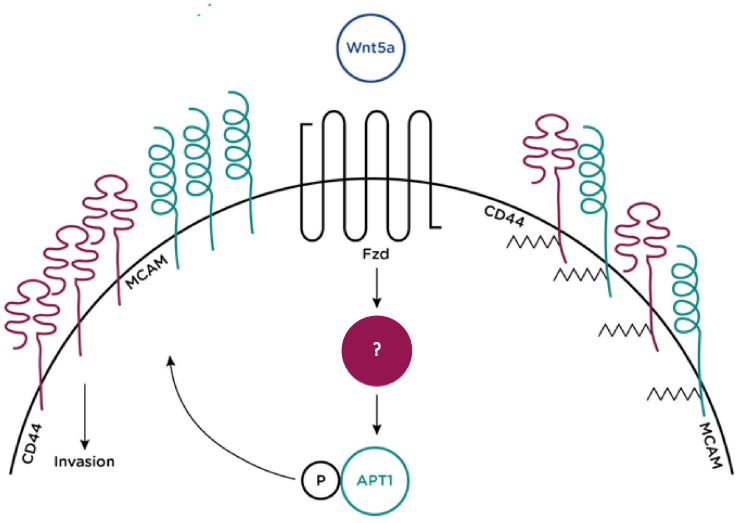

CHAPTER 2: CHARACTIZATION OF APT1'S ENZYMATIC ACTIVITY

OVERVIEW

In the subsequent chapter, we dive into further detail on the previously reported mass spectrometry data that led us to conclude APT1 can be phosphorylated (see Chapter 3), but for the interests of explaining Chapter 2's optimizations, we must clarify the APT1 tools we generated to study APT1's depalmitoylating activity. We generated APT1 phospho-mutants to study the phosphorylation/de-phosphorylation states of APT1 and the functional consequences of these modifications on its depalmitoylating activity. APT1 was previously reported to be phosphorylated on serine's 209 and 210 in laryngeal cancer cells, although how APT1 became phosphorylated and how the phosphorylation state affected APT1's activity and function remained unknown (Phosphosite.org, site group ID: 25299324 and 25299327). We mutated both of APT1's detected phospho-site serine's to alanine's, $APT1^{S209,210A}$, hereon referred to as $APT1^{SA}$, so that it can no longer be phosphorylated and thus it is a phospho-deficient mutant. Conversely, we mutated serine 209 to an aspartic acid, $APT1^{S209D}$, hereon referred to as $APT1^{SD}$, to mimic the negative charge that would exist in the phosphorylated state of APT1 and thus it is a phospho-mimetic mutant. To address if Wnt5a signaling was regulating APT1 depalmitoylating activity, we needed an accurate and consistent assay to study and measure APT1's depalmitoylating activity.

Previously, only a few assays had been developed that we could adapt to study APT1-mediated depalmitoylation and its enzymatic activity levels. In the attempt to finalize the assay we would use to study APT1-mediated depalmitoylation, we optimized a total of three different assays to find the most accurate representation of APT1's

enzymatic activity. Here, we outline the various assays performed, describe the optimization techniques used, and final conclusions drawn from results.

INTRODUCTION

Firstly, we tested a resorufin acetate hydrolysis assay that was previously used to measure hydrolase activity (Adapted from Hwang, S., 2015). The second assay we optimized was a fluorogenic palmitoyl-palmitoylation assay first characterized for lysosomal palmitoyl-protein thioesterase activity, or PPT found in the lysosome (Adapted from Van Diggelen et al., 1999). The final assay tested utilized synthetic small-molecule fluorophore depalmitoylation probe, or DPP-3 specifically, to monitor endogenous activity levels of S-palmitoylation (Kathayat et al., 2017). After careful interpretation of these assays, we concluded use of DPP-3 was the most accurate and consistent method to capture APT1's depalmitoylating activity. In addition, we were able to use this substrate with purified proteins and in live cells in combination with live cell imaging microscopy, which will be discussed in greater detail in the following chapter.

RESULTS

Resorufin acetate hydrolysis assay was originally developed to study hydrolase activity by using resorufin acetate as a fluorogenic substrate. In this assay, resorufin acetate (ResOAc) hydrolysis is measured as a proxy for APT1 enzymatic activity. Specifically, the acetyl group of ResOAc is hydrolyzed by APTs, producing a fluorescent Res^- product, which has distinct fluorescent properties compared to the initial substrate. Using a Tecan plate reader equipped with excitation and emission filters of λ_{ex}535(25) nm, λ_{em}590(20) nm respectively, you can measure the amount of product produced as a

means of analyzing the APT hydrolase activity (Figure 2.1A). Thus, the catalytic rate of APT1 is can be assayed by measuring the rate of fluorescent product production over time. One advantage of this technique was that it contained only a one-step reaction. However, there was not a palmitate group or another fatty acid group attached to the substrate. One could argue that it is too artificial since there is no real substrate specificity involved in the catalysis. $APT1^{WT}$, $APT1^{S209,210A}$, and $APT1^{S209D}$ were immunopurified from WM39A cells ectopically expressing wild-type APT1 or the APT1 phospho-mutants. The reaction was performed using resorufin acetate and fluorescence was measured over time. All three samples had similar measurements that increased over time and no differences were observed between the wild-type APT1 and the APT1 phospho-mutants (Figure 2.1B). Since this assay measures hydrolysis and the ResOAc substrate utilized is so dissimilar from a palmitoylated substrate, we concluded this assay might now be capturing an accurate representation of APT1's depalmitoylating activity. We aimed to use a substrate that more closely mimics APT1's palmitoylated substrates.

The fluorogenic palmitoyl-protein thioesterase assay was utilized next because of the artificial substrate contained a palmitoyl group. This assay was originally developed to study palmitoyl-protein thioesterase (PPT) activity from lysosomes (Van Diggelen et al., 1999). This assay also utilized a fluorophore synthetic substrate, although its structure differed considerably in terms of structure. To create the substrate, a palmitate group was added to the fluorochrome substrate 4-methylumbelliferyl-6-thiopalmitoyl-β-glucopyranoside via a thioester bond to create Mu-6S-Palm-β-Glc. The addition of purified APT1, either purified from bacteria or immunopurified from melanoma cells, to the substrate results in a non-fluorescent cleaved intermediate from the removal of palmitate. A second reaction with β-glucosidase results in the final fluorescent product,

which can be observed at λ449nm (Figure 2.1C). We adapted this protocol with the purpose of using the assay for immunopurified APT1, as opposed to whole cell lysate, which was used in the original publication. APT1 was immunopurified from WM239A cells ectopically expressing $APT1^{WT}$ or phospho-dead $APT1^{S209,210A}$ and the two reactions were performed using increasing concentrations of the Mu-6S-Palm-β-Glc substrate. At lower concentrations of substrate, $APT1^{WT}$ and $APT1^{S209,210A}$ (hereon referred to as $APT1^{SA}$) have similar activity. However, at the highest concentration $APT1^{WT}$ exhibited increased activity when compared to $APT1^{SA}$ (Figure 2.1D). When we tested $APT1^{WT}$ against phospho-mimetic $APT1^{S209D}$ ($APT1^{SD}$), $APT1^{SD}$ had higher enzymatic activity compared to $APT1^{WT}$, even at the lower concentrations of substrate (Figure 2.1E). When we treated WM239A cells ectopically expressing $APT1^{WT}$ or the catalytic inactive mutant $APT1^{S119A}$ with either purified Wnt5a or control buffer, then immunopurified APT1, and subsequently performed the fluorogenic palmitoyl-protein thioesterase assay, we observed increased depalmitoylation levels for Wnt5a-treated $APT1^{WT}$ but, observed no difference between Wnt5a untreated and untreated/treated catalytic inactive mutant $APT1^{S119A}$ (Figure 2.1F). These results suggest phospho-mimetic APT1 exhibits increased activity, and mutation mimicking phosphorylation is sufficient to increase its activity. Moreover, the results suggest Wnt5a-treated APT1 also results in increased depalmitoylating activity. Advantages of using the fluorogenic palmitoyl-protein transferase assay was that this substrate contained a palmitate group, and thus this reaction involved recognition of a more physiologically relevant substrate. However, a potential pitfall, which proved to create much difficulty in attempting to obtain consistent results, was that this substrate had solubility issues and the protocol contains two reaction steps. Therefore, using the fluorogenic palmitoyl-transferase assay

increased the chances of variability across repeated experiments and reduced reproducibility among the results. We could observe differences between wild-type and mutants, but only at higher concentrations of Mu-6S-Palm-β-Glc, which proved difficult to work with at such high concentrations due to its solubility issues and we did not want to run the risk of testing with inaccurate concentrations of available Mu-6S-Palm-β-Glc if it were not to be solubilized completely.

Lastly, we discovered a recent publication utilizing small-molecular fluorophores to monitor the depalmitoylation activity levels of APTs, called depalmitoylation probes or DPPs (Kathayat et al., 2017). The authors of this paper state that development and application of DPPs provide the ability to measure endogenous levels of depalmitoylation activity in live cells. We contacted the authors of this paper and had their probe, DPP-3, synthesized for our studies. Similar to the previous assays, this reaction results in cleavage of a fluorescent product, which is then measured as a proxy for APT1 depalmitoylating activity. After addition of purified APT1 with DPP-3 substrate, fluorescence intensity is measured using Tecan plate reader at λ_{ex} 490/9 nm and λ_{em} 545/20 nm over time. Although it is not a palmitate, DPP-3 does have a fatty acid attached (Kathayat et al., 2017). This approach seems to be the best compromise of having a substrate that can be easily worked with, including its ability to be used in live cells, but also mimics APT1's substrate as closely as possible. We expand more on this experiment, the applications of this probe, and its significance in Chapter 3. When we tested the depalmitoylating activity of wild-type APT1 and the APT1 phospho-mutants using DPP-3 as a substrate, we observed a significant increase of activity between $APT1^{SD}$ compared to $APT1^{WT}$ and negative control $APT1^{S119A}$ (Figure 2.1G).

FIGURES

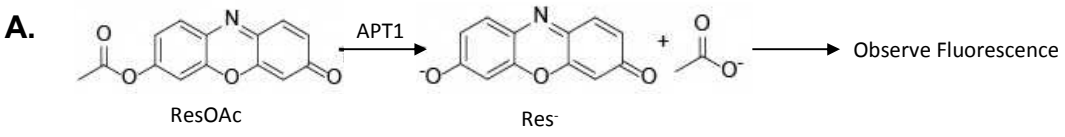
A.
APT1
Observe Fluorescence
ResOAc
Res-

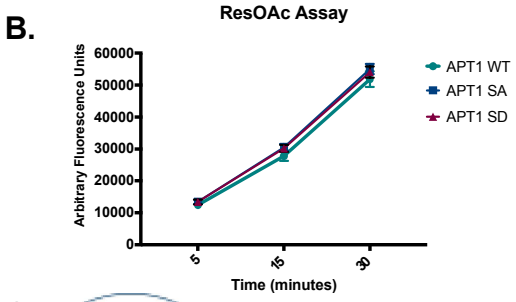
B.
ResOAc Assay
Arbitrary Fluorescence Units
60000
50000
40000
30000
20000
10000
0
5
15
30
Time (minutes)
APT1 WT
APT1 SA
APT1 SD

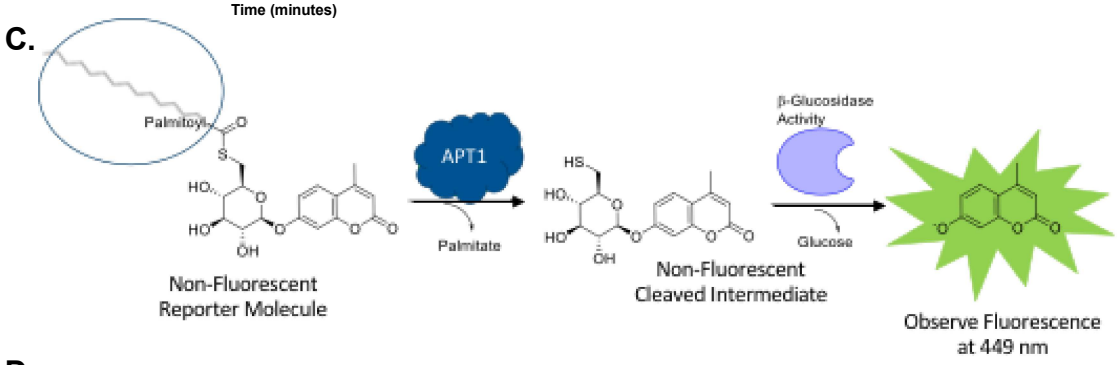
C.
Palmitoyl
APT1
Palmitate
β-Glucosidase Activity
Glucose
Non-Fluorescent Reporter Molecule
Non-Fluorescent Cleaved Intermediate
Observe Fluorescence at 449 nm

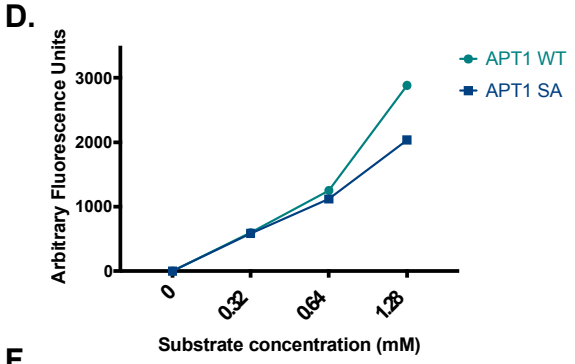
D.
Arbitrary Fluorescence Units
3000
2000
1000
0
0
0.32
0.64
1.28
Substrate concentration (mM)
APT1 WT
APT1 SA

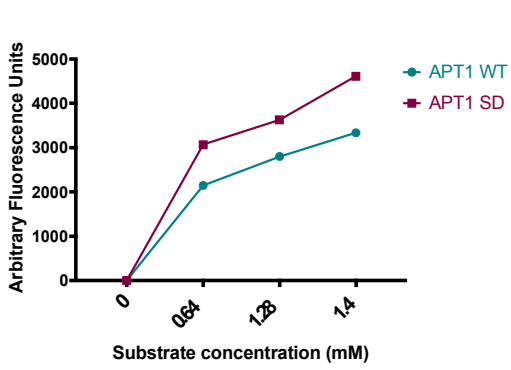
E.
Arbitrary Fluorescence Units
5000
4000
3000
2000
1000
0
0
0.64
1.28
1.4
Substrate concentration (mM)
APT1 WT
APT1 SD

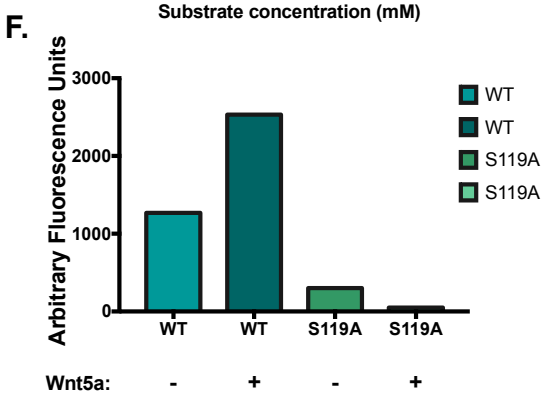
F.
Arbitrary Fluorescence Units
3000
2000
1000
0
WT
WT
S119A
S119A
Wnt5a:
-
+
-
+
WT
WT
S119A
S119A

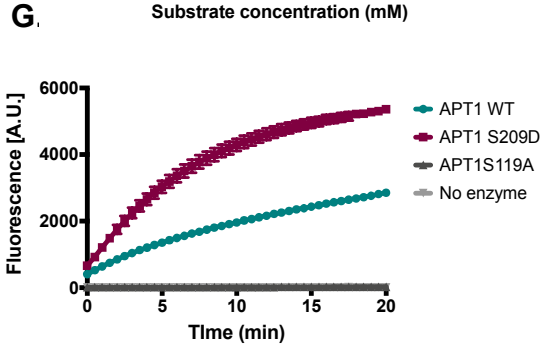
G.
Fluorescence [A.U.]
6000
4000
2000
0
0
5
10
15
20
TIme (min)
APT1 WT
APT1 S209D
APT1S119A
No enzyme

Figure 2.1. *Characterization and optimization of analyzing APT1's depalmitoylating activity.* (**A**) Schematic of resorufin acetate hydrolysis assay reaction. (**B**) Depalmitoylation activity measured by resorufin acetate hydrolysis assay of bacterially expressed and purified $APT1^{WT}$, $APT1^{S209,210A}$ ($APT1^{SA}$), and $APT1^{S209D}$ ($APT1^{SD}$) measured over time. n=3 replicates per condition. (**C**) Schematic of fluorogenic palmitoyl-protein thioesterase assay reactions. Adapted from Van Diggelen et al., 1999. (**D**) Depalmitoylation activity analyzed by fluorogenic palmitoyl-transferase assay of bacterially expressed and purified $APT1^{WT}$ and $APT1^{SA}$ measured with increasing concentrations of Mu-6S-Palm-β-Glc substrate. n=3 replicates per condition. Results shown are from a representative trial from three independent experiments. (**E**) Depalmitoylation activity analyzed by fluorogenic palmitoyl-protein thioesterase assay of bacterially expressed and purified $APT1^{WT}$ and $APT1^{SD}$ measured with increasing concentrations of Mu-6S-Palm-β-Glc substrate. n=3 replicates per condition. Results shown are from a representative trial from three independent experiments. (**F**) WM239A cells expressing $APT1^{WT}$ or catalytically inactive mutant $APT1^{S119A}$ were treated with purified 150 ng/ml Wnt5a or control buffer for 15 minutes, APT1 was immunopurified using anti-FLAG magnetic particles, and depalmitoylation activity was measured by fluorogenic palmitoyl-protein thioesterase assay using 0.64 mM Mu-6S-Palm-β-Glc. (**G**) DPP-3 depalmitoylation assay using 5 μM of depalmitoylation probe DPP-3 in HEPES (20 mM, pH 7.4, 150mM NaCl, 0.1% Triton X-100) with either 50 nM purified $APT1^{WT}$, $APT1^{S209D}$ or catalytically inactive $APT1^{S119A}$ and fluorescence emission was measured over time (λ_{ex}490/9 nm; λ_{em} 545/20 nm). Error bars indicate s.e.m., n=3 replicates per condition. Results shown are from a representative trial from three independent experiments.

DISCUSSION

The resorufin acetate hydrolysis assay had many pitfalls. The first being the use of the artificial substrate. We were afraid that we were not capturing the differences in catalytic activity between the mutants because the substrate utilized in this protocol was so unlike APT1's typical substrates and very artificial compared to a palmitoylated substrate. After confirmation that there were significant differences among the mutants using the other two assays, we decided this assay was not accurately capturing the true enzymatic activity of APT1.

Although the fluorogenic palmitoyl-palmitoylation assay with MU-6S-Palm-β-Glc utilized a substrate with a palmitate group, there proved to be many solubility issues that resulted in inconsistencies across repeated experiments. Furthermore, the additional reaction with β-glucosidase only added to those inconsistencies. Adding the extra layer of variability with β-glucosidase, we were unable to get consistent results and concluded this assay had too many variables and technical challenges.

After careful interpretation of these assays, we concluded use of the DPPs was the most accurate way to capture APT1's depalmitoylating activity. We go into detail about this experimental approach in the subsequent chapter, Chapter 3. We are able to use the DPP-3 substrate to study APT1's depalmitoylating activity in real time, resolved any solubility issues because the synthesized probe was easy to dissolve and work with, and are able to use the probe in important live cell imaging experiments. Because of these consistent results and added benefits, we utilized this unique technique for our remaining studies in the subsequent chapters.

METHODS

Resorufin acetate assay

Protocol is adapted from Hwang, S., 2015. Resorufin acetate was added to immunopurified APT1 wild-type or APT1 phospho-mutants. Fluorescent product was measured by using Tecan plate reader with excitation and emission filters of λ_{ex} 535(25) nm and λ_{em} 590(20) nm, respectively.

Fluorogenic palmitoyl protein thioesterase assay with MU-6S-Palm-ß-Glc

Protocol is adapted from Van Diggelen et al., 1999. 4-methylumbelliferyl 6 thio-palmitate-ß-D-glucopyranoside (Mu-6S-Palm-β-Glc) (Santa Cruz Biotechnology, Dallas, TX). Bacterially expressed and purified APT1 or immunopurified APT1 (see methods below) was added to increasing concentrations of Mu-6S-Palm-β-Glc substrate solution containing 15 mM DTT, 0.375% Triton-X-100. After a 1-hour incubation at 37°C, samples were boiled to stop the APT1 reaction and then allowed to cool. Almond β-glucosidase (Sigma) was added and the reaction mixture incubated again for 30 minutes at 37°C to hydrolyze the reaction intermediate MU-6-thio-β-glucoside. All enzymatic reactions were terminated by the addition of 200 µl of 0.5 M Na_2CO_3/$NaHCO_3$ pH 10.7, containing 0.025% Triton-X-100 and then the fluorescence was measured using a Tecan plate reader at λ449 nm.

Fluorogenic palmitoyl thioesterase assay with DPPs

APT1 was assayed for depalmitoylating activity as described previously (Kathayat et al. 2017).

Purification of APT1

Wild type and APT1 mutants (FLAG tagged) were cloned into the pET-28 plasmid backbone. Bacteria were grown overnight at 37°C in the presence of 100 µg/ml

ampicillin and 50 μg/ml chloramphenicol. Next, fresh LB or TB was inoculated with the overnight bacteria and grown for 4 hours at 37°C until OD_{600}= 0.6-1.0. Expression of APT1 was induced with final concentration of 1 mM IPTG for 2 hours at 37°C or overnight at 18ºC. Cells were pelleted at 8000 RPM for 15 minutes at 4°C. Pellet was resuspended in 50 mM HEPES pH 8.0, 300 mM NaCl, 1% Triton X-100, 20 mM Imidazole (Sigma), 1 mM Phenylmethylsulfonyl fluoride (PMSF), 1 mM dithiothreitol or 25 mM HEPES pH 7.5, 500 mM NaCl, 10% glycerol, 1mM PMSF, 10mM 2-Mercaptoethanol, complete EDTA free protease inhibitor cocktail (Pierce). Lysate was sonicated at 50% duty cycle for 30 second pulses two times on ice or 50% duty cycle for 30 pulses on and 30 pulses off for 30 minutes at 4ºC. Lysate was centrifuged at 12,000 RPM for 15 minutes at 4°C. Supernatant was incubated with Ni Sepharose 6 Fast Flow beads (GE Healthcare) at 4°C rocking for 3 hours or overnight. Beads were washed three times with wash buffer (50mM HEPES pH 8.0, 300mM NaCl, 40mM Imidazole) or 500mL of wash buffer (25 mM HEPES pH 7.5, 500 mM NaCl, 10% glycerol, 40 mM Imidazole, 10mM 2-Mercaptoethanol). Protein was eluted using 50 mM HEPES pH 8.0, 300 mM NaCl, 250 mM Imidazole by rocking for 45 minutes at 4°C or 50mL of 25 mM HEPES pH 7.5, 500mM NaCl, 300mM Imidazole, 10mM 2-Mercaptoethanol at 4°C.

Cell lines and culture conditions

Metastatic melanoma cell line WM239A (BRAF V600D) (Wistar Institute) were cultured in RPMI 1640 medium (Gibco-BRL, Grand Island, NY) supplemented with 10% fetal bovine serum (FBS) (GE Life Sciences). Cell lines were authenticated routinely by short tandem repeat profiling by the Wistar Institute prior to use.

Immunoprecipitation

WM239A cells ectopically expressing APT1-CFP-FLAG wild-type/mutants were treated with control buffer or 150 ng/ml Wnt5a for specified time period and then lysed in lysis buffer containing 1% Triton-X 100, 50 mM Tris pH 7.5, 150 mM NaCl supplemented with protease and phosphatase inhibitors (1μg/ml leupeptin, 1μg/ml aprotinin, 2μg/ml pepstatin A, 1mM PPi, 2nM $NaVO_4$, 150mM NaF). Insoluble cell debris was removed by centrifugation (13,000 RPM for 10 min at 4°C. Lysate was incubated with FLAG M2 magnetic beads (Sigma-Aldrich, St. Louis, MO) for 1.5 hours. Beads were washed with lysis buffer and protein was eluted using FLAG peptide for 1 hour at room temperature. Samples were separated by SDS-PAGE and transferred to either nitrocellulose membrane (Life Technologies, Thermo Fisher Scientific, Waltham, MA) for phospho-APT1 antibody (YenZym Antibodies, San Francisco, CA) or PVDF membrane (Millipore, Burlington, MA) for all other antibodies used.

Purification of recombinant Wnt5a and treatments with Wnt5a

Wnt5a was purified from mouse L-cells overexpressing human Wnt5a as described previously (Willert et al., 2003). Control cells were treated with control buffer with identical detergent conditions as the Wnt5a purification buffer.

CHAPTER 3: WNT5A SIGNALING INDUCED PHOSPHORYLATION INCREASES APT1 ACTIVITY AND PROMOTES MELANOMA METASTATIC BEHAVIOR

This chapter has been previously published in:

Sadeghi, R. S., Kulej, K., Kathayat, R. S., Garcia, B. A., Dickinson, B. C., Brady, D. C., and Witze, E. S. (2018) Wnt5a signaling induced phosphorylation increases APT1 activity and promotes melanoma metastatic behavior. eLife ***7***

OVERVIEW

Many studies have reported a correlation between elevated Wnt5a expression and melanoma and observations of increased motility and invasion mediated by Wnt5a signaling but fail to define the mechanistic details of how Wnt5a signaling is mediating these effects. Prior to this publication, there was a gap in the literature addressing how Wnt5a signaling, specifically Wnt5a induced APT1-mediated depalmitoylation, is contributing to metastatic behavior in melanoma. We hypothesized APT1 activity and function was being regulated by Wnt5a signaling and aimed to determine the mechanism of APT1 regulation. Here, we define a phospho-switch on APT1 that increases APT1's depalmitoylating activity, resulting in increased melanoma invasion, and decreased APT1 dimer formation.

INTRODUCTION

The Wnt5a signaling pathway plays a paramount role in important biological processes as it regulates cell polarity and polarized cell movement during embryonic development. Wnt5a expression is strongly correlated with melanoma progression and metastasis (Bitter et al., 2000, Carr et al., 2003). Melanoma is the deadliest form of skin

cancer, with a 5-year survival rate of only 17% for metastatic melanoma patients (Sandru et al., 2014). Previously, the elevated expression of Wnt5a in human melanoma samples and subsequent *in vitro* studies have suggested a role for Wnt5a in melanoma metastasis (Bitter et al., 2000, Carr et al., Forno et al.). Importantly, Wnt5a expression is positively correlated with poor outcome, with high Wnt5a expression being associated with decreased patient survival (Forno et al., 2008). With this information, it has been suggested that Wnt5a expression be used as a prognostic clinical risk factor (Forno et al., 2008). However, the exact mechanisms by which Wnt5a promotes metastatic behavior remains unknown. Thus, elucidation of the signaling events downstream of Wnt5a that promote polarized cell movement and metastatic behavior have the potential to enhance our understanding of the contribution of Wnt5a to melanoma metastasis.

Our lab and others have shown Wnt5a signaling promotes migration and invasion in melanoma cells (Dissanayake et al., 2007, Wang et al., 2015, Weeraratna at al., 2002). Wnt5a is a secreted ligand in the noncanonical Wnt signaling pathway and upon interacting with its Frizzled receptor, activates a signal transduction cascade (Sato et al., 2010). Wnt5a signaling controls cell polarity and directional cell movement, and Wnt5a treatment promotes recruitment and reorganization of proteins involved in cell adhesion and cell signaling (Witze et al., 2008, Wang et al., 2015). Wnt5a stimulation promotes asymmetrical localization of cell adhesion molecules, increases cell motility, and elevates levels of free Ca^{2+} to induce Ca^{2+} signaling in a polarized manner (Witze et al., 2008, Witze et al., 2013). The tyrosine kinase receptor ROR2, which is predominantly expressed in metastatic melanoma, has been shown to specifically interact with Wnt5a and mediate Wnt5a signaling (O'Connell et al., 2010). In addition to reorganization of the actin cytoskeleton and polarized localization of cell adhesion

molecules, others have shown that elevated Wnt5a expression promotes melanoma invasion and human biopsies directly correlated Wnt5a expression with tumor grade (Weeraratna at al., 2002).

Pro-metastatic cell adhesion molecules, such as transmembrane receptors CD44 and MCAM (Melanoma Cell Adhesion Molecule), have been shown to play a role in cell migration and metastasis. CD44 levels are elevated in multiple cancer types and MCAM is expressed in melanoma cells and not untransformed melanocytes (Weilenga et al., 1993, Shih et al., 1994a, Shih et al., 1994b). Palmitoylation of these cell adhesion molecules strongly influences protein function. CD44 has been shown to be palmitoylated and inhibiting CD44 palmitoylation through cysteine point mutations strongly enhanced breast cancer migration (Babina et al., 2014). Similarly, cysteine point mutations that block MCAM palmitoylation increases metastatic cell behavior in melanoma cells both *in vitro* and *in vivo* (Wang et al., 2015).

S-Palmitoylation is the reversible addition of a 16-carbon fatty acid to cysteine residues via a thioester linkage. Palmitate addition is mediated by palmitoyl-transferases and acyl protein thioesterases (APTs) remove palmitate from proteins to regulate protein localization, trafficking, and cell signaling (Vartak et al., 2014, Linder and Deschenes et al., 2007, Lin and Conibear at al., 2015). Acyl protein thioesterases 1 and 2 (APT1 and APT2; aka LYPLA1 and LYPLA2) are cytosolic depalmitoylases that have been proposed to act constitutively to depalmitoylate proteins from membranes. However, there is evidence that protein depalmitoylation is a signal regulated modification. Wnt5a stimulation has been shown to induce the depalmitoylation of both MCAM and CD44 through APT1 (Wang et al., 2015). Wnt5a mediated melanoma cell invasion is reduced by treatment with a small molecule inhibitor of APT proteins. Another group has also

shown that growth factor stimulation is also sufficient to inhibit depalmitoylating activity of APT proteins (Kathayat et al., 2016). Wang, et al. demonstrated that increased APT1 expression increased melanoma invasion in the absence of exogenous Wnt5a (Wang et al., 2015). It remains to be determined how Wnt5a signaling increases depalmitoylation through APT1. These results led us to investigate the link between Wnt5a signaling and regulation of APT1-mediated depalmitoylation. We hypothesized APT1 depalmitoylating activity could be regulated by upstream signaling events, specifically the Wnt5a signaling pathway.

Here, we uncover a mechanism by which the non-canonical Wnt signaling pathway increases the depalmitoylating activity of APT1. We have mapped a regulatory phosphorylation site on APT1 and utilizing site specific point mutations, we unravel the impact of phosphorylation on APT1 activity and its importance in melanoma cell invasion. Using a depalmitoylation probe (DPP) that measures depalmitoylating activity (Kathayat at al., 2016, Qiu et al., 2017 and Beck et al., 2017), we show APT1 phosphorylation increases its depalmitoylating activity. This is the first study showing a signaling pathway can direct protein depalmitoylation through a phospho-switch on APT1 that we propose functions to disrupt an inactive APT1 dimer.

RESULTS

Wnt5a Signaling Induces APT1 Phosphorylation

Wnt5a induced metastatic cell behavior was previously shown to be dependent on increased protein depalmitoylation driven by APT1 (Wang et al., 2015). We hypothesized a mechanism for increased depalmitoylation could be a result of regulatory post-translational modifications of APT1 that increases APT1 activity. To investigate if

APT1 is post-translationally modified in response to Wnt5a stimulation, we used mass spectrometry to identify Wnt5a dependent post-translational modifications (PTMs) of APT1. Low Wnt5a producing WM239A melanoma cells expressing CFP-FLAG tagged wild type APT1 ($APT1^{WT}$-CFP-FLAG) were treated with purified Wnt5a and APT1 was immunoprecipitated using anti-FLAG magnetic particles. APT1 was eluted with FLAG peptide. The immunopurified APT1 was alkylated and trypsinized and analyzed by mass spectrometry. The only phosphorylation sites identified on APT1 were on serine residues 209 and 210. Whereas single phosphorylation of either serine 209 or 210 was detected, we can't rule out the possibility of dual phosphorylation (Figure 3.1A and 3.1B). These findings are consistent with a previous high throughput mass spectrometry screen by another group that identified APT1 phosphorylation on serine residues 209 and 210 in laryngeal cancer cells (Phosphosite.org, site group ID: 25299324 and 25299327).

We generated separate phospho-specific antibodies to phospho-site Ser209 and Ser210 of APT1 (YenZym Antibodies) to detect phosphorylated APT1 in melanoma cell lysates. To validate the antibodies, WM239A cells ectopically expressing $APT1^{WT}$-CFP-FLAG were treated with purified Wnt5a for 15 minutes. $APT1^{WT}$-CFP-FLAG was then immunoprecipitated and separated by SDS-PAGE followed by immunoblotting. With phospho-APT1 antibodies to both serine 209 and serine 210, we detected phosphorylated APT1 (pS209-APT1/pS210-APT1) that increased following Wnt5a stimulation (Figure 3.1C). The induction of APT1 phosphorylation at Ser210 was detected in whole cell lysate without immunoprecipitation, showing a relatively high stoichiometry of phosphorylated APT1 to total APT1 after Wnt5a stimulation (Figure 3.1D). We also observe a similar, but weaker, increase in exogenous phospho-APT1 in whole cell lysate utilizing the pS209-APT1 antibody in response to Wnt5a (data not

shown). However, we were unable to detect phosphorylation of the endogenous APT1 in the whole cell lysate from these cells (data not shown). To determine the temporal kinetics of Wnt5a induced APT1 phosphorylation, WM239A cells ectopically expressing $APT1^{WT}$-CFP-FLAG were treated with purified Wnt5a for increasing lengths of time, $APT1^{WT}$-CFP-FLAG was then immunoprecipitated and APT1 phosphorylation was measured by immunoblotting. APT1 phosphorylation peaked at 30 min and began to decrease at 60 min (Figure 3.1E). To determine the function of the Wnt5a induced phosphorylation, a phospho-deficient APT1 double mutant was generated by mutating both serine residues 209 and 210 to alanine (from here on referred to as $APT1^{SA}$). When WM239A cells ectopically expressing $APT1^{SA}$ are treated with Wnt5a, the levels of phosphorylation of APT1 at Ser210 measured by immunoblotting were unchanged compared to cells expressing $APT1^{WT}$ (Figure 3.1F).

The crystal structure of APT1 has been previously determined (Devedjiev et al., 2000, Won at al., 2015) allowing us to model where the phosphorylated serine residues are positioned on the three-dimensional structure (PDB:5sym). We found that the phosphorylated serine residues 209 and 210 are solvent exposed on the lip of the hydrophobic putative acyl-binding channel and adjacent to the catalytic triad (Ser119, His208, Asp174), suggesting phosphorylation of these sites could influence APT1 activity (Figure 3.1G). Together, these results indicate Wnt5a signaling in melanoma cells induces APT1 phosphorylation at serine residues 209 and 210 and our phospho-specific antibodies are selective for these sites.

APT1 Phosphorylation Increases Depalmitoylating Activity

To investigate how Wnt5a induced phosphorylation of APT1 affects its function, phosphorylated serine 209 was mutated to a negatively charged aspartic acid ($APT1^{S209D}$) to mimic the negative charge of phosphate on serine 209. To measure APT1 activity, we utilized a recently developed fluorescent depalmitoylation probe, DPP-3, that contains a thiol conjugated 7 carbon fatty acid that when hydrolyzed, generates a fluorescent product that can be measured at λ_{ex}490/9 nm; λ_{em} 545/20 nm (Kathayat et al. 2017). This probe served as a reporter to measure the depalmitoylating activity of APT1 and APT1 mutants both *in vitro* and in live cells. 6x His-tagged APT1 expressed and purified from *E. coli* was incubated with DPP-3 and the relative fluorescence was measured over time. $APT1^{S209D}$ was found to have increased depalmitoylating activity compared to $APT1^{WT}$ (Figure 3.2A). A catalytically inactive mutant where catalytic serine 119 is mutated to alanine (referred to as $APT1^{S119A}$) was used as a negative control and generated minimal fluorescence throughout the duration of the assay (Figure 3.2A). We next evaluated the depalmitoylating activity of $APT1^{WT}$ and $APT1^{S209D}$ using DPP-3 in the presence of increasing concentrations of DPP-3 substrate to determine the initial velocities at multiple substrate concentrations (Figure 3.2B and 3.2C). We measured higher initial velocities for $APT1^{S209D}$ at each substrate concentration compared to $APT1^{WT}$ (Table 1).

To determine the effect of Wnt5a stimulation on APT1 depalmitoylating activity, WM239A cells were incubated with DPP-3 and fluorescence emission was measured at 15, 30, and 45 minutes post Wnt5a treatment by live-cell microscopy (Figure 3.2 – figure supplement 1A). We quantified fluorescence emission in individual cells and determined that Wnt5a stimulation significantly increased the fluorescence emission compared to control buffer treated cells, indicating an increase in endogenous APT1 activity (Figure

3.2D). To confirm the increase in fluorescence emission in response to Wnt5a was through APT1, we immunoprecipitated APT1 from WM239A APT1^{WT} cells stimulated with purified Wnt5a or untreated control cells, and measured depalmitoylating activity *in vitro* using DPP-3. APT1 isolated from Wnt5a stimulated cells showed an increase in depalmitoylating activity compared to untreated control (Figure 3.2 – figure supplement 1B). While the non-canonical Wnt ligand Wnt5a is sufficient to increase APT1 activity we found stimulation with the canonical Wnt ligand, Wnt3a, was unable to increase APT1 activity compared to Wnt5a and was similar to cells treated with control buffer (Figure 3.2E). We confirmed these cells are competent to respond to the Wnt3a concentration used because we observe stabilization of β-catenin beginning at 75 ng/ml of Wnt3a (Figure 3.2 – figure supplement 1C). Therefore, the ability to increase APT1 activity appears to be specific to the non-canonical Wnt pathway.

To directly assess how the phosphorylation state of APT1 affects depalmitoylation in live cells, WM239A melanoma cells expressing APT1^{WT} or the phospho-mutants APT1^{SA} and APT1^{S209D} were incubated with the DPP-3 probe for 30 minutes and fluorescence emission was measured by live-cell microscopy. Consistent with the *in vitro* results, APT1^{S209D} has greater depalmitoylating activity in cells compared to either APT1^{WT} or APT1^{SA} (Figure 3.2F, Figure 3.2 – figure supplement 1D). To determine the contribution of APT1 phosphorylation to the Wnt5a mediated increase in APT1 activity, we treated cells expressing either APT1^{WT}, APT1^{SA}, or APT1^{S209D} with Wnt5a or control buffer and measured the APT1 activity with the DPP-3 probe. Wnt5a treatment increases APT1^{WT} activity to levels higher than the phosphomimetic mutant APT1^{S209D}. As expected Wnt5a stimulation is unable to increase activity of phospho-

dead APT1^{SA} or further increase the constitutive elevated activity of APT1^{S209D} (Figure 3.2F).

To demonstrate that activity of a protein kinase is responsible for the Wnt5a-mediated increase in APT1 activity, we treated cells with pan protein kinase inhibitors to block the Wnt5a mediated increase in APT1 activity. We pre-treated WM239A cells expressing APT1^{WT} with either the serine/threonine kinase ATP-competitive inhibitor BI-D1870 or the broad-spectrum kinase inhibitor staurosporine for 1 hour, incubated the cells with the DPP-3 probe, and measured fluorescence over time by live-cell microscopy during treatment with Wnt5a or control buffer. Treatment with either protein kinase inhibitors inhibited the Wnt5a mediated increase in APT1 activity to levels comparable to unstimulated cells (Figure 3.2G). Although the identity of the Wnt5a regulated kinase remains unknown, these results suggest that phosphorylation of APT1 is a main driver of increased APT1 activity in response to Wnt5a.

Expression of APT1^{S209D} Decreases Levels of a Palmitoylated Protein Substrate

We next asked if we could observe a similar phosphorylation dependent increase in depalmitoylating activity by measuring palmitoylation of a protein substrate in cells. The extent of protein palmitoylation is the result of an equilibrium between palmitoylation and depalmitoylation of substrates. To determine the immediate effect of expressing the phospho-mutant forms of APT1 on protein palmitoylation before the cell adapts and reaches a new steady state, we generated an inducible expression system to measure the effects of acute expression of APT1^{WT} and the APT1 phosphorylation mutants on a specific depalmitoylation substrate. We chose MCAM (melanoma cell adhesion molecule), a known substrate of APT1 that is depalmitoylated in response to Wnt5a

stimulation, to investigate the contribution of APT1 phosphorylation on protein depalmitoylation (Wang et al., 2015). HEK 293T cells were co-transfected with a MCAM-GFP plasmid and a doxycycline inducible plasmid containing FLAG-tagged $APT1^{WT}$, $APT1^{SA}$, or $APT1^{S209D}$. Cells expressing $APT1^{WT}$ or mutants were induced with doxycycline for 15 hours. We found cells produced similar amounts of wild type and mutant APT1 protein (Figure 3.3A). The abundance of palmitoylated MCAM in each condition was then measured using the acyl biotin exchange assay (ABE). As a negative control, samples are processed without hydroxylamine (-HAM) leaving the palmitoylated cysteines intact and preventing biotin labeling. We found MCAM palmitoylation to be highest in $APT1^{SA}$ samples, indicating a decreased ability to depalmitoylate MCAM (Figure 3.3B). In contrast, the $APT1^{S209D}$ sample had the lowest level of palmitoylated MCAM, indicating the highest level of depalmitoylating activity. These results confirm the elevated depalmitoylating activity of $APT1^{S209D}$ we observe with the DPP-3 probe using a known palmitoylated protein in the cell. These data serve as evidence that the phosphorylation state of APT1 regulates depalmitoylation of endogenous substrates.

APT1 Phosphorylation Increases Metastatic Behavior in Melanoma Cells

Previous studies demonstrated increased APT1 expression results in increased invasion of melanoma cells embedded in collagen (Wang et al. 2015). To determine if this increased metastatic behavior was due to APT1 phosphorylation, we asked if APT1's phosphorylation state affects melanoma invasion using the APT1 phospho-mutants. Spheroids were formed from WM239A melanoma cells ectopically expressing CFP-FLAG-tagged $APT1^{WT}$, $APT1^{SA}$, or $APT1^{S209D}$, embedded in collagen, and the distance invaded was measured. We found that expression of $APT1^{SA}$ resulted in decreased invasion, similar to the negative control CFP, while $APT1^{S209D}$ significantly

increased melanoma invasion (Figure 3.3C and 3.3D). Since these melanoma cells are not Wnt5a treated, this dramatic increase in APT1^{S209D} melanoma invasion is due to the single point mutation that mimics phosphorylation alone. When the activity of APT1 is inhibited with the selective inhibitor ML348, invasion is blocked, demonstrating the increased invasion observed in cells expressing APT1^{S209D} is mediated by APT1 activity (Figure 3.3E). Together these results indicate phosphorylation of Ser209 increases depalmitoylating activity in cells, in turn increasing metastatic cell behavior.

Phosphorylation Reduces APT1 Dimerization

We next sought to determine how phosphorylation increases APT1 activity. We first asked if mutating the phospho-sites changed the thermostability of the protein using differential scanning fluorimetry of purified APT1^{WT}, APT1^{SA}, or APT1^{S209D} mutants (Figure 3.4A). We found that each mutant possessed similar thermostability to that of APT1^{WT}, indicating that the point mutations are not destabilizing the folding of the protein (Figure 3.4B). We next asked if the existing crystal structure might provide insight into the mechanism of APT1 activity.

Previous crystal structures of APT1 revealed a weak asymmetric dimer in which the active site was occluded by the dimer interface, suggestive of an inactive dimer (Devedjiev et al., 2000, Won et al., 2015). Our interrogation of the crystal structure revealed that the phosphorylation sites 209 and 210 reside in the interface of the dimer and could potentially destabilize the dimeric form and decrease the inhibitory dimeric interaction. We measured the distance between the serine residues to the methionine (Met 65) residue on the opposite dimer and found a short distance of less than 4 Å (Figure 3.4C). We therefore hypothesized that phosphorylation of one of these sites

would be less favorable for dimer formation. Studies confirming the dimeric state of APT1 in solution are lacking. We therefore asked if we could detect dimeric APT1. We next sought to distinguish the APT1 monomer from the dimer by size-exclusion chromatography. When APT1 was loaded on the column at a concentration of 0.1 mg/ml both $APT1^{WT}$ and $APT1^{S209D}$ eluted at the same time as a 29kD standard. When the protein concentration is increased to 0.25 mg/ml a second peak of $APT1^{WT}$ begins to resolve closer to the 44kD standard (Figure 3.4D). When the $APT1^{WT}$ protein concentration was increased to 0.375 mg/ml a second peak was resolved near the 44kD standard that was not observed with $APT1^{S209D}$. Additionally, the peak at 29kD for $APT1^{WT}$ is abolished at this concentration (Figure 3.4D). The identity of the protein in the shifted peak was confirmed as APT1 by visualizing the 25kD APT1 band by SDS-PAGE followed by Coomassie staining (Figure 3.4D). These results indicate APT1 does dimerize and phosphorylation of APT1 does not completely block dimerization but reduces the propensity for the dimer to form.

Serine 210 is mutated in cancer and increases APT1 activity

The APT1 gene is mutated in multiple tumor types, with the highest frequency of serine 210 mutated specifically to a leucine (Figure 3.5A) (Gao et al., 2013 & Cerami et al., 2012). To investigate if this mutation also increases APT1 activity, we mutated serine 210 to leucine of APT1 ($APT1^{S210L}$) and measured its depalmitoylating activity by incubating purified protein with the DPP-3 probe. After measuring fluorescence over time, we observed an increase in depalmitoylating activity of $APT1^{S210L}$ compared to $APT1^{WT}$. When we compare the depalmitoylating activity of $APT1^{S210L}$ to $APT1^{S209D}$, we find that S210L exhibits an almost identical increase in activity to the phospho-mimetic $APT1^{S209D}$ (Figure 3.5B). We also observe similar inhibition of APT1 depalmitoylation by

ML348 using the DPP-3 probe as a substrate for APT1^{S209D} and APT1^{S210L} (Figure 3.5 – figure supplement 1A). These results demonstrate that the high activity of the APT1 phospho-mutants are still inhibited with ML348. To visualize how a S210L mutation would affect dimerization, we modeled the substitution on the three-dimensional crystal structure and determined a leucine at position 210 is located 5.5 Å from the methionine of the adjacent APT1 monomer (Figure 3.5C). With a neutral charge leucine positioned a small distance from the dimer interface, we propose steric hindrance disrupts the dimerization of APT1.

We next asked if this mutation would also enhance the ability of APT1 to promote cell invasion, similar to what we observe in APT1^{S209D}. To test the APT1^{S210L} mutant's effect on cell behavior, we generated spheroids from WM239A melanoma cell expressing CFP-FLAG-tagged APT1^{WT} and APT1^{S210L}, embedded them in collagen, and measured cell invasion each day over the course of 9 days. Expression of APT1^{S210L} increased melanoma invasion when compared to APT1^{WT} and negative control CFP (Figure 3.5D, Figure 3.5 – figure supplement 1B). Similar to the phospho-mimetic APT1^{S209D}, treating spheroids expressing APT1^{S210L} with ML348 significantly reduces cell invasion (Figure 3.5 – figure supplement 1C). These results demonstrate that APT1^{S210L} increases metastatic behavior compared to wild type and this is dependent on the catalytic activity of APT1.

In patients, increased Wnt5a expression is known to correlate with increased tumor grade and metastasis. To investigate if phospho-APT1 levels were also elevated in human melanoma samples and to establish human disease relevance, we stained human melanoma tumor arrays with our phospho-antibody (anti-pS209-APT1) and for total APT1 (anti-APT1 antibody). We discovered a correlation between high pAPT1

staining and increased tumor grade (Figure 3.5E). When looking at melanoma metastatic samples we observed the same correlation (Figure 3.5F, Figure 3.5 – figure supplement 1D), implicating increased APT1 phosphorylation with increased tumor progression and metastasis.

FIGURES

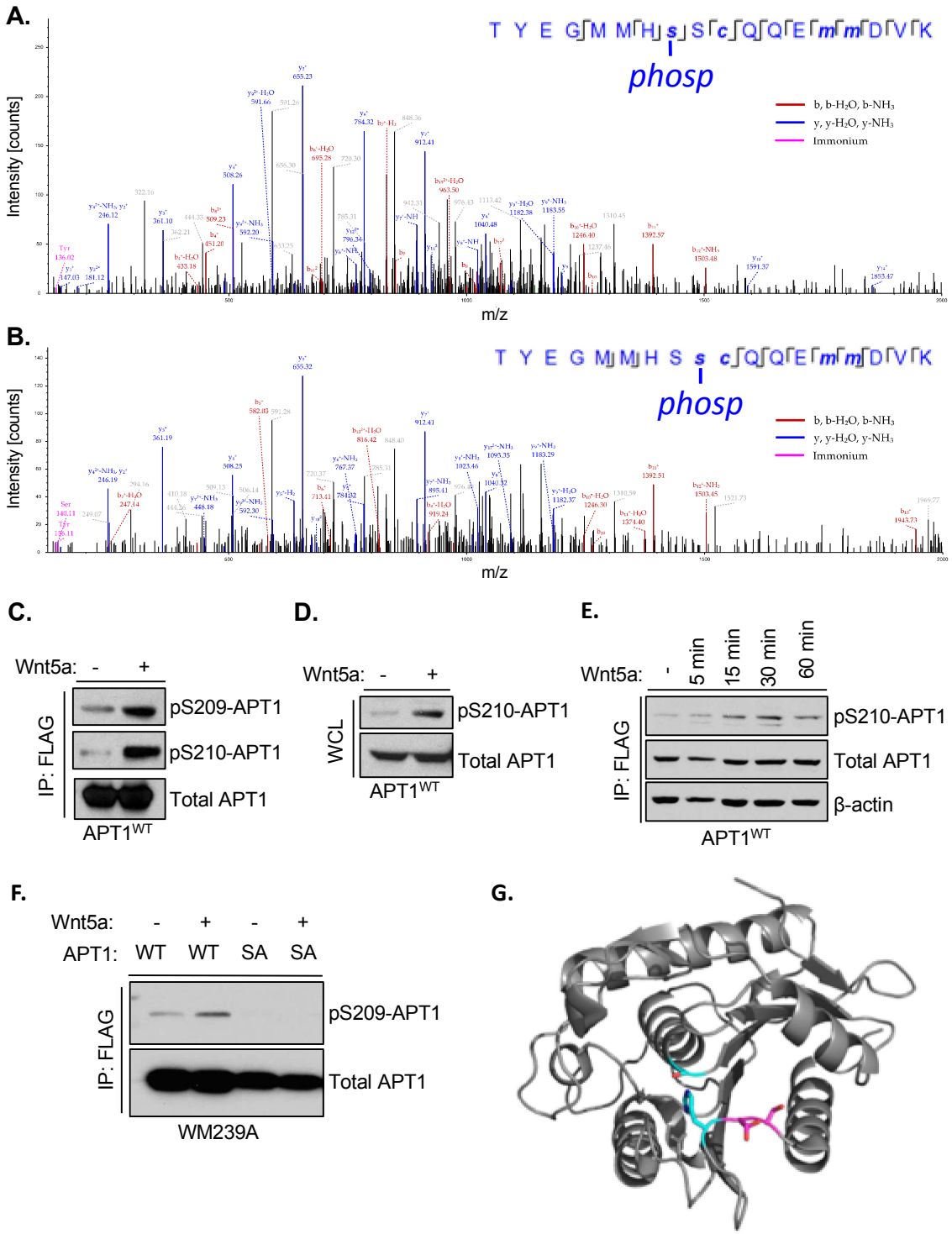

Figure 3.1. *Wnt5a signaling induces APT1 phosphorylation on serines 209 and 210.* (**A**) Annotated MS/MS spectrum of identified S209 phosphopeptide of protein APT1. The image represents the observed fragment ions collected using MS/MS (HCD). Colored

lines represent matches between observed and expected fragment ions of the given peptides. Specifically, blue lines represent matches with y-type fragments, red lines with b-type fragments, and purple lines show immonium ions. (**B**) Annotated MS/MS spectrum of identified S210 phosphopeptide of protein APT1, as described in A. (**C**) $APT1^{WT}$-CFP-FLAG was immunoprecipitated from lysates prepared from WM239A melanoma cells expressing $APT1^{WT}$-CFP-FLAG treated with control buffer or 150 ng/ml of purified Wnt5a for 15 minutes and analyzed by SDS-PAGE followed by immunoblotting to detect phosphorylated APT1 using antibodies to pS209-APT1 and pS210-APT1. (**D**) Western blot of whole cell lysate (WCL) from WM239A cells expressing $APT1^{WT}$-CFP-FLAG treated with control buffer or 150 ng/ml of Wnt5a for 15 minutes. (E) WM239A cells expressing $APT1^{WT}$-CFP-FLAG were treated with control buffer or 150 ng/ml of Wnt5a for increasing lengths of time and then $APT1^{WT}$-CFP-FLAG was immunoprecipitated and analyzed by SDS-PAGE and immunoblotting to detect phosphorylated APT1 with anti-pS210-APT1 antibody. (**F**) WM239A cells expressing $APT1^{WT}$-CFP-FLAG (WT) or $APT1^{SA}$ -CFP-FLAG (SA) were treated with control buffer or 150 ng/ml of Wnt5a for 15 minutes. APT1 was immunoprecipitated and analyzed by SDS-PAGE and immunoblotting to detect phosphorylated APT1 with anti-pS209-APT1 antibodies. (**G**) Three-dimensional model of APT1, showing the positions of Ser209 and Ser210 (magenta) adjacent to the catalytic residues Ser119, Asp174 and His208 (cyan).

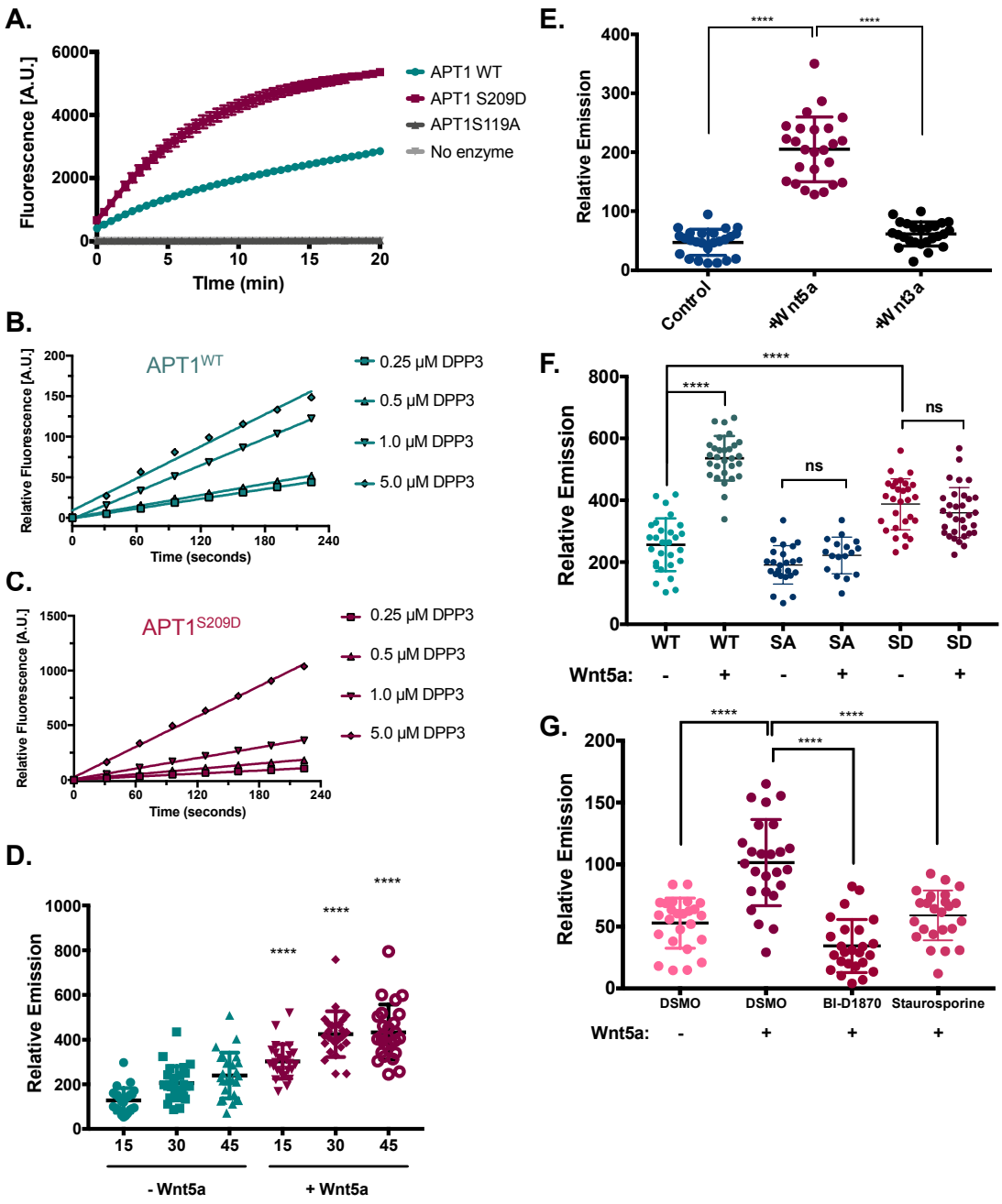

Figure 3.2. *Wnt5a stimulation increases APT1 depalmitoylating activity.* (**A**) *In vitro* fluorescence assay using 5 µM of depalmitoylation probe DPP-3 in HEPES (20 mM, pH 7.4, 150mM NaCl, 0.1% Triton X-100) with either 50 nM purified APT1^{WT}, APT1^{S209D} or catalytically inactive APT1^{S119A} and fluorescence emission was measured over time (λ_{ex}490/9 nm; λ_{em} 545/20 nm). Error bars indicate s.e.m., n=3 replicates per condition. Results shown are from a representative trial from three independent experiments. (**B**) Linear regression of APT1^{WT} (WT) enzymatic activity measured by fluorescence

emission of increasing DPP-3 substrate concentrations over time. Results are averaged from six independent experiments. (**C**) Linear regression of $APT1^{S209D}$ (SD) enzymatic activity measured by fluorescence emission of increasing DPP-3 substrate concentrations over time. Results are averaged from 6 independent runs. (**D**) Quantification of relative fluorescence of WM239A cells treated with control buffer or 150 ng/ml of Wnt5a, loaded with 10 μM DPP-3, and then analyzed by live-cell fluorescence microscopy over time. Error bars indicate s.d., n=25 cells per condition, ****p<0.0001 by unpaired t-test analysis. Results shown are from three experiments. (E) Quantification of relative fluorescence of WM239A cells expressing $APT1^{WT}$ treated with control buffer, 150 ng/ml of Wnt5a, or 150 ng/ml of Wnt3a, loaded with 5 μM DPP-3, and then analyzed by live-cell fluorescence microscopy after 30 minutes. Error bars indicate s.d., n=25 cells per condition, ****p<0.0001 by unpaired t-test analysis. Results shown are from three experiments. (**F**) Quantification of relative fluorescence generated by WM239A cells expressing either $APT1^{WT}$ (WT), $APT1^{SA}$ (SA), or $APT1^{S209D}$ (SD) treated with control buffer or 150 ng/ml Wnt5a, loaded with 10 μM DPP-3, and then analyzed by live-cell fluorescence microscopy after 30 minutes. Error bars indicate s.d., n=17-32 cells per condition, ****p<0.0001 by unpaired t-test analysis. Results shown are from three experiments. (**G**) Quantification of relative fluorescence of WM239A $APT1^{WT}$ cells treated with kinases inhibitors 10 μM BI-D1870, or 0.2 μM staurosporine or DMSO control for 1 hour, loaded with 10 μM DPP-3, treated with Wnt5a, and analyzed by live-cell fluorescence microscopy after 30 minutes. Error bars indicate s.d., n=25 cells per condition, ****p<0.0001 by unpaired t-test analysis. Results shown are from three experiments. Quantification for all live-cell microscopy was determined by measuring the mean intensity of relative fluorescence for region of interests (background fluorescence was subtracted from mean intensity).

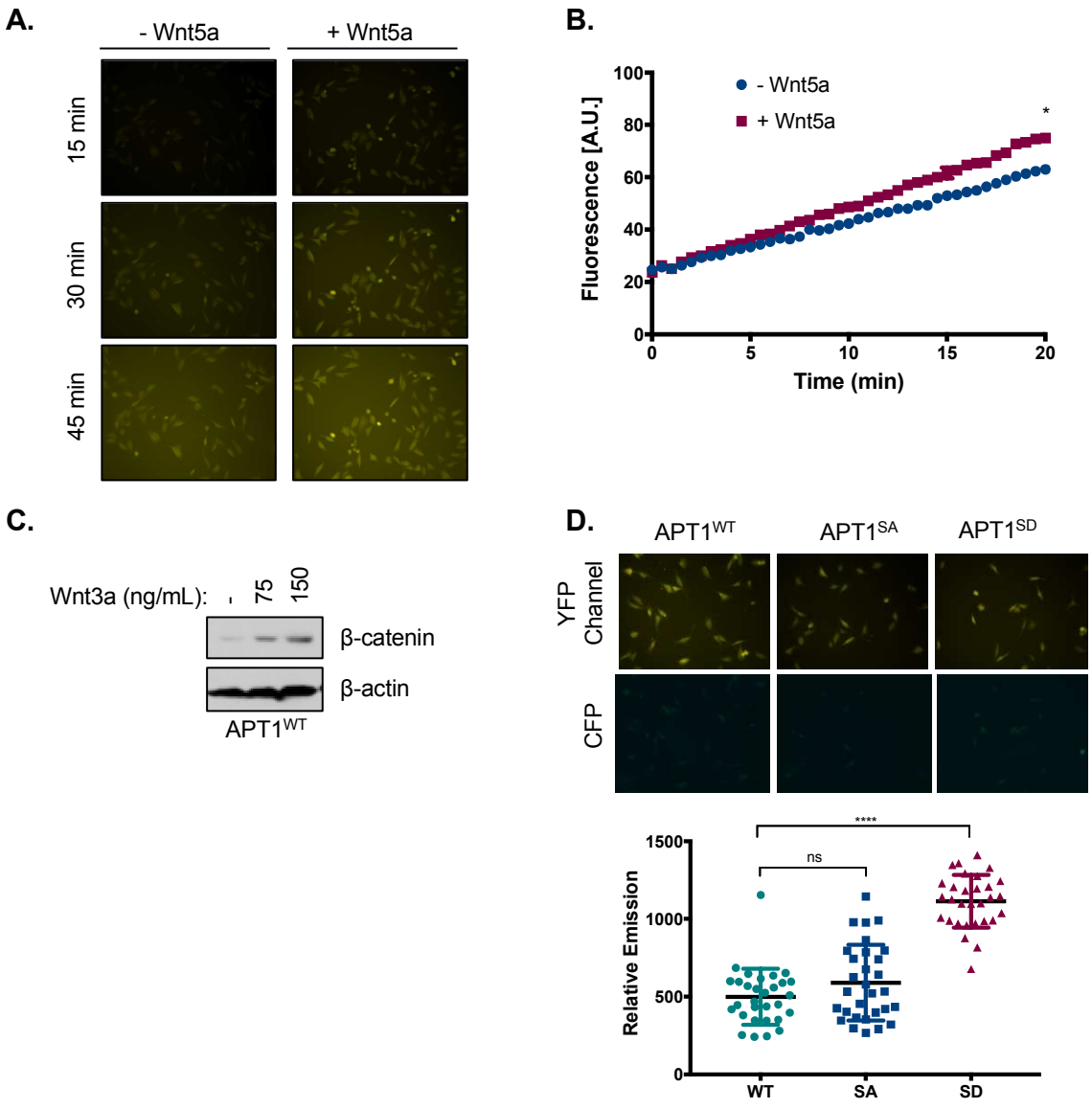

Figure 3.2 – figure supplement 1. *Activity of APT1 in response to Wnt5a stimulation or the phosphomimetic mutation.* (**A**) Representative images of WM239A cells loaded with 10 μM DPP-3, treated with control buffer or 150 ng/ml Wnt5a, and then analyzed by live-cell fluorescence microscopy at 15 minutes, 30 minutes, and 45 minutes, quantified in Figure 2D. (**B**) APT1^{WT} was immunoprecipitated from WM239A whole cell lysate pre-treated with control buffer or 150 ng/ml Wnt5a and analyzed by *in vitro* fluorescence assay. *p <0.05 by unpaired t-test analysis of – Wnt5a and + Wnt5a groups. (**C**) WM239A APT1^{WT} cells were treated with control buffer, 75 ng/ml, or 150 ng/ml of recombinant Wnt3a for 1 hour, lysate was harvested and analyzed by SDS-PAGE to determine β-catenin stabilization. (**D**) Top panel: Representative images of APT1^{WT}, APT1^{SA} and APT1^{S209D} WM239A cells treated with 10 μM of DPP-3 for 15 minutes, and then analyzed by live-cell microscopy. Bottom panel: Quantification of relative

fluorescence of WM239A APT1^{WT} (WT), APT1^{SA} (SA), and APT1^{S209D} (SD) cells treated with control buffer or 150 ng/ml Wnt5a, loaded with 10 μM DPP-3, and then analyzed by live-cell fluorescence microscopy after 30 minutes. Error bars indicate s.d., n=17-32 cells per condition, ****p<0.0001 by unpaired t-test analysis.

	Fluoresence/Time (V_0)	
Substrate	APT1^{WT}	APT1^{SD}
0.25µM	0.2012 ± 0.008627	0.4704 ± 0.01765
0.5µM	0.2316 ± 0.02656	0.8083 ± 0.03173
1.0µM	0.5496 ± 0.01478	1.612 ± 0.04416
5.0µM	0.6573 ± 0.03547	4.627 ± 0.2237

Table 1. *Enzyme kinetics of APT1^{WT} and APT1^{S209D}*. Table of initial velocities (V_0) of APT1^{WT} and APT1^{S209D}. Values were determined by incubating purified APT1^{WT} and APT1^{S209D} with increasing concentrations of DPP-3 substrates and measuring fluorescence for 240 seconds. The initial velocity of the reactions for APT1^{WT} and APT1^{S209D} activity was calculated by fitting the linear regression of the fluorescence vs. time. Results are averaged from six independent experiments.

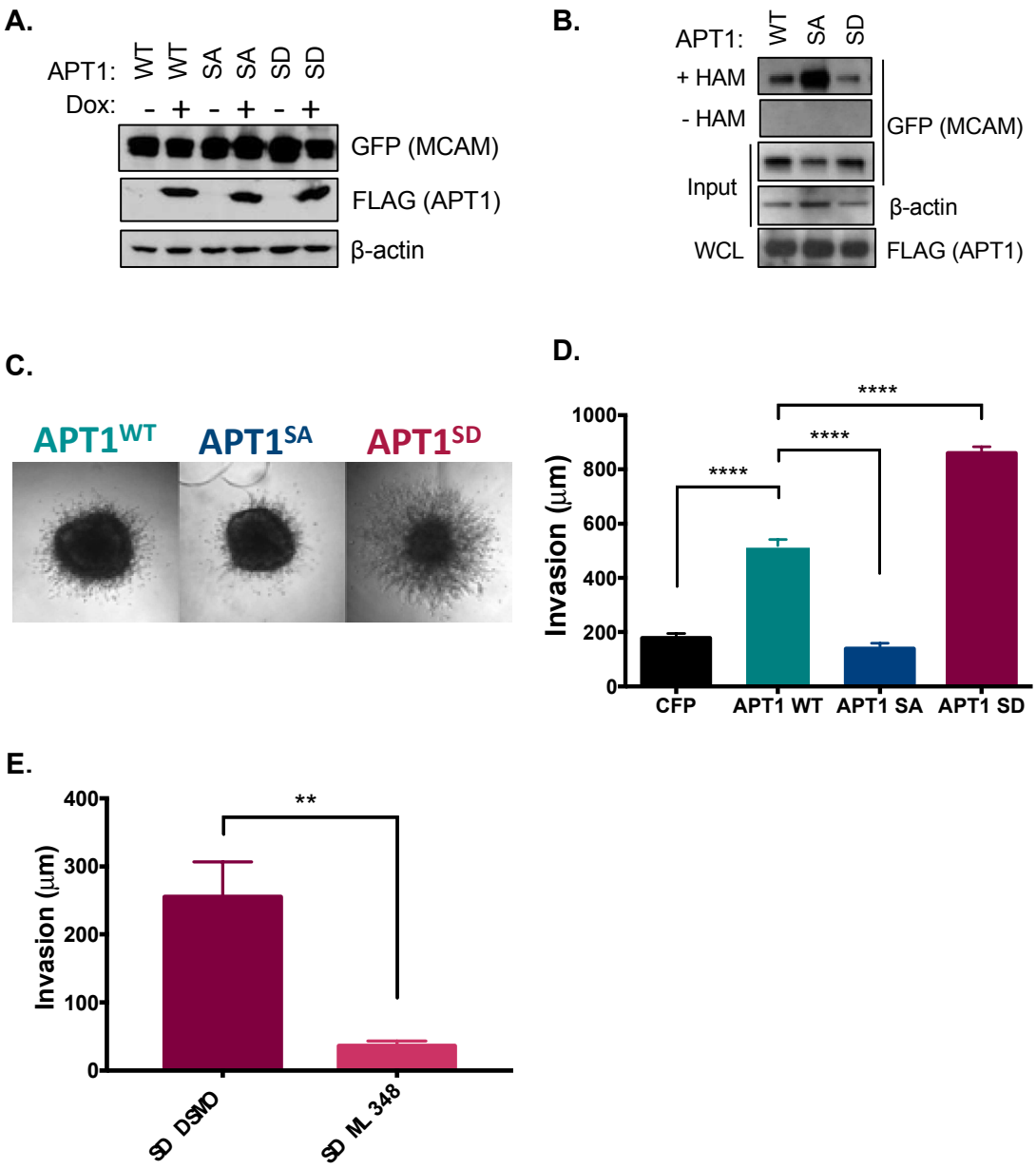

Figure 3.3. *APT1 phosphorylation increases APT1 depalmitoylating activity in cells and increases melanoma invasion.* (**A**) HEK 293T cells transfected with constitutively transcribed MCAM-GFP and doxycycline inducible APT1^{WT}-FLAG (WT), APT1^{SA}-FLAG (SA), or APT1^{S209D}-FLAG (SD). After 15 hours of induction with 1 μg/ml doxycycline, APT1 protein expression was determined by immunoblotting with anti-GFP (MCAM-GFP) and anti-FLAG (APT1-FLAG) antibodies. (**B**) An acyl-biotin exchange (ABE) assay was used to measure MCAM palmitoylation in cell lysates from cell lines described in (A). In the ABE assay addition of hydroxylamine (+HAM) removes palmitate from cysteine residues that are then conjugated to biotin-HPDP. Biotinylated proteins are then isolated on streptavidin beads and palmitoylated proteins are analyzed by SDS-PAGE

followed by immunoblotting. Hydroxylamine is withheld as a negative control (-HAM) MCAM-GFP is detected with anti-GFP antibodies and APT1-FLAG is detected with anti-FLAG antibodies. Results shown are a representative trial from three independent experiments. (**C**) WM239A melanoma cells expressing $APT1^{WT}$ (WT), $APT1^{SA}$ (SA), or $APT1^{S209D}$ (SD) were grown on agarose to form spheroids that were embedded in collagen and images were taken on day 7 and the distance invaded was measured. Representative images from day 7 are shown. (**D**) Quantification of WM239A spheroid invasion assay in (C). Error bars indicate s.e.m., n=14-34 spheroids counted per condition, ****p<0.0001 by unpaired t-test analysis. Results shown are from four experiments. (**E**) Quantification of WM239A spheroid invasion assay of $APT1^{S209D}$ (SD) treated with DSMO control or 10 μM ML348, every other day for 7 days and distance invaded measured at day 7. Error bars indicate s.e.m., n=6 spheroids counted per condition, **p=0.0017 by unpaired t-test analysis. Results shown are a representative trial from three independent experiments.

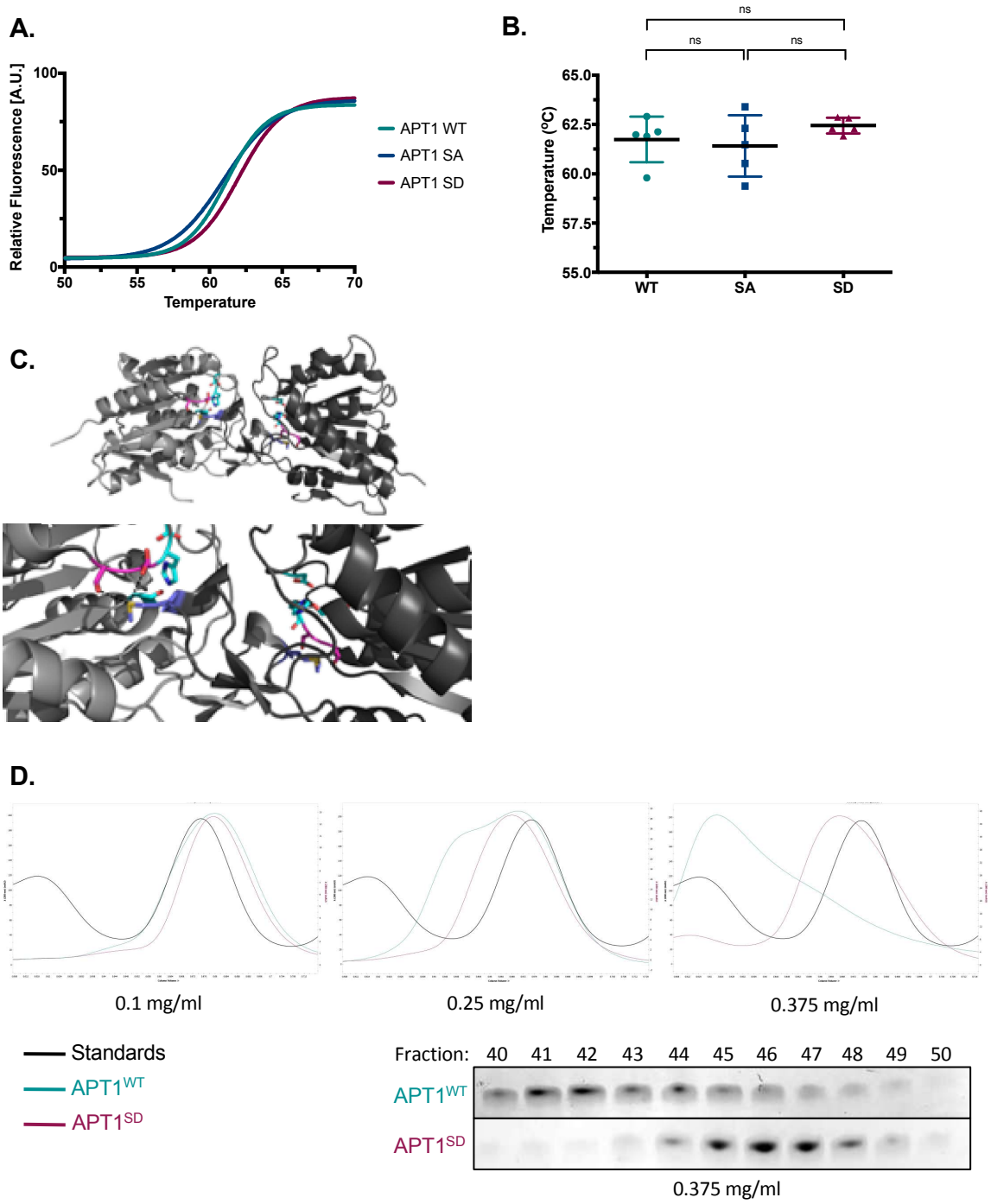

Figure 3.4. *APT1 phosphorylation impedes dimer formation.* (**A**) Differential scanning fluorimetry (DSF) of purified APT1^{WT}, APT1^{SA} and APT1^{S209D}. (**B**) Melting curves of purified APT1^{WT}, APT1^{SA} and APT1^{S209D} as determined by DSF. Results shown from DSF analysis are a representative trial from three independent experiments. (**C**) Top panel: Three-dimensional model of crystal structure of APT1 dimer interface. Ser209 and

Ser210 (pink) are located 4.3 Å away from Met65 (blue) of the adjacent APT1 monomer. Catalytic triad Ser119, Asp174 and His208 are highlighted (cyan). Bottom panel: Zoom in of APT1 dimer interface. (**D**) Top panels: Chromatogram of purified $APT1^{WT}$ (cyan) and $APT1^{S209D}$ (magenta) from size-exclusion chromatography at three protein concentrations. Bottom panel: SDS-PAGE followed by Coomassie staining of eluted fractions after separation by size-exclusion chromatography of $APT1^{WT}$ and $APT1^{S209D}$.

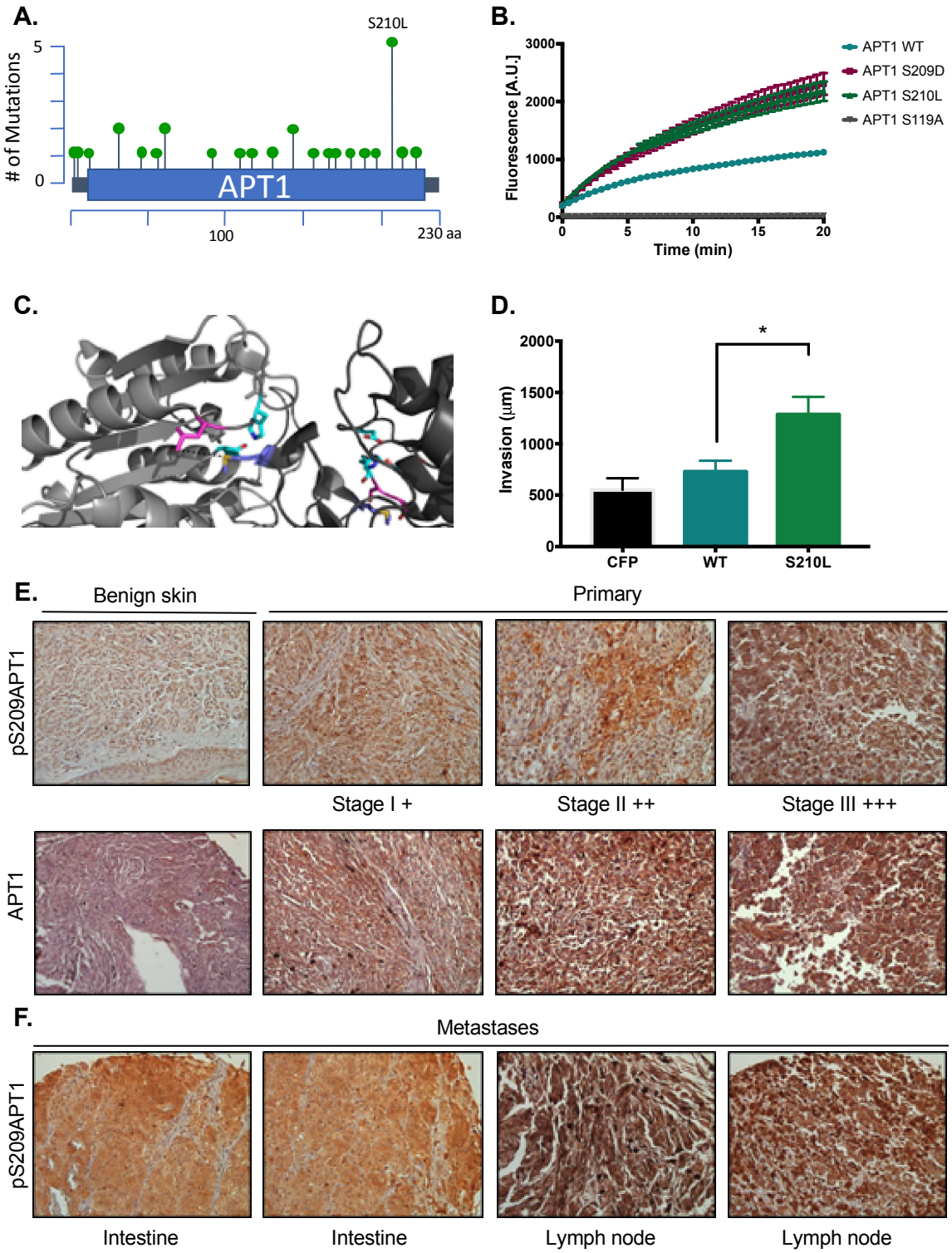

Figure 3.5. *Increased phospho-APT1 staining correlates with increased tumor grade and metastasis.* (**A**) Schematic of APT1 mutations from human tumor samples. Adapted from results generated using cBioPortal (Gao et al., 2013; Cerami et al., 2012). (**B**) *In*

vitro fluorescence assays of 5 μM of DPP-3 with either 50 nM purified $APT1^{WT}$, $APT1^{S210L}$ $APT1^{S209D}$, or catalytically inactive $APT1^{S119A}$ and fluorescence emission was measured (λ_{ex}490/9 nm; λ_{em} 545/20 nm). Error bars indicate s.e.m., n=3 replicates per condition. Results shown are a representative trial from three independent experiments. (**C**) Three-dimensional model of crystal structure of APT1 dimer interface with Ser210 to Leu mutation. Ser210Leu (pink) is located 5.5 Å away from Met65 (blue) of the adjacent APT1 monomer. Catalytic triad Ser119, Asp174 and His208 are shown in cyan. (**D**) Quantification of WM239A CFP-FLAG (CFP), $APT1^{WT}$-CFP-FLAG (WT), and $APT1^{S210L}$-CFP-FLAG (S210L) spheroids embedded in collagen and distance invaded measured at day 8. Error bars indicate s.e.m., n=8 spheroids per condition, *p=0.0150 by unpaired t-test analysis. Results shown are from three independent experiments. (**E**) Immunohistochemistry staining of melanoma tumors in a human melanoma tumor array using pS209-APT1 and APT1 antibodies. (**F**) Immunohistochemistry staining of metastatic tumor samples in a human melanoma tumor array using anti-pS209-APT1.

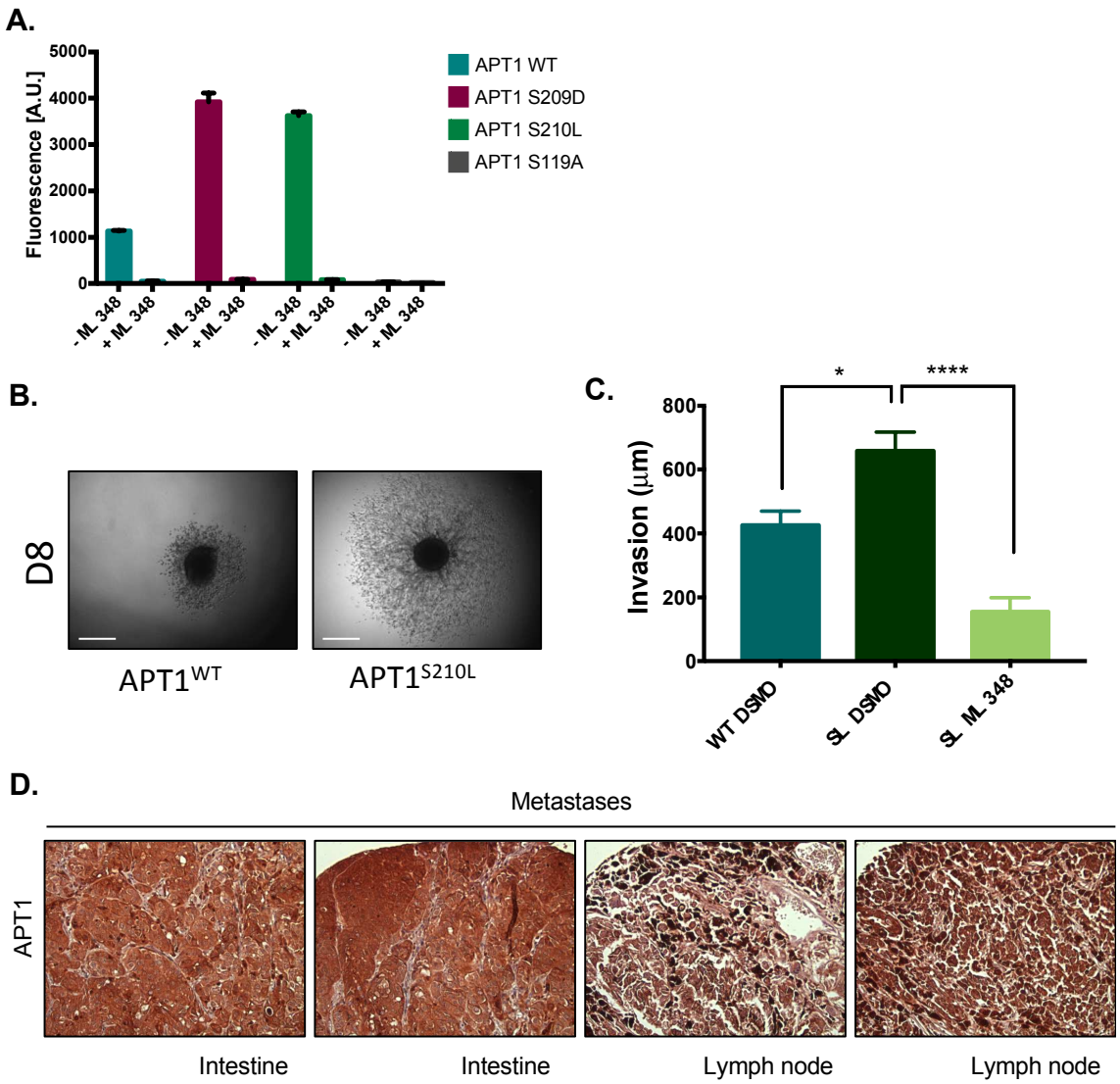

Figure 3.5 – figure supplement 1. *Response of APT1^{S210L} mutant to APT1 inhibitor ML348.* (**A**) Quantification of fluorescence response of 5 μM DPP-3 treated with either 50 nM purified APT1 (APT1^{WT}, APT1^{S209D}, APT1^{S210L}, or catalytically inactive APT1^{S119A}) for 30 min each in the presence or absence of 50 μM ML348 (λ_{ex}490/9 nm; λ_{em} 545/20 nm). Error bars indicate s.d., n=3 replicates per condition. Results shown are a representative trial from three experiments. (**B**) Representative images of APT1^{WT} and APT1^{S210L} collagen invasion assay in Figure 5D. Images are of spheroids on day 8 (D8). Scale bar = 500 μm. (**C**) Quantification of WM239A spheroid invasion assay of APT1^{S210L} (SL) treated with DSMO control or 10 μM ML348 every other day for 7 days and distance invaded measured on day 7. Error bars indicate s.e.m., n=5-6 spheroids per condition, ****p<0.0001 by unpaired t-test analysis. Results are from three independent experiments. (**D**) Immunohistochemistry staining of metastatic tumors in a human melanoma tumor array using anti-APT1 antibodies.

DISCUSSION

Protein palmitoylation is often considered a constitutive modification required for correct protein localization and function. Here, we uncover a molecular switch that promotes protein depalmitoylation in response to non-canonical Wnt signaling. We demonstrate Wnt5a signaling induces APT1 phosphorylation and this activates APT1, increasing its depalmitoylating activity and thus depalmitoylation of its substrates. While phosphorylation of these serine residues has been observed in mass spectrometry studies, this is the first example of differential phosphorylation of APT1 in response to an extracellular signal. Ultimately, activation of APT1 signaling results in increased depalmitoylating activity, leading to increased melanoma invasion, and correlating with increased tumor grade and metastasis.

Understanding APT1 protein function has been hindered by a deficiency in assays for measuring thioesterase activity either *in vitro* or in cells. Here, we take advantage of a recently developed small molecule fluorophore, DPP-3, which allowed us to measure the activity of APT1 both *in vitro* and in cultured cells. This assay revealed the phospho-mimetic mutant APT1 has greater thioesterase activity compared to wild-type APT1. The increase in activity was also observed by live cell imaging and the phospho-dead mutant had similar activity to wild-type APT1. Using live imaging, we were able to demonstrate that the ability to increase endogenous APT1 activity is specific to Wnt5a and the noncanonical Wnt pathway, as we found Wnt3a lacks this ability.

The first crystal structure of APT1 revealed a dimer with the active site buried in the dimer interface (Devedjiev et al., 2000), suggesting the dimer must dissociate prior to interaction with its substrate. The phosphorylation sites are located on the edge of the hydrophobic channel distant from the site of catalysis but at the dimer interface. Our

proposed model is phosphorylation impedes the formation of an inactive dimer. Few studies have examined if APT1 forms a dimer in solution. Using both size-exclusion chromatography and chemical crosslinking, we find evidence of dimeric APT1 in solution. When measured by crosslinking, the phospho-mimetic mutation decreases but does not eliminate the dimeric pool of APT1. However, size-exclusion chromatography detected a complete shift of the $APT1^{WT}$ monomer population to the dimer. The shift was dependent on the concentration of APT1 since at the $APT1^{WT}$ dimer concentration $APT1^{S209D}$ remains a monomer. Furthermore, using three-dimensional modeling, we were able to determine the distance between the serine's that are phosphorylated and the neighboring APT1 in the dimer interface to be 4.3 Å. With such a short distance between the serine and the adjacent APT1, it is consistent with the idea that phosphorylation of this serine would impede the dimerization of APT1. However, it is still unclear if this reduction in dimer formation is sufficient to account for the increase in APT1 activity. We still don't know if the higher activity of $APT1^{S209D}$ compared to $APT1^{WT}$ is caused by reduced dimer formation or a conformational change in the protein that increases activity. Alternatively, phosphorylation could alter the conformation of APT1 allowing it to accommodate the lipid substrate or increase the rate of catalysis independent of dimer formation.

When analyzing the results of the *in vitro* fluorogenic palmitoylation assay using the DPP-3 probe and the acyl-biotin exchange assay measuring palmitoylation of MCAM as a protein substrate, there is a small discrepancy between the two assays for phospho-deficient mutant $APT1^{SA}$. In the acyl-biotin exchange assay, we observe $APT1^{SA}$ displaying decreased activity compared to $APT1^{WT}$ cells. Whereas in our *in vitro* depalmitoylation assay with the DPP-3 probe, we do not observe a significant difference

between the APT1^{SA} mutant and APT1^{WT}. It is important to note that in whole cells there are other factors that play a role in this signaling pathway and this might contribute to the difference in the acyl-biotin exchange assay, where we are measuring depalmitoylation of a protein APT1 substrate in this signaling pathway. It is possible that modifications of the substrate MCAM affect how its accessed or preference for depalmitoylation. Adaptor proteins may hinder or ease the depalmitoylation of the protein. Due to decreased melanoma invasion in collagen observed in APT1^{SA} expressing cells, we hypothesize that the decreased depalmitoylation of MCAM may play a role in the APT1 mediated invasion. Thus, this is a more physiologically relevant measure of the depalmitoylation activity than solely using the artificial probe *in vitro*. Concerning the DPP-3 probe, it is still a reliable tool to assess APT1 depalmitoylation, when taken together with other data, which we have been able to do in this study.

The APT1 gene, LYPLA1, is amplified across a wide variety of tumor types, including 31.8%, 23.2%, and 13.8%, in neuroendocrine prostate cancer, uterine carcinosarcoma, and invasive breast carcinoma, respectively. Other cancers with amplified LYPLA1 include metastatic prostate adenocarcinoma, ovarian serous cystadenocarcinoma, and uveal melanoma (Beltran et al., 2016, Getz et al., 2013, and Eirew et al., 2015). Serine 210 is mutated not only in melanoma (Krauthammer et al., 2012) but also in multiple tumor types including colorectal adenocarcinoma and lung squamous cell carcinoma (Giannakis, et al., 2016, Hammerman et al., 2012, Campbell et al., 2016). This bulky residue behaves similarly to the phosphorylated APT1 *in vitro*, suggesting this disease relevant mutation might result in increased depalmitoylation and thus increased invasion in patients. Using three-dimensional modeling, we find the leucine to be positioned 5.5 Å next the dimer interface and based on modeling, this

mutation will not accommodate dimeric conformation. Due to this finding, this signaling pathway becomes increasingly important, not only in Wnt5a driven cancers mentioned above but also for patients who present with APT1 mutations in other tumor types. There is a possibility an APT1 mutation in this phospho-site could be regulating cancer metastasis across other tumor types. Not surprisingly, the S210L mutation in APT1 is observed at a much lower frequency compared to well-established oncogenes frequently mutated in melanoma, such as BRAF or NRAS. We, therefore, think it is unlikely APT1 mutations contribute significantly to oncogenesis and tumor initiation. We did map the positions in the three-dimensional structure of the other mutations in APT1 cataloged in the TCGA database (Figure 5A). The only mutation that is positioned within the dimer interface is S210L, making it unlikely that the other low-frequency mutations would increase APT1 activity through reduced dimerization. Therefore, $APT1^{S210L}$ may provide some selective advantage to tumor growth *in vivo* since it occurs at a higher frequency than the other mutations in APT1.

The data we present offers insights into the Wnt5a signaling pathway and its contribution to tumor progression and metastasis. Patients who present with elevated Wnt5a expression are in dire need of effective therapy and directly targeting the Wnt5a pathway is one possible avenue (Prasad et al., 2015). By identifying increased APT1 activity through either gene amplification or mutation of serine 210 as a driver of this pathway, we could expand the number of patients who can benefit from inhibition of the Wnt5a-APT1 pathway. This suggests APT1 signaling may play a larger role as a possible target for treating metastatic melanoma patients, especially those with APT1 amplification/mutations or disease recurrence after other treatments.

Here we show regulation of protein depalmitoylation by activation of the Wnt5a signaling pathway. This novel discovery allows us to better understand how secreted signals regulate protein function and polarized cell behavior. Wnt5a signaling directly regulates APT1 depalmitoylating activity and protein function, with activation or mutations in this pathway contributing to their metastatic behavior. Novel therapeutics for Wnt5a driven cancers are lacking in the clinic. Understanding the signaling mechanism behind Wnt5a driven tumor progression and metastasis is imperative if we aim to create novel therapies against this pathway and to achieve our goal of increasing cancer patient survival.

METHODS

Purification of recombinant Wnt5a and treatments with Wnt5a and Wnt3a

Wnt5a was purified from mouse L-cells overexpressing human Wnt5a as described previously (Willert et al., 2003). Control cells were treated with control buffer with identical detergent conditions as the Wnt5a purification buffer. For experiments utilizing Wnt3a treatment, cells were treated with recombinant Wnt3a (R&D Systems, Minneapolis, MN) for 1 hour at 37 °C before lysate was harvested as described.

Cell lines and culture conditions

Metastatic melanoma cell line WM239A (BRAF V600D) (Wistar Institute) were cultured in RPMI 1640 medium (Gibco-BRL, Grand Island, NY) supplemented with 10% fetal bovine serum (FBS) (GE Life Sciences). Cell lines were authenticated routinely by short tandem repeat profiling by the Wistar Institute prior to use.

Mass spectrometry analysis of APT1 phosphorylation sites

All chemicals used for preparation of mass spectrometry samples were of at least sequencing grade and purchased from Sigma-Aldrich (St Louis, MO), unless otherwise stated. The 1% TritonX-100 detergent was removed from samples prior MS analysis by precipitation using chloroform (CHCl3)-methanol (MeOH) precipitation [Wessel et al.]. The protein pellet from CHCl3-MeOH precipitation was resuspended in 6 M urea/2 M thiourea in 50 mM ammonium bicarbonate, pH 8.3 supplemented with Phosphatase and Protease Inhibitors Mix (Thermo Fisher Scientific, Waltham, MA). Samples were reduced with 10mM DTT for 1 hour at room temperature and the carbamidomethylated with 20 mM iodoacetamide (IAA) for 30 minutes at room temperature in the dark. After alkylation proteins were digested first with endopeptidase Lys-C (Wako, Cambridge, MA; MS grade) for 3 hours, after which the solution was diluted 10 times with 20 mM ammonium bicarbonate, pH 8.3. Subsequently, samples were digested with trypsin (Promega, Madison, WI) at an enzyme to substrate ratio of approximately 1:50 for 12 hours at room temperature. After digestion, the samples were concentrated to the volume of ~100 µl by lyophilization. Phosphopeptide enrichment using titanium dioxide (TiO2) chromatographic resin was performed as previously described [Thingholm et al., Enghold et al.]. The lyophilized phosphorylated peptide samples were reconstituted in 0.1% trifluoroacetic acid (TFA) and desalted using Poros Oligo R3 RP (PerSeptive Biosystems, Framingham, MA) P200 columns. The peptide samples were subsequently lyophilized and stored at −80 °C for further analysis.

Dried samples were resuspended in buffer-A (0.1% formic acid) and loaded onto an Easy-nLC system (Thermo Fisher Scientific, San Jose, CA), coupled online with an Orbitrap Fusion Tribrid mass spectrometer (Thermo Fisher Scientific, San Jose, CA).

Peptides were loaded into a picofrit 25 cm long fused silica capillary column (75 µm inner diameter) packed in-house with reversed-phase Repro-Sil Pur C18-AQ 3 µm resin. The gradient length was 75 min. The gradient was from 2–26% buffer-B (100% ACN/0.1% formic acid) at a flow rate of 300 nl/min. The MS method was set up in a data-dependent acquisition (DDA) mode. For full MS scan, the mass range of 350–1200 m/z was analyzed in the Orbitrap at 120,000 FWHM (200 m/z) resolution and 5 × 10e5 AGC target value. HCD (higher energy collision dissociation) collision energy was set to 32, AGC target to 10e4 and maximum injection time to 200 msec. Detection of MS/MS fragment ions was performed in the ion trap in the rapid mode using the TopSpeed mode (2 s).

Raw MS-files were analyzed using Proteome Discoverer (v2.1, Thermo Scientific, Bremen, Germany). MS/MS spectra were converted to mgf files and searched against the UniProt-Human LYPLA1 (APT1) database (version June 2017) using SequestHT. Database searching was performed with the following parameters: precursor mass tolerance 10 ppm; MS/MS mass tolerance 0.6 Da; enzyme trypsin (Promega), with two missed cleavages allowed; fixed modification was cysteine carbamidomethylation; variable modifications were methionine oxidation, serine/threonine/tyrosine phosphorylation, asparagine and glutamine deamidation. Peptides were filtered for <1% false discovery rate, Sequest ion score >0.9. All MS-APT1 raw files have been deposited in the CHORUS database under project number 1456 (https://chorusproject.org/).

Structural modeling

Modeling of catalytic triad (serine 119, aspartate 174, and histidine 208) and serine residues 209 and 210 identified to be phosphorylated by MS analysis was performed in

MacPyMOL with the three-dimensional co-crystal structure of human APT1 in complex with an isoform selective inhibitor, ML348 at 1.55 A˚ (PDB 5SYM). Modeling of the distance between the distance between the oxygen side chain of the serine residues 209 and 210 in monomer A and the thiol group of methionine 65 in monomer B was performed in MacPyMOL with the three-dimensional co-crystal structure of human APT1 in complex with an isoform selective inhibitor, ML348 at 1.55 A˚ (PDB 5SYM). Modeling of serine 210 to leucine mutation identified in several cancers and the distance between the leucine backbone in monomer A and the thiol group of methionine 65 in monomer B was performed in MacPyMOL with the three-dimensional co-crystal structure of human APT1 in complex with an isoform selective inhibitor, ML348 at 1.55 A˚ (PDB 5SYM).

Immunoprecipitation

WM239A cells ectopically expressing APT1-CFP-FLAG mutants were treated with control buffer or 150 ng/ml Wnt5a for specified time period and then lysed in lysis buffer containing 1% Triton-X 100, 50 mM Tris pH 7.5, 150 mM NaCl supplemented with protease and phosphatase inhibitors (1μg/ml leupeptin, 1μg/ml aprotinin, 2μg/ml pepstatin A, 1mM PPi, 2nM $NaVO_4$, 150mM NaF). Insoluble cell debris was removed by centrifugation (13,000 RPM for 10 min at 4°C. Lysate was incubated with FLAG M2 magnetic beads (Sigma-Aldrich, St. Louis, MO) for 1.5 hours. Beads were washed with lysis buffer and protein was eluted using FLAG peptide for 1 hour at room temperature. Samples were separated by SDS-PAGE and transferred to either nitrocellulose membrane (Life Technologies, Thermo Fisher Scientific, Waltham, MA) for phospho-APT1 antibody (YenZym Antibodies, San Francisco, CA) or PVDF membrane (Millipore, Burlington, MA) for all other antibodies used.

Western blot analysis and antibodies

Cells were harvested and lysed in 1% Triton X-100, 50mM Tris pH 7.5, 150mM NaCl supplemented with protease and phosphatase inhibitors (1μg/ml leupeptin, 1μg/ml aprotinin, 2μg/ml pepstatin A, 1mM PPi, 2nM $NaVO_4$, 150mM NaF). Insoluble cell debris was removed by centrifugation (13,000 RPM for 10 min at 4°C. The protein concentration was determined by DC Protein method (BioRad, Hercules, CA). Equal amounts of total protein were separated by SDS-PAGE and transferred to either nitrocellulose membrane (Life Technologies, Thermo Fisher Scientific, Waltham, MA) for phosphor-APT1 antibody or PVDF membrane (Millipore, Burlington, MA) for all other antibodies used. The nitrocellulose membranes were blocked with 5% bovine serum albumin (BSA) in TBST (TBS, 0.1% Tween). The PVDF membranes were blocked with 5% dry milk in TBST. All membranes were immunoblotted with different antibodies diluted in 5% BSA in TBST.

The rabbit anti-human APT1 antibody (Abcam, Cambridge, MA) was used at 1:1000. The rabbit anti-human beta-actin (Cell Signaling Technologies, Danvers, MA) was used at 1:5000. The mouse anti-human MCAM antibody (Santa Cruz Biotechnology, Dallas, TX) was used at 1:1000. The secondary antibodies were HRP-conjugated 1:10000 diluted in 5% BSA in TBST. Membranes were washed three times with TBST between the different steps.

Spheroid Assay

96-well plates were coated with 50 μl per well of sterile 1.5% noble agar and solidified at room temperature for 10 min. 200 μl of 2.5×10^4 cells/ml cell suspension was added to each well. Spheroids formed at 37°C and at 4% CO_2 for 48 h. Collagen matrices were

prepared on ice using Pur Col purified bovine collagen (Advanced Biomatrix, Carlsbad, CA), Hyclone RPMI 1640 (5X) with sodium biocarbonate diluted to 1X in total volume and 10% FBS. Sterile NaOH was added to correct the collagen pH. 75 μl of collagen matrix was added to new wells and allowed to solidify at 37°C for 1 h. Spheroids were resuspended in 125 μl of collagen matrix and transferred to wells containing 75 μl of collagen. After collagen solidified at 37°C, 100 μl of fresh medium was added on top of the collagen. Medium was changed every other day. Images were taken every 24 h for 1 – 10 days. For the invasion assays including ML348 and LGK-974: 10μM of ML348 (Sigma-Aldrich, St. Louis, MO) was added to fresh media on the spheroids and changed every other day.

Acyl-biotin exchange assay

The ABE assay was performed as described (Wan et al., 2007).

Purification of APT1

Wild type and APT1 mutants (FLAG tagged) were cloned into the pET-28 plasmid backbone. Bacteria were grown overnight at 37°C in the presence of 100 μg/ml ampicillin and 50 μg/ml chloramphenicol. Next, fresh LB or TB was inoculated with the overnight bacteria and grown for 4 hours at 37°C until OD_{600}= 0.6-1.0. Expression of APT1 was induced with final concentration of 1 mM IPTG for 2 hours at 37°C or overnight at 18°C. Cells were pelleted at 8000 RPM for 15 minutes at 4°C. Pellet was resuspended in 50 mM HEPES pH 8.0, 300 mM NaCl, 1% Triton X-100, 20 mM Imidazole (Sigma), 1 mM Phenylmethylsulfonyl fluoride (PMSF), 1 mM dithiothreitol or 25 mM HEPES pH 7.5, 500mM NaCl, 10% glycerol, 1mM PMSF, 10mM 2-

Mercaptoethanol, complete EDTA free protease inhibitor cocktail (Pierce). Lysate was sonicated at 50% duty cycle for 30 second pulses two times on ice or 50% duty cycle for 30 pulses on and 30 pulses off for 30 minutes at 4°C. Lysate was centrifuged at 12,000 RPM for 15 minutes at 4°C. Supernatant was incubated with Ni Sepharose 6 Fast Flow beads (GE Healthcare) at 4°C rocking for 3 hours or overnight. Beads were washed three times with wash buffer (50mM HEPES pH 8.0, 300mM NaCl, 40mM Imidazole) or 500mL of wash buffer (25 mM HEPES pH 7.5, 500 mM NaCl, 10% glycerol, 40 mM Imidazole, 10mM 2-Mercaptoethanol). Protein was eluted using 50 mM HEPES pH 8.0, 300 mM NaCl, 250 mM Imidazole by rocking for 45 minutes at 4°C or 50mL of 25 mM HEPES pH 7.5, 500mM NaCl, 300mM Imidazole, 10mM 2-Mercaptoethanol at 4°C. For SEC experiments, 50 mL of eluted APT1 was dialyzed against 25 mM HEPES pH7.5, 150mM NaCl, 10mM 2-Mercaptoethanol overnight at 4°C. Dialyzed APT1 was concentrated using an Amicon Ultra-15 centrifugal filter unit to 500 μL and injected onto NGC Liquid Chromatography System (Bio-Rad) equipped with a Superdex 200 Increase 10/300GL (GE) size-exclusion chromatography (SEC) equilibrated in 25 mM HEPES pH7.5, 150mM NaCl, 10mM 2-Mercaptoethanol. Fractions containing homogeneous APT1 were utilized for analytical SEC at various protein concentrations.

Fluorogenic palmitoyl thioesterase assays

APT1 was assayed for depalmitoylating activity as described previously (Kathayat et al. 2017).

Fluorogenic palmitoyl thioesterase assay from immunopurified APT1-CFP-FLAG

WM239A cells ectopically expressing APT1-CFP-FLAG mutants were treated with control buffer or 150 ng/ml of purified Wnt5a and lysed in lysis buffer containing 1%

Triton-X 100, 50 mM Tris pH 7.5, 150 mM NaCl supplemented with protease and phosphatase inhibitors (1μg/ml leupeptin, 1μg/ml aprotinin, 2μg/ml pepstatin A, 1mM PPi, 2nM $NaVO_4$, 150mM NaF). Insoluble cell debris was removed by centrifugation (13,000 RPM for 10 min at 4°C. Lysate was incubated with FLAG M2 magnetic beads (Sigma-Aldrich, St. Louis, MO) for 1.5 hours. Beads were washed with lysis buffer and fluorogenic palmitoyl thioesterase assay was performed as described previously (Kathayat et al. 2017).

Crosslinking Experiments

APT1 mutants were purified using technique mentioned above. After quantification, 4.5 μM of APT1 was incubated with the following buffer for a final concentration of 35 mM HEPES pH 8, 210 mM NaCl. All crosslinking experiments were crosslinked with a final concentration of 1mg/ml disuccinimidyl glutarate, over time. Crosslinking was quenched by incubating samples with 5X SDS loading buffer and boiled.

Differential scanning fluorimetry

Differential scanning fluorimetry data were collected on a QuantStudio3TM Real-Time PCR Detection System (Applied Biosystems) at a APT1 protein concentration of 1.42 μM in either 50 mM HEPES pH 8.0 using SYPRO orange as described previously {Niesen:2007eh}. The melting temperature was calculated by fitting the normalized data curve to the Boltzmann sigmoid equation in Prism 6 (GraphPad) as described previously{Niesen:2007eh}.

Size-exclusion chromatography

Homogenous $APT1^{WT}$ or $APT1^{S209D}$ at 0.1 mg/mL, 0.25 mg/mL, or 0.375 mg/mL were injected onto NGC Liquid Chromatography System (Bio-Rad) equipped with a Superdex 200 Increase 10/300GL (GE) size-exclusion chromatography (SEC) equilibrated in 25 mM HEPES pH 7.5, 150 mM NaCl, 10 mM 2-Mercaptoethanol. Fractions corresponding to molecular weight standards between 44kD (Ovalbumin) and 29kD (Carbonic anhydrase) were evaluated by Coomassie Brilliant Blue (CBB).

Enzyme kinetics

Purified APT1 protein (purification mentioned above) was incubated with increasing concentrations of DPP-3 substrate and fluorescence was measured over time to measure depalmitoylation (Kathayat et al. 2017). Initial velocities were calculated by fitting the linear regression of the fluorescence vs. time for $APT1^{WT}$ or $APT1^{S209D}$ at each DPP-3 substrate concentration.

Immunohistochemistry

Melanoma tumor arrays (US Biomax, Inc, ME1004b and ME1004e) were immuno-stained with primary antibody 1:50 anti-pS209APT1 and 1:200 anti-APT1. Staining procedure was performed as described in Walter et al., 2017. Images were obtained using 20X objective using a Leica DMI6000 B inverted microscope.

Statistics

* denotes a P-value between 0.0150-0.0205, ** denotes a P-value of 0.0017 and **** denotes a P-value of less than 0.0001 in an unpaired, two-tailed Students t-test, assuming normal distribution and equal variance. Each experiment was performed at least three times.

CHAPTER 4: IDENTIFYING APT1'S KINASE

OVERVIEW

After discovering Wnt5a signaling results in the phosphorylation of APT1, increasing its depalmitoylating activity to promote melanoma invasion, the obvious question remained unanswered: What is the identity of the candidate kinase responsible for phosphorylating APT1 in response to activation of Wnt5a signaling? My advisor, Eric S. Witze, obtained data from a previous screen used in a publication (Witze et al., 2013) where he performed proteomics profiling to determine changes in localization of proteins in response to Wnt5a treatment. In that screen, he identified lymphocyte-oriented kinase, hereon referred to as LOK and also known as STK10, became associated with the cytoskeleton in response to Wnt5a treatment. This led us to investigate LOK's candidacy in being the Wnt5a responsive kinase for APT1's serine's 209/210.

INTRODUCTION

LOK belongs to the Ste20 family of serine/threonine kinases. LOK, also referred to as lymphocyte-oriented kinase or STK10 (serine/threonine kinase 10), had been previously reported as highly expressed in lymphocytes in mice and similar expression patterns are observed in human tissues. Additionally, LOK is expressed highest in rapidly proliferating tissues but is also detected in other tissues profiled (Walter et al., 2003). Interestingly, LOK was detected in many different tumor cells lines and has the ability to auto-phosphorylate itself (Walter et al., 2003). LOK has been determined to be a major ERM kinase that phosphorylates ERM proteins to regulate cortical reorganization through the following observations: identification of LOK colocalizing with

cpERM (C terminus phosphorylated ERM), confirming LOK phosphorylates ERM proteins and determining LOK knockout mice have decreased ERM phosphorylation (Belkina et al., 2009). ERM (ezrin-radixin-moesin) proteins regulate linkage of the actin cytoskeleton to the plasma membrane and rapid dephosphorylation of these proteins facilitates lymphocyte polarization (Belkina et al., 2009, Brown et al., 2003). Additionally, ERM N-terminus binds to the plasma membrane by both direct interactions with phospholipids and by binding cytoplasmic tails of transmembrane proteins such as CD44.

After parsing out the data of kinases in WM239A cells that become associated with the cytoskeleton in response to Wnt5a treatment, STK10 kinase (or LOK) was determined to have a shifted peak in the Wnt5a treatment sample, showing an increase in abundance in the organelle fraction containing the cytoskeleton (data from screen used in Witze et al., 2013). LOK was the only kinase that was detected in this screen to have any sort of shift in organelle association in response to Wnt5a. This preliminary data suggests LOK becomes associated with the cytoskeleton in response to Wnt5a signaling. Since LOK fits the profile of being a serine/threonine kinase, in combination with the Wnt5a-mediated cytoskeletal association, we hypothesized this kinase might be APT1's Wnt5a regulated kinase responsible for phosphorylating APT1 on serine's 209/210 in response to Wnt5a signaling, regulating downstream events such as depalmitoylation of cell adhesion molecules and ultimately promoting melanoma invasion.

RESULTS

Inhibition or knockdown of LOK reduces pAPT1 levels and Wnt5a treatment increases LOK-MCAM interactions

After reviewing Witze et al., 2013 database of kinases that shifted their abundance in various organelle fractions, STK10, hereon referred to as LOK, was found to have increased abundance in the cytoskeletal fractions in response to Wnt5a stimulation (Figure 4.1A, adapted from data obtained in Witze et al, 2013). These results suggest Wnt5a signaling promotes LOK association to the cytoskeleton. Since Wnt5a treatment is inducing an increased association with the cytoskeleton, there was the possibility that LOK could be changing its intracellular localization in response to Wnt5a signaling. We questioned if we could observe the changes in LOK's localization in response to Wnt5a signaling. By the same token, we were interested if we could detect any similarities to MCAM's asymmetrical localization response to Wnt5a signaling by determining if LOK also becomes asymmetrically localized in Wnt5a treated cells. To answer this question, we performed immunostaining of fixed WM239A cells to compare the localization of MCAM and LOK post-Wnt5a treatment, followed by immunofluorescence imaging. Treatment of WM239A cells with purified Wnt5a results in asymmetric localization of not only MCAM, as expected, but also LOK (Figure 4.1B). If Wnt5a signaling results in asymmetric localization of LOK, we wanted to understand how LOK's localization was being modified following Wnt5a treatment. As we described in detail in the earlier chapters, protein palmitoylation is known to regulate protein localization. Our lab has shown Wnt5a signaling regulates protein palmitoylation status of various proteins. The evidence showing LOK becomes asymmetrically localized in response to Wnt5a led us to ask the question, is LOK palmitoylated? The abundance of palmitoylated LOK in each condition was then measured using the acyl-biotin exchange assay (ABE) in parental WM239A cells and $APT1^{WT}$ expressing WM239A cells. As a negative control, samples are processed without hydroxylamine (-HAM) leaving the palmitoylated cysteines intact and preventing biotin labeling. We found LOK to be

palmitoylated in both parental WM239A cells and APT1^{WT} expressing cells (Figure 4.1C). These results suggest LOK can be palmitoylated and palmitoylation could be the mechanism driving asymmetric localization of LOK in response to activated Wnt5a signaling. Our next goal was to determine if phosphorylation of APT1 is reduced with LOK inhibition.

BI-D1870 is an ATP analog, which acts as an ATP competitor, and is known to inhibit LOK's kinase activity (Edgar et al., 2014). We treated WM239A APT1^{WT} cells with either control buffer or purified Wnt5a and DSMO or 10 μM of BI-D1870, immunopurified APT1 with anti-FLAG magnetic beads, processed the samples by SDS-PAGE, and blotted for pS209APT1 to determine the phospho-APT1 levels. Inhibition of LOK with BI-D1870 treatment results in a reduction in phospho-APT1 levels (Figure 4.1D). We generated a short-hairpin to LOK in order to study how knockdown of LOK affects phosphorylation of APT1. Knockdown of LOK reduces phospho-APT1 levels compared to control cells (Figure 4.1E). These results suggest LOK is necessary to phosphorylate APT1 and LOK phosphorylates APT1 in response to Wnt5a signaling.

After determining LOK is asymmetrically localized in response to Wnt5a, and located in close proximity to MCAM in the cell via our imaging experiments, we asked do LOK and MCAM interact? Parental and APT1^{WT} expressing WM239A cells were treated with control buffer or purified Wnt5a, endogenous MCAM was immunopurified, and LOK-MCAM interaction was determined by SDS-PAGE followed by immunoblotting for LOK. In the basal control buffer-treated state, LOK is unable to be pulled down with MCAM. However, in Wnt5a treated cells LOK is co-immunoprecipitated with MCAM (Figure 4.1F). Not only does Wnt5a signaling induce increased interaction of LOK and MCAM, but this interaction is augmented with ectopic expression of APT1 (Figure 4.1F). This observation leads us to conclude APT1 is increasing LOK-MCAM interactions, likely

through a complex formation. Since APT1 expression clearly augments LOK-MCAM interactions, we asked if a depalmitoylation mutant of MCAM, $MCAM^{C590G}$ would be able to interact with LOK. Our hypothesis was that APT1 would not be necessary for depalmitoylation of MCAM, and thus regardless of Wnt5a treatment, the APT1-LOK complex would then not interact with the palmitoylation mutant of MCAM ($MCAM^{C590G}$, hereon referred to as $MCAM^{CG}$). Cells expressing $APT1^{WT}$ as a control, or $MCAM^{WT}$ or $MCAM^{CG}$ were treated with control buffer or purified Wnt5a. MCAM was immunopurified and we detected LOK levels by immunoblotting. Palmitoylation mutant $MCAM^{CG}$ is unable to pull down LOK, while in $APT1^{WT}$ and $MCAM^{WT}$ expressing cells MCAM interacts with LOK in response to Wnt5a stimulation (Figure 4.1G). This might suggest that LOK phosphorylating APT1 is the event that promotes LOK-MCAM interactions. Then, when MCAM is unable to be depalmitoylated, it doesn't end up interacting with the APT1/LOK complex. With these results combined, we determined LOK can be palmitoylated, is asymmetrically localized in response to Wnt5a, is able to interact with MCAM, and inhibition or knockdown of LOK reduces phospho-APT1 levels. We wanted to better understand LOKs role in the ability of the Wnt5a signaling pathway to promote metastatic behavior.

Inhibition or knockdown of LOK inhibits Wnt5a induced melanoma invasion

Since inhibition or knockdown of LOK reduces phospho-APT1 levels, we wanted to better understand if inhibition and/or knockdown of LOK could block Wnt5a induced melanoma invasion. Previously, we have shown Wnt5a induced melanoma invasion requires APT1 activity, and APT1 activity can be increased through phosphorylation of APT1. If LOK is the kinase that phosphorylates APT1, and thereby increases its depalmitoylating activity, then inhibition or knockdown of LOK should reduce Wnt5a

stimulated melanoma invasion. We treated WM239A melanoma spheroids embedded in collagen with purified Wnt5a and either DSMO or 10 μM BI-D1870 every other day and measured invasion on day 7. Treatment of WM239A spheroids with BI-D1870 significantly reduced melanoma invasion compared to DSMO negative control (Figure 4.2A). Similarly, in $APT1^{WT}$ cells, treatment with BI-D1870 reduces melanoma invasion (Figure 4.2B). When we combine that data to compare the values observed with WM239A parental cells and those expressing $APT1^{WT}$, we see that even $APT1^{WT}$ cells' high invasiveness is reduced with BI-1870 treatment (Figure 4.2C). This tells us that inhibition of LOK can significantly reduce Wnt5a induced melanoma invasion.

Next, we treated $APT1^{WT}$ control, and two clones of shLOK, shLOK2.3, and shLOK2.4 melanoma spheroids cells embedded with collagen with purified Wnt5a and measured melanoma invasion on day 7. $APT1^{WT}$ control cells display a high level of invasiveness, as expected since the spheroids are treated with Wnt5a which promotes invasion (Figure 4.2D, 4.2F). Knockdown of LOK, shown with two shRNA clones, dramatically reduces Wnt5a mediated invasion in melanoma cells in both parental WM239A and $APT1^{WT}$ expressing cells (Figure 4.2D, 4.2E, 4.2F). Taken together, these results suggest APT1 phosphorylation, mediated by LOK, is driving melanoma invasion and that LOK inhibition or knockdown can significantly reduce Wnt5a induced melanoma invasion.

FIGURES

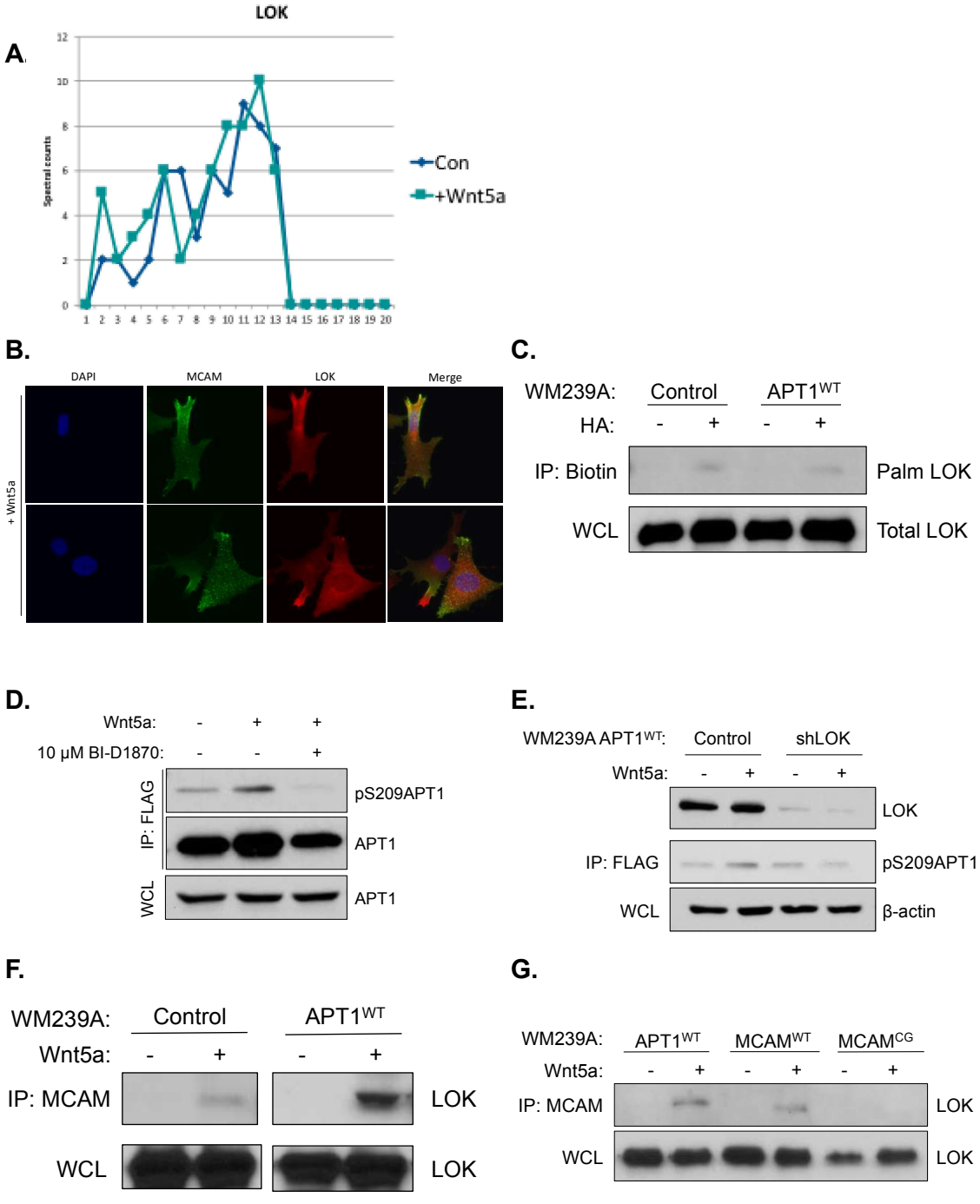

Figure 4.1. *Inhibition or knockdown of LOK/STK10 reduces pAPT1 levels and Wnt5a treatment increases LOK-MCAM interactions.* (**A**) Proteomics profiling of Wnt5a treated WM239A melanoma cell lysates, with LOK kinase, also known as STK10, results shown.

(Data obtained through screen from Witze, E., et al., 2013). Lysates were subjugated to density gradient centrifugation followed by protein digestion and mass spectrometry. Fraction 2 corresponds to the cytoskeleton fraction. (**B**) Immunostaining of Wnt5a treated WM239A cells and cellular localization of LOK and MCAM observed by immunofluorescence microscopy. DAPI staining indicates nuclei. Merge images combines all filtered images shown. (**C**) Acyl-biotin exchange assay of WM239A control and $APT1^{WT}$ cells showing palmitoylation levels of LOK (Palm LOK) compared to total LOK by western blot analysis using anti-LOK antibodies. (**D**) WM239A ectopically expressing $APT1^{WT}$ were treated with control buffer or 150 ng/ml of purified Wnt5a and either DSMO or 10 μM of BI-D1870. $APT1^{WT}$ was immunopurified and phosphorylation levels of APT1 was analyzed by western blot analysis. (**E**) Western blot of WM239A $APT1^{WT}$ control and $APT1^{WT}$ shLOK cells treated with control buffer or 150 ng/ml purified Wnt5a. APT1 was then immunopurified to determine phospho-APT1 levels using pS209APT1 antibodies. β-actin was immunoblotted for as a loading control. (**F**) WM239A control or $APT1^{WT}$ cells were treated with control buffer or 150 ng/ml purified Wnt5a, MCAM was immunopurified, samples analyzed by SDS-PAGE, and immunoblotted for LOK. (**G**) WM239A cells ectopically expressing $APT1^{WT}$, $MCAM^{WT}$, or $MCAM^{C590G}$ ($MCAM^{CG}$) were treated with control buffer or 150 ng/ml Wnt5a, MCAM was immunopurified, samples analyzed by SDS-PAGE, and immunoblotted for LOK using anti-LOK antibodies.

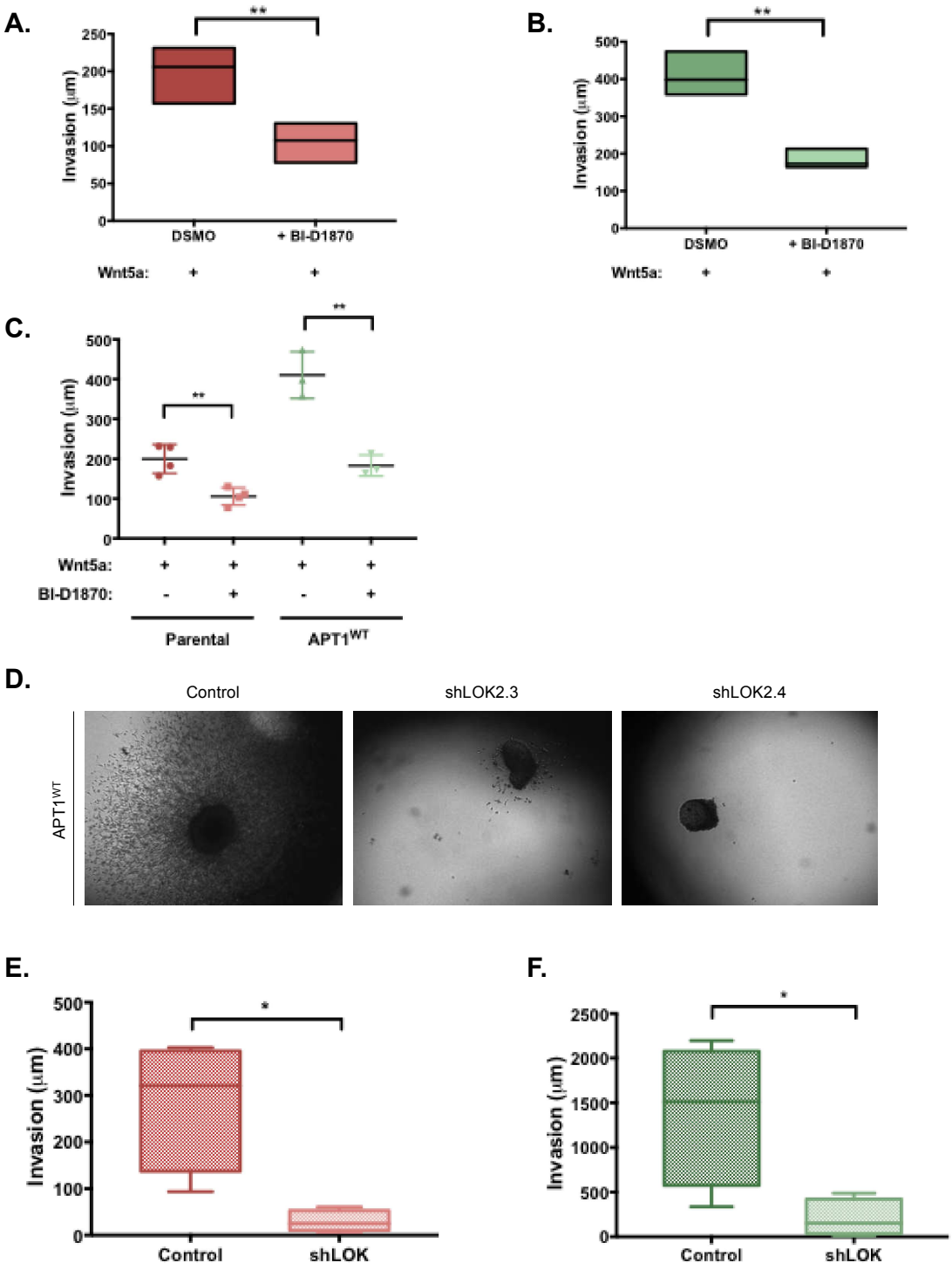

Figure 4.2. *Inhibition or knockdown of LOK/STK10 inhibits Wnt5a induced melanoma invasion.* (**A**) WM239A melanoma cells were grown on agarose to form spheroids that were embedded in collagen, purified Wnt5a and DSMO or 10 µM BI-D1870 were added to the wells every other day, images were taken on day 7, and the distance invaded was measured. Quantification of WM239A spheroid invasion assay. n=4 spheroids counted

per condition, **p=0.0044 by unpaired t-test analysis. (**B)** WM239A APT1^{WT} cells were grown on agarose to form spheroids that were embedded in collagen, purified Wnt5a and DSMO or 10 μM BI-D1870 were added to the wells every other day, images were taken on day 7, and the distance invaded was measured. Quantification of WM239A spheroid invasion assay. n=4 spheroids counted per condition, **p=0.0036 by unpaired t-test analysis. (**C**) Combined data from (A) and (B). (**D**) WM239A APT1^{WT} control, two clones of shLOK, shLOK2.3 and shLOK2.4, cells were grown on agarose to form spheroids that were embedded in collagen, purified Wnt5a and DSMO or 10 μM BI-D1870 were added to the wells every other day, images were taken on day 7, and the distance invaded was measured. Representative images of each sample are shown. (**E**) Quantification of WM239A spheroid invasion assay of control and shLOK cells. n=4 spheroids counted per condition. *p=0.0113 by unpaired t-test analysis. (**F**) Quantification of WM239A APT1^{WT} spheroid invasion assay of control and shLOK cells. n=4 spheroids counted per condition. *p=0.0274 by unpaired t-test analysis.

DISCUSSION

Here, we uncover evidence to suggest LOK may be the Wnt5a-mediated kinase that phosphorylates APT1 in response to activation of the Wnt5a pathway in melanoma. We have shown LOK to be palmitoylated, something that had not yet been reported. Having this kinase be spatially regulated by palmitoylation opens up the possibility that LOK's regulation itself can go awry in cancer cells who have palmitoylation in palmitoyl transferases. Identification of LOK's palmitoylation sites might help us better understand how LOK's palmitoylated state affects its interactions with its targets. Furthermore, identification of LOKs palmitoyltransferase will help us piece together this puzzle. If LOKs palmitoyl transferase is also mutated frequently in cancer, there are other ways this signaling pathway can be augmented to promote metastasis, as well as other angles to pursue in terms of therapeutic options. It's important to also investigate how LOKs palmitoylation status affects its ability to interact with other LOK targets. For example, if palmitoylation blocks, or conversely increases, LOKs ability to phosphorylate ERM proteins and influences how cells migrate, then increased palmitoylation cycling regulated by Wnt5a signaling could be affecting more than APT1 activity but also downstream players that promote migration. Understanding how palmitoylation of LOK affects its interaction with its targets and the ability to phosphorylate them is an important next step for us to investigate to better understand LOKs role in normal, untransformed cells, and the role it plays in promoting cancer metastasis.

Our findings of LOK's Wnt5a-induced asymmetry can be interpreted in different ways. One possibility is that activation of Wnt5a signaling could result in an adaptor or scaffolding proteins increased interaction with LOK, such as Dvl, which we know plays a role in Wnt signaling. The scaffolding protein could bring the kinase in close proximity to APT1 so that it can be phosphorylated, and this event is responsible for the Wnt5a-

induced asymmetry of LOK that we observe. Another possibility is Wnt5a signaling results in LOK becoming depalmitoylated, and the depalmitoylation of LOK is what is responsible for LOKs induced asymmetry, and there it interacts with APT1 alone. One way to start to determine if Dvl is binding LOK to bring it in close proximity to APT1 is to answer the question, do Dvl and LOK interact? One could perform co-immunoprecipitation assays and reciprocal co-immunoprecipitation assays to determine if they interact in a complex. After that, one could clone the various domains of Dvl to determine which domain specifically is responsible for this interaction by co-immunoprecipitation experiments. To determine if asymmetric LOK is primarily in its palmitoylated or depalmitoylated state, one could perform an acyl-biotin exchange assay on fixed cells on a coverslip and then image via fluorescence microscopy. If depalmitoylated LOK is mainly asymmetrical, this might provide us with evidence that LOK is depalmitoylated, and once its depalmitoylated it is able to move freely about the cell, either on its own or as part of a complex, to act on downstream targets such as APT1. Another added layer of mechanistic clarity would be provided if live imaging experiments were performed using tagged LOK and MCAM to determine the temporal events and can be used to define which of these players becomes asymmetrical in response to Wnt5a first, or if they occur at the same time.

If somehow, activation of Wnt5a signaling is activating LOK itself to phosphorylate APT1, LOK activation could potentially have a feedback loop associated with it. It would be interesting to investigate if any modifications arise in LOK post Wnt5a treatment, especially since we know LOK can phosphorylate itself. For example, Wnt5a signaling could result in LOK itself being phosphorylated by either itself or another kinase, and this could be an explanation for increased phosphorylation of APT1 in response to Wnt5a signaling. That observation, in combination with LOK being

palmitoylated/depalmitoylated, adds an extra layer to LOK regulation. Palmitoylation of LOK could be part of the feedback loop proposed. A potential mechanism can include any of the following two possibilities. Wnt5a signaling increasing LOK's proximity to APT1 or Wnt5a signaling results in a regulatory modification of LOK, such as phosphorylation or autophosphorylation or palmitoylation/depalmitoylation, to increase its affinity for APT1. Of course, there is the possibility that both of these are involved in some capacity in the mechanism of how LOK phosphorylates APT1 in response to Wnt5a signaling. Further studies would need to be performed to tease out these details.

METHODS

Purification of recombinant Wnt5a and treatments with Wnt5a

Wnt5a was purified from mouse L-cells overexpressing human Wnt5a as described previously (Willert et al., 2003). Control cells were treated with control buffer with identical detergent conditions as the Wnt5a purification buffer.

Cell lines and culture conditions

Metastatic melanoma cell line WM239A (BRAF V600D) (Wistar Institute) were cultured in RPMI 1640 medium (Gibco-BRL, Grand Island, NY) supplemented with 10% fetal bovine serum (FBS) (GE Life Sciences). Cell lines were authenticated routinely by short tandem repeat profiling by the Wistar Institute prior to use.

Immunoprecipitation

WM239A cells ectopically expressing APT1-CFP-FLAG mutants were treated with control buffer or 150 ng/ml Wnt5a for specified time period and then lysed in lysis buffer containing 1% Triton-X 100, 50 mM Tris pH 7.5, 150 mM NaCl supplemented with

protease and phosphatase inhibitors (1μg/ml leupeptin, 1μg/ml aprotinin, 2μg/ml pepstatin A, 1mM PPi, 2nM $NaVO_4$, 150mM NaF). Insoluble cell debris was removed by centrifugation (13,000 RPM for 10 min at 4°C. Lysate was incubated with FLAG M2 magnetic beads (Sigma-Aldrich, St. Louis, MO) for 1.5 hours. Beads were washed with lysis buffer and protein was eluted using FLAG peptide for 1 hour at room temperature. Samples were separated by SDS-PAGE and transferred to either nitrocellulose membrane (Life Technologies, Thermo Fisher Scientific, Waltham, MA) for phospho-APT1 antibody (YenZym Antibodies, San Francisco, CA) or PVDF membrane (Millipore, Burlington, MA) for all other antibodies used.

Western blot analysis and antibodies

Cells were harvested and lysed in 1% Triton X-100, 50mM Tris pH 7.5, 150mM NaCl supplemented with protease and phosphatase inhibitors (1μg/ml leupeptin, 1μg/ml aprotinin, 2μg/ml pepstatin A, 1mM PPi, 2nM $NaVO_4$, 150mM NaF). Insoluble cell debris was removed by centrifugation (13,000 RPM for 10 min at 4°C. The protein concentration was determined by DC Protein method (BioRad, Hercules, CA). Equal amounts of total protein were separated by SDS-PAGE and transferred to either nitrocellulose membrane (Life Technologies, Thermo Fisher Scientific, Waltham, MA) for phosphor-APT1 antibody or PVDF membrane (Millipore, Burlington, MA) for all other antibodies used. The nitrocellulose membranes were blocked with 5% bovine serum albumin (BSA) in TBST (TBS, 0.1% Tween). The PVDF membranes were blocked with 5% dry milk in TBST. All membranes were immunoblotted with different antibodies diluted in 5% BSA in TBST.

The rabbit anti-human APT1 antibody (Abcam, Cambridge, MA) was used at 1:1000. The rabbit anti-human beta-actin (Cell Signaling Technologies, Danvers, MA) was used at 1:5000. The mouse anti-human MCAM antibody (Santa Cruz Biotechnology, Dallas, TX) was used at 1:1000. The rabbit anti-human LOK antibody was use 1:1000 (Bethyl Laboratories, Montgomery, TX). The secondary antibodies were HRP-conjugated 1:10000 diluted in 5% BSA in TBST. Membranes were washed three times with TBST between the different steps.

Immunofluorescence

Parental WM239A cells were plated on glass coverslips and treated with 150 ng/ml purified Wnt5a, fixed with formalin solution (10% neutral buffered) for 10 minutes, and cell membranes were permeabilized with 0.1% Triton X-100 in PBS for 10 minutes, and blocked with 5% BSA in TBST solution for 30 minutes. Primary antibodies of MCAM (Santa Cruz Biotechnology, Dallas, TX) and LOK (Bethyl Laboratories, Montgomery, TX) were added 1:500 overnight at 4°C. Primary antibody was washed off with three washes of TBST. Secondary antibodies were added at 1:1000 for 1 hour at room temperature, washed in TBST, and mounted with DAPI mount (SouthernBiotech, Birmingham, AL). Cells were imaged using Leica DMI6000 B inverted microscope.

Acyl-biotin exchange assay

The ABE assay was performed as described (Wan et al., 2007).

Spheroid assay

96-well plates were coated with 50 μl per well of sterile 1.5% noble agar and solidified at room temperature for 10 min. 200 μl of 2.5×10^4 cells/ml cell suspension was added to each well. Spheroids formed at 37°C and at 4% CO_2 for 48 h. Collagen matrices were

prepared on ice using Pur Col purified bovine collagen (Advanced Biomatrix, Carlsbad, CA), Hyclone RPMI 1640 (5X) with sodium biocarbonate diluted to 1X in total volume and 10% FBS. Sterile NaOH was added to correct the collagen pH. 75 μl of collagen matrix was added to new wells and allowed to solidify at 37°C for 1 h. Spheroids were resuspended in 125 μl of collagen matrix and transferred to wells containing 75 μl of collagen. After collagen solidified at 37°C, 100 μl of fresh medium was added on top of the collagen. Medium was changed every other day. Images were taken every 24 h for 1 – 10 days. For the invasion assays including BID-1870: 10μM of BID-1870 (Sigma-Aldrich, St. Louis, MO) was added to fresh media on the spheroids and changed every other day.

Statistics

* denotes a P-value between 0.0113-0.0274, ** denotes a P-value of 0.0036-0.0044 in unpaired two-tailed Students t-test, assuming normal distribution and equal variance. Each experiment was performed at least 3 times.

CHAPTER 5: FUTURE DIRECTIONS

OVERVIEW

As we summarize our findings and conclude our discussion, we end with an examination on future directions of this thesis project. We provide proposals for future experiments that will validate our findings, make suggestions of various avenues to pursue that could provide valuable insight, and outline how breakthroughs on defining this pathway further can open up possibilities to create better therapies for cancer patients.

CONFIRMING LOK AS APT1'S KINASE

More experiments confirming LOK as APT1's candidate kinase must be performed in order to validate our findings. One could strengthen this argument by cloning a recombinant catalytically inactive mutant of LOK, expressing this in WM239A cells, treating the cells with purified Wnt5a, and determining the levels of phosphorylated APT1. We expect catalytically inactive LOK would be unable to phosphorylate APT1 and thus, we would not be able to detect phospho-APT1. Conversely, if one were to clone LOK and perform an in vitro kinase assay with purified APT1, we would expect LOK to be sufficient to phosphorylate APT1.

Our findings of LOK's Wnt5a induced asymmetry and its temporal response remain to be validated. It would be interesting and valuable to determine the temporal events that result in Wnt5a induced asymmetry of LOK and if this occurs before, during, or after MCAM's Wnt5a induced asymmetry. By creating different fluorescently tagged LOK and MCAM, we could perform live cell imaging experiments on Wnt5a treated

WM239A cells and observe the timing of the asymmetry. Particularly, it would be interesting to determine if we performed that same experiment with catalytic inactive LOK or with a palmitoylation mutant of LOK, after the LOK sites have been mapped, if this would change the Wnt5a induced asymmetry. Based on my initial observations, I would hypothesize the palmitoylation mutant LOK would no longer be able to be asymmetrically distributed in response to Wnt5a signaling. As far as the catalytic inactive mutant, we would need to understand how LOKs catalytic activity affects it assembling in a LOK-MCAM-APT1 complex, if it does. Hence, further studies would need to be done to clarify this sort of complex and what regulates it.

How LOK becomes primed for APT1 phosphorylation in response to Wnt5a signaling remains unknown. Understanding how activation of Wnt5a signaling leads to increased phosphorylation of APT1 by LOK is important to understand and parsing out the other pathway players involved in this signaling axis would help provide clarity to this issue. One possibility is cytosolic adaptor or scaffold proteins, such as Dishevelled, bringing LOK in close proximity to APT1. Activation of Wnt5a-Ror signaling has been shown to phosphorylate the scaffolding protein Dishevelled (Dvl), while the absence of Ror signaling leads to a phenotype that mirrors Wnt5a null mutant mice (Ho et al., 2012), providing evidence that Dvl is a Wnt5a-Ror signaling target. I have obtained preliminary evidence that Dvl binds APT1 shown by a co-immunoprecipitation of APT1 and Dvl. For this reason, generating Dvl domain mutants and determining if Dvl can bind to LOK, or any of the depalmitoylation targets of APT1, such as MCAM and CD44, would help tease out the role Dvl plays in the Wnt5a/APT1 signaling axis.

Other unanswered questions remain within LOK's palmitoylation and regulation of palmitoylation. For example, the identification of the palmitoyl transferase responsible for palmitoylating LOK remains unknown. Additionally, identifying the palmitoylation

site(s) on LOK would be another important piece of information that would help us understand how LOK's activity and function could be regulated. One could map the likely palmitoylation sites by looking at the various LOK domains, identify the cysteines, map those via a palmitoylation software, and then create palmitoylation mutants of each to study which of those cysteines are the likely palmitoylation targets using acyl-biotin exchange assays. In addition, it would be interesting to determine if LOK is depalmitoylated by APT1. If we review Figure 4.1C, where we show LOK's palmitoylation levels, they appear to be lower in the cells ectopically expressing $APT1^{WT}$ which would suggest APT1 can depalmitoylate LOK. It would be interesting to investigate how expressing the APT1 phospho-mutants, $APT1^{SA}$ and $APT1^{SD}$, and then measure the effects LOK palmitoylation levels. If the high activity of $APT1^{SD}$, or phospho-APT1, are overserved with LOK as a substrate, and there are decreased LOK palmitoylation levels when you express $APT1^{SD}$, then this could suggest APT1 regulating LOK's localization in a feedback mechanism. LOK could phosphorylate APT1, APT1 can then become 'activated', depalmitoylate LOK, and LOK can then become more dynamic in the cell, allowing more freedom for movement throughout the cell and asymmetric localize. One possibility is this feedback loop allows LOK to better access its targets, another is that it could increase APT1's phosphorylation in specific areas of the cell so that APT1 can increase its depalmitoylated of targets. This possibility, alongside or in combination with the scaffolding complex, might help explain why we see the asymmetric localization of LOK in response to Wnt5a. If LOK is able to re-localize to a specific region of the cell, then there it could phosphorylate other downstream targets, such as ERM proteins, which could be resulting in changes in the cytoskeleton and thus, increased migration and motility.

IDENTIFICATION OF OTHER PROTEINS THAT MIGHT PLAY A ROLE IN THE WNT5A SIGNALING PATHWAY

More than 2000 human proteins have either been shown or predicted to be palmitoylated (Blanc et al., 2015). This represents 12% of the proteome and identification of the proteins whose depalmitoylation is Wnt5a responsive would provide further clarity on downstream players and the role they play in promoting metastasis. We know many proteins are palmitoylated and palmitoylation can affect how they signal, traffic, and how they interact with their pathway players. However, detailing the events that cause their palmitoylation or depalmitoylation are yet to be provided for many of palmitoylated proteins. To better understand the role Wnt5a signaling plays on the global palmitoylation landscape, I treated WM239A cells with control buffer or purified Wnt5a, performed an acyl-biotin exchange assay, processed samples by SDS-PAGE, and determined the global palmitoylation landscape proteins by silver stain analysis. Many bands appear in the control buffer lane, indicating a large number of palmitoylated proteins exist in the untreated state, while a large selection of those bands disappear in the Wnt5a treated sample, suggesting they are no longer in their palmitoylated state when Wnt5a signaling is activated. When we treat the cells with an APT inhibitor, Palmostatin B, prior to Wnt5a treatment, and then perform the same analysis, many bands return that disappeared in the Wnt5a treated sample. This suggests APT1 activity is required for the Wnt5a mediated depalmitoylation of those proteins. This preliminary data I obtained suggests Wnt5a signaling promotes a large subset of proteins to be depalmitoylated, and this is specifically mediated by APT1 activity (data not shown). It would be interesting to identify those proteins that are depalmitoylated by APT1 in response to Wnt5a signaling. With this information, we can begin testing how their palmitoylation state affects their function and overall cell behavior, and how those

proteins play a role in metastasis. One could perform the same experiment, but instead of a silver stain analysis one could perform a Coomassie stain and analyze the differences via mass spectrometry analysis to identify the proteins. Once the candidates have been identified, test their how palmitoylation state affects metastatic behavior. This may help round out the picture of how palmitoylated/depalmitoylated proteins are promoting metastasis.

UNDERSTANDING THE ROLE OF APT1 PHOSPHORYLATION *IN VIVO*

Understanding APT1's activity *in vivo* would provide invaluable information on how phosphorylated APT1 functions in tissues. We could do this by introducing APT1 wild-type and the APT1 phospho-mutants into human melanoma cells or into transformed primary human melanocytes and study melanoma invasion via an organotypic model. This type of model allows us to recapitulate the human skin by using all human components including keratinocytes, primary melanocytes, basement membranes, and investigate three-dimensional melanoma invasion on a mouse (Ridky et al., 2010). We can introduce genetic events that are commonly found in human melanoma, such as $BRAF^{V600E}$ and p53 inactivation, and the wild-type or phospho-mutants of APT1, allow the skin to grow, graft it onto a mouse, and study melanoma invasion over time by examining invasion through immunostaining after time. Validating phospho-APT1 or the disease-relevant mutation, $APT1^{S209D}$ and $APT1^{S210L}$, respectively, increase metastatic behavior *in vivo* would further strengthen the argument that Wnt5a induced phosphorylation of APT1, or patients who present with this mutation in their melanoma, are likely to have metastatic disease. An alternative technique to do this to remove the possibilities of issues with overexpression vectors is to mutate the endogenous APT1 using CRISPR technology.

INVESTIGATING THE WNT5A/APT1 SIGNALING AXIS IN OTHER CANCERS

Other studies have investigated Wnt5a's role in cancer cell migration, proliferation, and survival across a wide variety of tumor types. Wnt5a enhances activation of Rac1/2 by inducing receptor tyrosine kinase-like orphan receptor 1 (Ror1) to interact with DOCK2, leading to Wnt5a enhanced cell proliferation (Hasan et al., 2018). Previous studies have down a role for Wnt5a in osteosarcoma. Wnt5a stimulates migration and invasion of osteosarcoma cells (Wang, X. et al 2018). Similarly, Wnt5a-induced cell migration in osteosarcoma cells is through activation of PI3K/Akt/RhoA signaling (Dai et al., 2018).

It is worth investigating the Wnt5a/APT1 signaling axis in other cancers to confirm the mechanism we have uncovered is conserved among other tumor types and to help us better understand how to target the Wnt5a signaling pathway as a therapeutic option for patients who have abnormalities in this pathway. Previous studies showed Wnt5a overexpression increased clone formation, migration, invasion, as well as played a role in promoting EMT and metastasis in non-small-cell lung cancer (NSCLC) (Wang, B. et al 2017). Similarly, loss of E-cadherin and gain of N-cadherin has been reported in melanomas transitioning from radial growth phase to vertical growth phase (Danen et al., 1996; Hsu et al., 1996). Additionally, expression of Wnt5a significantly enhanced migration, proliferation, and invasiveness in pancreatic cancer cells. Wnt5a expression was reported to be associated with a modulation of genes associated with EMT in pancreatic cells as well (Ripka et al., 2007). Importantly, Wnt5a expression was also found to be upregulated early during pancreatic carcinogenesis and in invasive pancreatic adenocarcinomas (Ripka et al., 2007). Frizzled2 (Fzd2) and Wnt5a are highly expressed in metastatic samples and their expression, along with activation of

noncanonical Wnt components like PKC and JNK, correlates with EMT markers (Dissanayake et al., 2007). Taken together, these observations and studies suggest the Wnt5a signaling pathway could not only be contributing to EMT in melanoma but other cancers as well (Dissanayake et al., 2007; Jordan et al., 2013; Scheel et al., 2011). Investigating the details of how Wnt5a expression is driving epithelial-mesenchymal transition can help us better understand its role in EMT and identifying how to prevent Wnt5a from promoting EMT in cancer patients. These findings can help us not only develop novel therapies but also develop better therapies for patients who experience disease recurrence and chemoresistance from EMT, for those who develop EMT induced chemoresistance, for example (Fischer et al., 2015).

Inhibition of the Wnt5a signaling pathway has been previously proposed as a novel treatment for cancer patients. This thesis corroborates those proposals and even emphasizes how large of a role Wnt5a signaling plays in not only melanoma metastasis, but also likely is Wnt5a's role in other cancer types. Patients with abnormalities in this signaling pathway or patients who either do not respond or respond negatively to the current standard of care, which includes BRAF inhibitors, among other treatments are in dire need of more targeted therapies. There are numerous possibilities of targets within this pathway, all with certain benefits and potential pitfalls, and some that may prove more effective than others. One option includes inhibition of Wnt5a signaling using Box5 for patients with tumors with elevated Wnt5a expression. Wnt5a has been shown to play a role in resistance to BRAF inhibitors in melanoma patients. Treatment of six BRAF mutant melanoma cell lines with increasing does of BRAF inhibitor PLX4032 resulted in three cell lines developing resistance to PLX4032 while upregulating expression of Wnt5a and activating MAPK signaling (Tap et al., 2010). Another study showed a positive correlation between Wnt5a expression and BRAFi resistance (O'Connell et al.,

2013). Stimulating the cells with recombinant Wnt5a increased BRAFi resistance. Knockdown of co-receptor ROR2 increased response to BRAF inhibitor PLX4720 (O'Connell et al., 2013). These results suggest Wnt5a signaling plays a role in cancer cells developing resistance to BRAF inhibitors and targeting the Wnt5a pathway, in this case through knockdown or ROR2, results in a better response to BRAF inhibitor PLX4720. The authors tied these results to clinical data they obtained on patients demonstrating patients who relapsed while on BRAFi therapy showed increased positivity for Wnt5a expression, indicating a role for Wnt5a in developing BRAFi resistance (O'Connell et al., 2013). A similar observation was reported in BRAFi-resistant melanoma tumors from another study, where 7 of the 11 patients showed increased Wnt5a expression compared to pretreated samples (Anastas et al., 2014). These studies suggest that inhibition of Wnt5a signaling might present as a viable co-treatment option for those patients undergoing BRAF inhibitor therapies as a supplemental therapy. Another possibility to inhibit this pathway in patients is inhibition of LOK kinase activity by BI-D1870 treatment or development of a more specific inhibitor to LOK. Inhibition of polo-like kinase 1, of which LOK has been shown to be an upstream regulator of, has been proposed as a possible target for cancer therapy (Walter et al., 2003; Strebhardt, K. and Ullrich, A., 2006). However, since LOK plays a diverse role in the cell and inhibition of LOK may include a larger set of side effects. Wnt5a treatment for BRAFi-resistant melanoma has been previously proposed (Prasad et al., 2015), but inhibition of APT1 activity as a therapy for cancer patients is a novel idea that is supported by the evidence presented in this thesis and is worth investigating further. The APT1 specific inhibitor, ML348, has been more recently developed and tested *in vitro* (Won et al., 2016). However, testing ML348 efficacy *in vivo* by using mouse models of cancer progression and metastasis and ultimately how patients respond to inhibition with

ML348 in a clinical setting is imperative to help us understand if APT1 inhibition is a viable human therapy for cancer patients. By inhibiting APT1 activity, we can inhibit the downstream Wnt5a signaling events that have been shown to drive melanoma metastasis.

CONCLUDING REMARKS

Here, we uncover the mechanistic details of the downstream signaling events that contribute to Wnt5a mediated metastatic melanoma. Targeting the Wnt5a/APT1 signaling axis, specifically through APT1 inhibition, would be a novel approach to treating Wnt5a driven melanoma. There is also the potential for a wider range of applications from the findings in this thesis for treating other types of Wnt5a driven cancers which have either upregulated Wnt5a or ROR2 expression, other tumor types with mutations in APT1, or even those with elevated LOK expression or LOK mutations. Metastatic melanoma patients are in dire need of targeted therapies to the players involved in this signaling axis and inhibition of APT1 activity might be a viable option to explore further. Our goal is for the findings obtained in this thesis to contribute to the scientific community in helping to understand why and how cancers hijack the Wnt5a signaling pathway and how we can best serve patients in the future. Below is a schematic of the model we have proposed in this thesis.

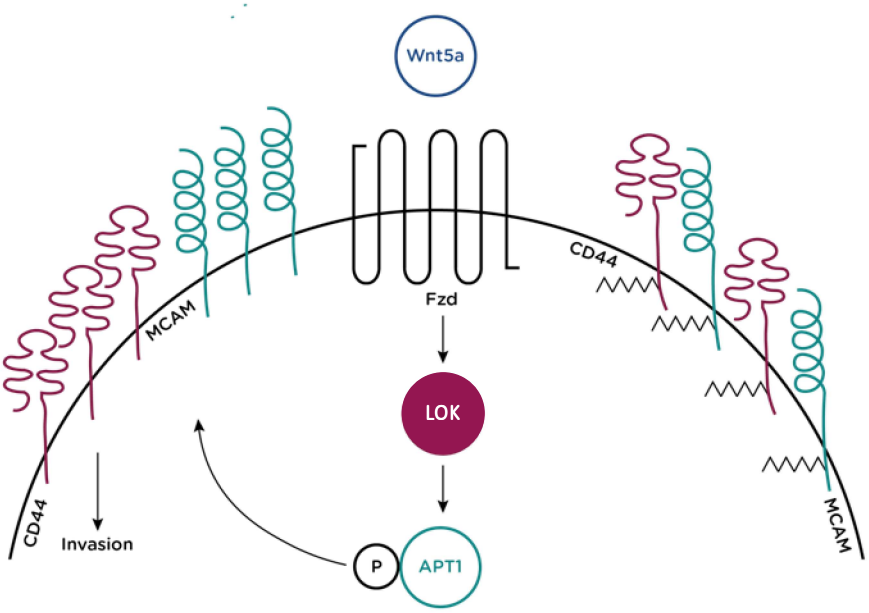
Wnt5a
Fzd
CD44
MCAM
LOK
CD44
Invasion
P
APT1
MCAM

BIBLIOGRAPHY

American Cancer Society. Facts & Figures 2018. American Cancer Society. Atlanta, Ga. 2018.

Anastas, J. N., and Moon, R. T. (2013) WNT signalling pathways as therapeutic targets in cancer. Nat. Rev. Cancer 13, 11–26

Anastas, J. N., Kulikauskas, R. M., Tamir, T., Rizos, H., Long, G. V., von Euw, E. M., Yang, P.-T. T., Chen, H.-W. W., Haydu, L., Toroni, R. A., Lucero, O. M., Chien, A. J., and Moon, R. T. (2014) WNT5A enhances resistance of melanoma cells to targeted BRAF inhibitors. J. Clin. Invest. 124, 2877–90

Babina, I., McSherry, E., Donatello, S., Hill, A., and Hopkins, A. (2014) A novel mechanism of regulating breast cancer cell migration via palmitoylation-dependent alterations in the lipid raft affiliation of CD44. Breast Cancer Research 16, R19

Beck, M., Kathayat, R., Cham, C., Chang, E., and Dickinson, B. (2017) Michael addition-based probes for ratiometric fluorescence imaging of protein S -depalmitoylases in live cells and tissues. Chem Sci 8, 7588–7592

Belkina, N. V., Liu, Y., Hao, J.-J. J., Karasuyama, H., and Shaw, S. (2009) LOK is a major ERM kinase in resting lymphocytes and regulates cytoskeletal rearrangement through ERM phosphorylation. Proc. Natl. Acad. Sci. U.S.A. 106, 4707–12

Beltran, H., Prandi, D., Mosquera, J.M., Benelli, M., Puca, L., Cyrta, J., Marotz, C., Giannopoulou E., Chakravarthi, B.V., Varambally, S., Tomlins, S.A., Nanus, D.M., Tagawa, S.T., Van Allen, E.M., Elemento, A., Sboner, A., Garraway, L.A., Rubin, M.A., and Demichelis, F. (2016) Divergent cloncal evolution of castration-resistant neuroendocrine prostate cancer. Nature Medicine. 22, 298–305

Bittner M, Meltzer P, Chen Y, Jiang Y, Seftor E, Hendrix M, Radmacher M, Simon R, Yakhini Z, Ben-Dor A, Sampas N, Dougherty E, Wang E, Marincola F, Gooden C, Lueders J, Glatfelter A, Pollock P, Carpten J, Gillanders E, et al. (2000) Molecular classification of cutaneous malignant melanoma by gene expression profiling. Nature 406:536–540.

Blanc M, David F, Abrami L, et al. SwissPalm: protein palmitoylation database. F1000Res. 2015;4:261.

Briele, H. A. & Das Gupta, T.K. Natural history of cutaneous malignant melanoma. World J. Surg. 3, 255–270 (1979).

Brown, M. J., Nijhara, R., Hallam, J. A., Gignac, M., Yamada, K. M., Erlandsen, S. L., Delon, J., Kruhlak, M., and Shaw, S. (2003) Chemokine stimulation of human peripheral blood T lymphocytes induces rapid dephosphorylation of ERM proteins, which facilitates loss of microvilli and polarization. Blood 102, 3890–9

Burger, M., Zimmermann, T., Kondoh, Y., Stege, P., Watanabe, N., Osada, H., Waldmann, H., and Vetter, I. (2011) Crystal structure of the predicted phospholipase

LYPLAL1 reveals unexpected functional plasticity despite close relationship to acyl protein thioesterases. J Lipid Res 53, 43–50

Campbell, J., Alexandrov, A., Kim, J., Wala, J., Berger, A., Pedamallu, C., Shukla, S., Guo, G., Brooks, A., Murray, B., Imielinski, M., Hu, X., Ling, S., Akbani, R., Rosenberg, M., Cibulskis, C., Ramachandran, A., Collisson, E., Kwiatkowski, D., Lawrence, M., Weinstein, J., Verhaak, R., Wu, C., Hammerman, P., Cherniack, A., Getz, G., Zenklusen, J., Zhang, J., Felau, I., Demchok, J., Yang, L., Wang, Z., Ferguson, M., Tarnuzzer, R., Hutter, C., Sofia, H., Pihl, T., Wan, Y., Chudamani, S., Liu, J., Sun, C., Naresh, R., Lolla, L., Wu, Y., Creighton, C., Rathmell, W., Auman, J., Balu, S., Bodenheimer, T., Hayes, D., Hoadley, K., Hoyle, A., Jones, C., Jefferys, S., Meng, S., Mieczkowski, P., Mose, L., Perou, C., Roach, J., Shi, Y., Simons, J., Skelly, T., Soloway, M., Tan, D., Wu, J., Veluvolu, U., Parker, J., Wilkerson, M., Boice, L., Huang, M., Thorne, L., Getz, G., Noble, M., Zhang, H., Heiman, D., Cho, J., Gehlenborg, N., Saksena, G., Voet, D., Lin, P., Frazer, S., Kim, J., Lawrence, M., Chin, L., Tsao, M.-S., Allison, F., Chadwick, D., Muley, T., Meister, M., Dienemann, H., Kucherlapati, R., Park, P., Bowen, J., Gastier-Foster, J., Gerken, M., Leraas, K., Lichtenberg, T., Ramirez, N., Wise, L., Zmuda, E., Stuart, J., Collisson, E., Peifer, M., Kwiatkowski, D., Campbell, J., Murray, B., Cherniack, A., Berger, A., Sougnez, C., Schumacher, S., Shih, J., Beroukhim, R., Zack, T., Gabriel, S., Meyerson, M., Byers, L., Davidsen, T., Laird, P., Weisenberger, D., Berg, D., Bootwalla, M., Lai, P., Maglinte, D., Baylin, S., Herman, J., Danilova, L., Cope, L., Crain, D., Curley, E., Gardner, J., Lau, K., Mallery, D., Morris, S., Paulauskis, J., Penny, R., Shelton, C., Shelton, T., Sherman, M., Yena, P., Mills, G., Artyomov, M., Schreiber, R., Govindan, R., and Meyerson, M. (2016) Distinct patterns of somatic genome alterations in lung adenocarcinomas and squamous cell carcinomas. Nat Genet 48, 607–616

Carr, K., Bittner, M., and Trent, J. (2003) Gene-expression profiling in human cutaneous melanoma. Oncogene 22, 3076–80

Cerami, E., Gao, J., Dogrusoz, U., Gross, B. E., Sumer, S. O., Aksoy, B. A. A., Jacobsen, A., Byrne, C. J., Heuer, M. L., Larsson, E., Antipin, Y., Reva, B., Goldberg, A. P., Sander, C., and Schultz, N. (2012) The cBio cancer genomics portal: an open platform for exploring multidimensional cancer genomics data. Cancer Discov 2, 401–4

Chamberlain LH, Shipston MJ. (2015) The physiology of protein S-acylation. Physiol Rev. 95(2):341-376.

Costin, G.-E. E., and Hearing, V. J. (2007) Human skin pigmentation: melanocytes modulate skin color in response to stress. FASEB J. 21, 976–94

Curto, J., Del Valle-Pérez, B., Villarroel, A., Fuertes, G., Vinyoles, M., Peña, R., García de Herreros, A., and Duñach, M. (2018) CK1ε and p120-catenin control Ror2 function in noncanonical Wnt signaling. Mol Oncol 12, 611–629

Da Forno, P., Pringle, J., Hutchinson, P., Osborn, J., Huang, Q., Potter, L., Hancox, R., Fletcher, A., and Saldanha, G. (2008) WNT5A Expression Increases during Melanoma Progression and Correlates with Outcome. Clin Cancer Res 14, 5825–5832

Dai, B., Yan, T., and Zhang, A. (2017) ROR2 receptor promotes the migration of osteosarcoma cells in response to Wnt5a. Cancer Cell Int. 17, 112

Danen, E.H., de Vries, T.J., Morandini, R., Ghanem, G.G., Ruiter, D.J., van Muijen, G.N. (1996) E-cadherin expression in human melanoma. Melanoma Res. 6, 127–131

Daniotti, J. L., Pedro, M. P., and Valdez Taubas, J. (2017) The role of S-acylation in protein trafficking. Traffic 18, 699–710

Devedjiev, Y., Dauter, Z., Kuznetsov, S., Jones, T., and Derewenda, Z. (2000) Crystal structure of the human acyl protein thioesterase I from a single X-ray data set to 1.5 A. Struct Lond Engl 1993 8, 1137–46

Dissanayake, S., Wade, M., Johnson, C., O'Connell, M., Leotlela, P., French, A., Shah, K., Hewitt, K., Rosenthal, D., Indig, F., Jiang, Y., Nickoloff, B., Taub, D., Trent, J., Moon, R., Bittner, M., and Weeraratna, A. (2007) The Wnt5A/Protein Kinase C Pathway Mediates Motility in Melanoma Cells via the Inhibition of Metastasis Suppressors and Initiation of an Epithelial to Mesenchymal Transition. Journal of Biological Chemistry 282, 17259–17271

Du, S. J., Purcell, S. M., Christian, J. L., McGrew, L. L., and Moon, R. T. (1995) Identification of distinct classes and functional domains of Wnts through expression of wild-type and chimeric proteins in Xenopus embryos. Mol. Cell. Biol. 15, 2625–34

Duncan JA, Gilman AG. (1998) A cytoplasmic acyl-protein thioesterase that removes palmitate from G protein alpha subunits and p21(RAS). J Biol Chem. 273(25):15830-15837.

Edgar, A. J., Trost, M., Watts, C., and Zaru, R. (2014) A combination of SILAC and nucleotide acyl phosphate labelling reveals unexpected targets of the Rsk inhibitor BI-D1870. Bioscience Rep 34, e00091

Eirew, P., Steif, A., Khattra, J., Ha, G., Yap, D., Farahani, H., Gelmon, K., Chia, S., Mar, C., Wan, A., Laks, E., Biele, J., Shumansky, K., Rosner, J., McPherson, A., Nielsen, C., Roth, A., Lefebvre, C., Bashashati, A., Souza, C., Siu, C., Aniba, R., Brimhall, J., Oloumi, A., Osako, T., Bruna, A., Sandoval, J., Algara, T., Greenwood, W., Leung, K., Cheng, H., Xue, H., Wang, Y., Lin, D., Mungall, A., Moore, R., Zhao, Y., Lorette, J., Nguyen, L., Huntsman, D., Eaves, C., Hansen, C., Marra, M., Caldas, C., Shah, S., and Aparicio, S. (2015) Dynamics of genomic clones in breast cancer patient xenografts at single-cell resolution. Nature 518, 422–426

Fischer, K. R., Durrans, A., Lee, S., Sheng, J., Li, F., Wong, S. T., Choi, H., El Rayes, T., Ryu, S., Troeger, J., Schwabe, R. F., Vahdat, L. T., Altorki, N. K., Mittal, V., and Gao, D. (2015) Epithelial-to-mesenchymal transition is not required for lung metastasis but contributes to chemoresistance. Nature 527, 472–6

Ford, C. E., Punnia-Moorthy, G., Henry, C. E., Llamosas, E., Nixdorf, S., Olivier, J., Caduff, R., Ward, R. L., and Heinzelmann-Schwarz, V. (2014) The non-canonical Wnt ligand, Wnt5a, is upregulated and associated with epithelial to mesenchymal transition in epithelial ovarian cancer. Gynecol. Oncol. 134, 338–45

Gao, J., Aksoy, B. A. A., Dogrusoz, U., Dresdner, G., Gross, B., Sumer, S. O., Sun, Y., Jacobsen, A., Sinha, R., Larsson, E., Cerami, E., Sander, C., and Schultz, N. (2013) Integrative analysis of complex cancer genomics and clinical profiles using the cBioPortal. Sci Signal 6, pl1

Getz, G., Gabriel, S., Cibulskis, K., Lander, E., Sivachenko, A., Sougnez, C., Lawrence, M., Kandoth, C., Dooling, D., Fulton, R., Fulton, L., Kalicki-Veizer, J., McLellan, M., O'Laughlin, M., Schmidt, H., Wilson, R., Ye, K., Ding, L., Mardis, E., Ally, A., Balasundaram, M., Birol, I., Butterfield, Y., Carlsen, R., Carter, C., Chu, A., Chuah, E., Chun, H.-J., Dhalla, N., Guin, R., Hirst, C., Holt, R., Jones, S., Lee, D., Li, H., Marra, M., Mayo, M., Moore, R., Mungall, A., Plettner, P., Schein, J., Sipahimalani, P., Tam, A., Varhol, R., Robertson, A., Cherniack, A., Pashtan, I., Saksena, G., Onofrio, R., Schumacher, S., Tabak, B., Carter, S., Hernandez, B., Gentry, J., Salvesen, H., Ardlie, K., Getz, G., Winckler, W., Beroukhim, R., Gabriel, S., Meyerson, M., Hadjipanayis, A., Lee, S., Mahadeshwar, H., Park, P., Protopopov, A., Ren, X., Seth, S., Song, X., Tang, J., Xi, R., Yang, L., Zeng, D., Kucherlapati, R., Chin, L., Zhang, J., Auman, J., Balu, S., Bodenheimer, T., Buda, E., Hayes, D., Hoyle, A., Jefferys, S., Jones, C., Meng, S., Mieczkowski, P., Mose, L., Parker, J., Perou, C., Roach, J., Shi, Y., Simons, J., Soloway, M., Tan, D., Topal, M., Waring, S., Wu, J., Hoadley, K., Baylin, S., Bootwalla, M., Lai, P., Jr, T., Berg, D., Weisenberger, D., Laird, P., Shen, H., Chin, L., Zhang, J., Getz, G., Cho, J., DiCara, D., Frazer, S., Heiman, D., Jing, R., Lin, P., Mallard, W., Stojanov, P., Voet, D., Zhang, H., Zou, L., Noble, M., Lawrence, M., Reynolds, S., Shmulevich, I., Aksoy, B., Antipin, Y., Ciriello, G., Dresdner, G., Gao, J., Gross, B., Jacobsen, A., Ladanyi, M., Reva, B., Sander, C., Sinha, R., Sumer, S., Taylor, B., Cerami, E., Weinhold, N., Schultz, N., Shen, R., Benz, S., Goldstein, T., Haussler, D., Ng, S., Szeto, C., Stuart, J., Benz, C., Yau, C., Zhang, W., Annala, M., Broom, B., Casasent, T., Ju, Z., Liang, H., Liu, G., Lu, Y., Unruh, A., Wakefield, C., Weinstein, J., Zhang, N., Liu, Y., Broaddus, R., Akbani, R., Mills, G., Adams, C., Barr, T., Black, A., Bowen, J., Deardurff, J., Frick, J., Gastier-Foster, J., Grossman, T., Harper, H., Hart-Kothari, M., Helsel, C., Hobensack, A., Kuck, H., Kneile, K., Leraas, K., Lichtenberg, T., McAllister, C., Pyatt, R., Ramirez, N., Tabler, T., Vanhoose, N., White, P., Wise, L., Zmuda, E., Barnabas, N., Berry-Green, C., Blanc, V., Boice, L., Button, M., Farkas, A., Green, A., MacKenzie, J., Nicholson, D., Kalloger, S., Gilks, C., Karlan, B., Lester, J., Orsulic, S., Borowsky, M., Cadungog, M., Czerwinski, C., Huelsenbeck-Dill, L., Iacocca, M., Petrelli, N., Rabeno, B., Witkin, G., Nemirovich-Danchenko, E., Potapova, O., Rotin, D., Berchuck, A., Birrer, M., DiSaia, P., Monovich, L., Curley, E., Gardner, J., Mallery, D., Penny, R., Dowdy, S., Winterhoff, B., Dao, L., Gostout, B., Meuter, A., Teoman, A., Dao, F., Olvera, N., Bogomolniy, F., Garg, K., Soslow, R., Levine, D., Abramov, M., Bartlett, J., Kodeeswaran, S., Parfitt, J., Moiseenko, F., Clarke, B., Goodman, M., Carney, M., Matsuno, R., Fisher, J., Huang, M., Rathmell, W., Thorne, L., Le, L., Dhir, R., Edwards, R., Elishaev, E., Zorn, K., Broaddus, R., Goodfellow, P., Mutch, D., Schultz, N., Liu, Y., Akbani, R., Cherniack, A., Cerami, E., Weinhold, N., Shen, H., Hoadley, K., Kahn, A., Bell, D., Pollock, P., Wang, C., Wheeler, D., Shinbrot, E., Karlan, B., Berchuck, A., Dowdy, S., Winterhoff, B., Goodman, M., Robertson, A., Beroukhim, R., Pashtan, I., Salvesen, H., Laird, P., Noble, M., Stuart, J., Ding, L., Kandoth, C., Gilks, C., Soslow, R., Goodfellow, P., Mutch, D., Broaddus, R., Zhang, W., Mills, G., Kucherlapati, R., Mardis, E., Levine, D., Ayala, B., Chu, A., Jensen, M., Kothiyal, P., Pihl, T., Pontius, J., Pot, D., Snyder, E., Srinivasan, D., Kahn, A., Shaw, K., Sheth, M., Davidsen, T., Ferguson, G., Demchok, J., Yang, L., Guyer, M., Ozenberger, B., Sofia, H., Kandoth, C., Schultz, N., Cherniack, A., Akbani,

R., Liu, Y., Shen, H., Robertson, A., Pashtan, I., Shen, R., Benz, C., Yau, C., Laird, P., Ding, L., Zhang, W., Mills, G., Kucherlapati, R., Mardis, E., and Levine, D. (2013) Integrated genomic characterization of endometrial carcinoma. Nature 497, nature12113

Giannakis, M., Mu, X. J., Shukla, S. A., Qian, Z. R., Cohen, O., Nishihara, R., Bahl, S., Cao, Y., Amin-Mansour, A., Yamauchi, M., Sukawa, Y., Stewart, C., Rosenberg, M., Mima, K., Inamura, K., Nosho, K., Nowak, J. A., Lawrence, M. S., Giovannucci, E. L., Chan, A. T., Ng, K., Meyerhardt, J. A., Van Allen, E. M., Getz, G., Gabriel, S. B., Lander, E. S., Wu, C. J., Fuchs, C. S., Ogino, S., and Garraway, L. A. (2016) Genomic Correlates of Immune-Cell Infiltrates in Colorectal Carcinoma. Cell Reports 15, 857–865

Hammerman, P., Lawrence, M., Voet, D., Jing, R., Cibulskis, K., Sivachenko, A., Stojanov, P., McKenna, A., Lander, E., Gabriel, S., Getz, G., Sougnez, C., Imielinski, M., Helman, E., Hernandez, B., Pho, N., Meyerson, M., Chu, A., Chun, H.-J., Mungall, A., Pleasance, E., Robertson, A., Sipahimalani, P., Stoll, D., Balasundaram, M., Birol, I., Butterfield, Y., Chuah, E., Coope, R., Corbett, R., Dhalla, N., Guin, R., He, A., Hirst, C., Hirst, M., Holt, R., Lee, D., Li, H., Mayo, M., Moore, R., Mungall, K., Nip, K., Olshen, A., Schein, J., Slobodan, J., Tam, A., Thiessen, N., Varhol, R., Zeng, T., Zhao, Y., Jones, S., Marra, M., Saksena, G., Cherniack, A., Schumacher, S., Tabak, B., Carter, S., Pho, N., Nguyen, H., Onofrio, R., Crenshaw, A., Ardlie, K., Beroukhim, R., Winckler, W., Hammerman, P., Getz, G., Meyerson, M., Protopopov, A., Zhang, J., Hadjipanayis, A., Lee, S., Xi, R., Yang, L., Ren, X., Zhang, H., Shukla, S., Chen, P.-C., Haseley, P., Lee, E., Chin, L., Park, P., Kucherlapati, R., Socci, N., Liang, Y., Schultz, N., Borsu, L., Lash, A., Viale, A., Sander, C., Ladanyi, M., Auman, J., Hoadley, K., Wilkerson, M., Shi, Y., Liquori, C., Meng, S., Li, L., Turman, Y., Topal, M., Tan, D., Waring, S., Buda, E., Walsh, J., Jones, C., Mieczkowski, P., Singh, D., Wu, J., Gulabani, A., Dolina, P., Bodenheimer, T., Hoyle, A., Simons, J., Soloway, M., Mose, L., Jefferys, S., Balu, S., O'Connor, B., Prins, J., Liu, J., Chiang, D., Hayes, D., Perou, C., Cope, L., Danilova, L., Weisenberger, D., Maglinte, D., Pan, F., Berg, D., Jr, T., Herman, J., Baylin, S., Laird, P., Getz, G., Noble, M., Voet, D., Saksena, G., Gehlenborg, N., DiCara, D., Zhang, J., Zhang, H., Wu, C.-J., Liu, S., Lawrence, M., Zou, L., Sivachenko, A., Lin, P., Stojanov, P., Jing, R., Cho, J., Nazaire, M.-D., Robinson, J., Thorvaldsdottir, H., Mesirov, J., Park, P., Chin, L., Schultz, N., Sinha, R., Ciriello, G., Cerami, E., Gross, B., Jacobsen, A., Gao, J., Aksoy, B., Weinhold, N., Ramirez, R., Taylor, B., Antipin, Y., Reva, B., Shen, R., Mo, Q., Seshan, V., Paik, P., Ladanyi, M., Sander, C., Akbani, R., Zhang, N., Broom, B., Casasent, T., Unruh, A., Wakefield, C., Cason, R., Baggerly, K., Weinstein, J., Haussler, D., Benz, C., Stuart, J., Zhu, J., Szeto, C., Scott, G., Yau, C., Ng, S., Goldstein, T., Waltman, P., Sokolov, A., Ellrott, K., Collisson, E., Zerbino, D., Wilks, C., Ma, S., Craft, B., Wilkerson, M., Auman, J., Hoadley, K., Du, Y., Cabanski, C., Walter, V., Singh, D., Wu, J., Gulabani, A., Bodenheimer, T., Hoyle, A., Simons, J., Soloway, M., Mose, L., Jefferys, S., Balu, S., Marron, J., Liu, Y., Wang, K., Liu, J., Prins, J., Hayes, D., Perou, C., Creighton, C., Zhang, Y., Travis, W., Rekhtman, N., Yi, J., Aubry, M., Cheney, R., Dacic, S., Flieder, D., Funkhouser, W., Illei, P., Myers, J., Tsao, M.-S., Penny, R., Mallery, D., Shelton, T., Hatfield, M., Morris, S., Yena, P., Shelton, C., Sherman, M., Paulauskis, J., Meyerson, M., Baylin, S., Govindan, R., Akbani, R., Azodo, I., Beer, D., Bose, R., Byers, L., Carbone, D., Chang, L.-W., Chiang, D., Chu, A., Chun, E., Collisson, E., Cope, L., Creighton, C., Danilova, L., Ding, L., Getz, G., Hammerman, P., Hayes, D., Hernandez, B., Herman, J., Heymach, J., Ida, C., Imielinski, M., Johnson, B., Jurisica, I., Kaufman, J., Kosari, F., Kucherlapati, R., Kwiatkowski, D., Ladanyi, M., Lawrence, M.,

Maher, C., Mungall, A., Ng, S., Pao, W., Peifer, M., Penny, R., Robertson, G., Rusch, V., Sander, C., Schultz, N., Shen, R., Siegfried, J., Sinha, R., Sivachenko, A., Sougnez, C., Stoll, D., Stuart, J., Thomas, R., Tomaszek, S., Tsao, M.-S., Travis, W., Vaske, C., Weinstein, J., Weisenberger, D., Wigle, D., Wilkerson, M., Wilks, C., Yang, P., Zhang, J., Jensen, M., Sfeir, R., Kahn, A., Chu, A., Kothiyal, P., Wang, Z., Snyder, E., Pontius, J., Pihl, T., Ayala, B., Backus, M., Walton, J., Baboud, J., Berton, D., Nicholls, M., Srinivasan, D., Raman, R., Girshik, S., Kigonya, P., Alonso, S., Sanbhadti, R., Barletta, S., Greene, J., Pot, D., Tsao, M.-S., Bandarchi-Chamkhaleh, B., Boyd, J., Weaver, J., Wigle, D., Azodo, I., Tomaszek, S., Aubry, M., Ida, C., Yang, P., Kosari, F., Brock, M., Rogers, K., Rutledge, M., Brown, T., Lee, B., Shin, J., Trusty, D., Dhir, R., Siegfried, J., Potapova, O., Fedosenko, K., Nemirovich-Danchenko, E., Rusch, V., Zakowski, M., Iacocca, M., Brown, J., Rabeno, B., Czerwinski, C., Petrelli, N., Fan, Z., Todaro, N., Eckman, J., Myers, J., Rathmell, W., Thorne, L., Huang, M., Boice, L., Hill, A., Penny, R., Mallery, D., Curley, E., Shelton, C., Yena, P., Morrison, C., Gaudioso, C., Bartlett, J., Kodeeswaran, S., Zanke, B., Sekhon, H., David, K., Juhl, H., Le, X., Kohl, B., Thorp, R., Tien, N., Bang, N., Sussman, H., Phu, B., Hajek, R., Hung, N., Khan, K., Muley, T., Shaw, K., Sheth, M., Yang, L., Buetow, K., Davidsen, T., Demchok, J., Eley, G., Ferguson, M., Dillon, L., Schaefer, C., Guyer, M., Ozenberger, B., Palchik, J., Peterson, J., Sofia, H., Thomson, E., Hammerman, P., Hayes, D., Wilkerson, M., Schultz, N., Bose, R., Chu, A., Collisson, E., Cope, L., Creighton, C., Getz, G., Herman, J., Johnson, B., Kucherlapati, R., Ladanyi, M., Maher, C., Robertson, G., Sander, C., Shen, R., Sinha, R., Sivachenko, A., Thomas, R., Travis, W., Tsao, M.-S., Weinstein, J., Wigle, D., Baylin, S., Govindan, R., and Meyerson, M. (2012) Comprehensive genomic characterization of squamous cell lung cancers. Nature 489, nature11404

Hasan, M. K., Yu, J., Widhopf, G. F., Rassenti, L. Z., Chen, L., Shen, Z., Briggs, S. P., Neuberg, D. S., and Kipps, T. J. (2018) Wnt5a induces ROR1 to recruit DOCK2 to activate Rac1/2 in chronic lymphocytic leukemia. Blood

Ho, H.-Y. H. Y., Susman, M. W., Bikoff, J. B., Ryu, Y. K., Jonas, A. M., Hu, L., Kuruvilla, R., and Greenberg, M. E. (2012) Wnt5a-Ror-Dishevelled signaling constitutes a core developmental pathway that controls tissue morphogenesis. Proc. Natl. Acad. Sci. U.S.A. 109, 4044–51

Hsu, M.Y., Wheelock, M.J., Johnson, K.R., Herlyn, M. (1996) Shifts in cadherin profiles between human normal melanocytes and melanomas. J. Investig. Dermatol. Symp. Proc. 1, 188–194.

Hu, B., Wang, Q., Wang, Y. A., Hua, S., Sauvé, C.-E. G., Ong, D., Lan, Z. D., Chang, Q., Ho, Y. W., Monasterio, M. M., Lu, X., Zhong, Y., Zhang, J., Deng, P., Tan, Z., Wang, G., Liao, W.-T., Corley, L. J., Yan, H., Zhang, J., You, Y., Liu, N., Cai, L., Finocchiaro, G., Phillips, J. J., Berger, M. S., Spring, D. J., Hu, J., Sulman, E. P., Fuller, G. N., Chin, L., Verhaak, R. G. W., and DePinho, R. A. (2016) Epigenetic Activation of WNT5A Drives Glioblastoma Stem Cell Differentiation and Invasive Growth. Cell 167, 1281–1295.e18

Hwang, S., 2015, Biochemical characterization of isoform-specific inhibition of acyl proteion thioesterase enzymes, University of Michigan, Ann Arbor, MI.

Iozzo, R., Eichstetter, I., and Danielson, K. G. (1995) Aberrant expression of the growth factor Wnt-5a in human malignancy. Cancer Research 55, 3495-3499

Jenei, V., Sherwood, V., Howlin, J., Linnskog, R., Säfholm, A., Axelsson, L., and Andersson, T. (2009) A t-butyloxycarbonyl-modified Wnt5a-derived hexapeptide functions as a potent antagonist of Wnt5a-dependent melanoma cell invasion. Proc. Natl. Acad. Sci. U.S.A. 106, 19473–8

Jimbow, K., Roth, S. I., Fitzpatrick, T. B., and Szabo, G. (1975) Mitotic activity in non-neoplastic melanocytes in vivo as determined by histochemical, autoradiographic, and electron microscope studies. J. Cell Biol. 66, 663–70

Johnson, J.P., Rummel, M.M., Rothbacher, U., Sers, C. (1996) MUC18: A cell adhesion molecule with a potential role in tumor growth and tumor cell dissemination. Attempts to Understand Mestastasis Formation I.

Jordan, N.V., Prat, A., Abell, A.N., Zawistowski, J.S., Sciacky, N., Karginova, O.A., Zhou, B., Golitz, B.T., Perou, C.M., and Johnson, G.L. (2013) SWI/SNF chromatin-remodeling factor Smarcd3/Baf60c controls epithelial-mesenchymal transition by inducing Wnt5a signaling. Mol. Cell. Biol. 33, 3011-3025

Kathayat, R., Elvira, P. & Dickinson, B. (2016) A fluorescent probe for cysteine depalmitoylation reveals dynamic APT signaling. Nat Chem Biol 13, 150–152

Krauthammer, M., Kong, Y., Ha, B., Evans, P., Bacchiocchi, A., McCusker, J., Cheng, E., Davis, M., Goh, G., Choi, M., Ariyan, S., Narayan, D., Dutton-Regester, K., Capatana, A., Holman, E., Bosenberg, M., Sznol, M., Kluger, H., Brash, D., Stern, D., Materin, M., Lo, R., Mane, S., Ma, S., Kidd, K., Hayward, N., Lifton, R., Schlessinger, J., Boggon, T., and Halaban, R. (2012) Exome sequencing identifies recurrent somatic RAC1 mutations in melanoma. Nat Genet 44, ng.2359

Lehmann, J. M., Riethmüller, G., and Johnson, J. P. (1989) MUC18, a marker of tumor progression in human melanoma, shows sequence similarity to the neural cell adhesion molecules of the immunoglobulin superfamily. Proceedings of the National Academy of Sciences 86, 9891–9895

Lehmann, JM, Holzmann, B, and research, B.-E. (1987) Discrimination between benign and malignant cells of melanocytic lineage by two novel antigens, a glycoprotein with a molecular weight of 113,000 and a protein with a molecular weight of 76,000. Cancer Reseach. 47;841-845

Liao, W.-T. T., Corley, L. J., Yan, H., Zhang, J., You, Y., Liu, N., Cai, L., Finocchiaro, G., Phillips, J. J., Berger, M. S., Spring, D. J., Hu, J., Sulman, E. P., Fuller, G. N., Chin, L., Verhaak, R. G., and DePinho, R. A. (2016) Epigenetic Activation of WNT5A Drives Glioblastoma Stem Cell Differentiation and Invasive Growth.Cell 167, 1281–1295.e18

Lin, D. T., and Conibear, E. (2015) Enzymatic protein depalmitoylation by acyl protein thioesterases. Biochem. Soc. Trans. 43, 193–8

Lin, D. T., and Conibear, E. (2015) ABHD17 proteins are novel protein depalmitoylases that regulate N-Ras palmitate turnover and subcellular localization. Elife 4, e11306

Linder, M. E., and Deschenes, R. J. (2007) Palmitoylation: policing protein stability and traffic. Nat. Rev. Mol. Cell Biol. 8, 74–84

Liu, T., DeCostanzo, A. J., Liu, X., Wang, H., Hallagan, S., Moon, R. T., and Malbon, C. C. (2001) G protein signaling from activated rat frizzled-1 to the beta-catenin-Lef-Tcf pathway. Science 292, 1718–1722

Lu, C., Wang, X., Zhu, H., Feng, J., Ni, S., and Huang, J. (2015) Over-expression of ROR2 and Wnt5a cooperatively correlates with unfavorable prognosis in patients with non-small cell lung cancer. Oncotarget 6, 24912–21

Mort, R. L., Jackson, I. J., and Patton, E. E. (2015) The melanocyte lineage in development and disease. Development 142, 620–32

Nguyen, D., Bos, P., and Massagué, J. (2009) Metastasis: from dissemination to organ-specific colonization. Nat Rev Cancer 9, 274–284

O'Connell, M., Fiori, J., Xu, M., Carter, A., Frank, B., Camilli, T., French, A., Dissanayake, S., Indig, F., Bernier, M., Taub, D., Hewitt, S., and Weeraratna, A. (2009) The orphan tyrosine kinase receptor, ROR2, mediates Wnt5A signaling in metastatic melanoma. Oncogene 29, 34–44

O'Connell, M., Marchbank, K., Webster, M., Valiga, A., Kaur, A., Vultur, A., Li, L., Herlyn, M., Villanueva, J., Liu, Q., Yin, X., Widura, S., Nelson, J., Ruiz, N., Camilli, T., Indig, F., Flaherty, K., Wargo, J., Frederick, D., Cooper, Z., Nair, S., Amaravadi, R., Schuchter, L., Karakousis, G., Xu, W., Xu, X., and Weeraratna, A. (2013) Hypoxia induces phenotypic plasticity and therapy resistance in melanoma via the tyrosine kinase receptors ROR1 and ROR2. Cancer Discov 3, 1378–93

Orian-Rousseau, V., Chen, L., Sleeman, J. P., Herrlich, P., and Ponta, H. (2002) CD44 is required for two consecutive steps in HGF/c-Met signaling. Genes Dev. 16, 3074–86

Ponta, H., Sherman, L., and Herrlich, P. (2003) CD44: From adhesion molecules to signalling regulators. Nat Rev Mol Cell Bio 4, 33–45

Prasad, C., Mohapatra, P., and Andersson, T. (2015) Therapy for BRAFi-Resistant Melanomas: Is WNT5A the Answer? Cancers 7, 1900–1924

Qiu, T., Kathayat, R. S., Cao, Y., Beck, M. W., and Dickinson, B. C. (2018) A Fluorescent Probe with Improved Water Solubility Permits the Analysis of Protein S-Depalmitoylation Activity in Live Cells. Biochemistry 57, 221–225

Ridky, T. W., Chow, J. M., Wong, D. J., and Khavari, P. A. (2010) Invasive three-dimensional organotypic neoplasia from multiple normal human epithelia. Nat. Med. 16, 1450–5

Ripka, S., König, A., Buchholz, M., Wagner, M., Sipos, B., Klöppel, G., Downward, J., Gress, T., and Michl, P. (2007) WNT5A—target of CUTL1 and potent modulator of tumor cell migration and invasion in pancreatic cancer. Carcinogenesis 28, 1178–1187

Rusch M, Zimmermann TJ, Bürger M, et al. Identification of acyl pro- tein thioesterases 1 and 2 as the cellular targets of the Ras-signaling modulators palmostatin B and M. Angew Chem Int Ed Engl. 2011;50(42):9838-9842.

Sadeghi, R. S., Kulej, K., Kathayat, R. S., Garcia, B. A., Dickinson, B. C., Brady, D. C., and Witze, E. S. (2018) Wnt5a signaling induced phosphorylation increases APT1 activity and promotes melanoma metastatic behavior. Elife 7

Sandru, A., Voinea, S., Panaitescu, E., and Blidaru, A. (2014) Survival rates of patients with metastatic malignant melanoma. Journal of Medicine and Life. 7, 572-576

Sato, A., Yamamoto, H., Sakane, H., Koyama, H., and Kikuchi, A. (2010) Wnt5a regulates distinct signalling pathways by binding to Frizzled2. EMBO J. 29, 41–54

Scheel, C., Eaton, E., Li, S., Chaffer, C., Reinhardt, F., Kah, K.-J., Bell, G., Guo, W., Rubin, J., Richardson, A., and Weinberg, R. (2011) Paracrine and Autocrine Signals Induce and Maintain Mesenchymal and Stem Cell States in the Breast. Cell 145, 926–940

Shain, A. H., and Bastian, B. C. (2016) From melanocytes to melanomas. Nat. Rev. Cancer 16, 345–58

Sheldahl, L. C., Slusarski, D. C., Pandur, P., Miller, J. R., Kühl, M., and Moon, R. T. (2003) Dishevelled activates Ca2+ flux, PKC, and CamKII in vertebrate embryos. J. Cell Biol. 161, 769–77

Shih, I., Elder, D., Hsu, M., and Herlyn, M. (1994) Regulation of Mel-CAM/MUC18 expression on melanocytes of different stages of tumor expression by normal keratinocytes. American Journal of Pathology 145, 837-845 (A)

Shih, I. M., Elder, D. E., Speicher, D., Johnson, J. P., and Herlyn, M. (1994) Isolation and functional characterization of the A32 melanoma-associated antigen. Cancer Res. 54, 2514–20 (B)

Shih I. M. (1999) The role of CD146 (Mel-CAM) in biology and pathology. The Journal of Pathology 189; 4-11

Strebhardt, K., and Ullrich, A. (2006) Targeting polo-like kinase 1 for cancer therapy. Nat Rev Cancer 6, 321–330

Stuelten, C. H., Parent, C. A., and Montell, D. J. (2018) Cell motility in cancer invasion and metastasis: insights from simple model organisms. Nat. Rev. Cancer 18, 296–312

Tap, W. D., Gong, K.-W. W., Dering, J., Tseng, Y., Ginther, C., Pauletti, G., Glaspy, J. A., Essner, R., Bollag, G., Hirth, P., Zhang, C., and Slamon, D. J. (2010) Pharmacodynamic characterization of the efficacy signals due to selective BRAF inhibition with PLX4032 in malignant melanoma. Neoplasia 12, 637–49

Tian L, McClafferty H, Knaus HG, Ruth P, Shipston MJ. (2012) Distinct acyl protein transferases and thioesterases control surface expression of calcium-activated potassium channels. J Biol Chem. 287(18):14718-14725.

Tomatis VM, Trenchi A, Gomez GA, Daniotti JL. (2010) Acyl-protein thioes- terase 2 catalyzes the deacylation of peripheral membrane- associated GAP-43. PLoS One. 5(11):e15045.

Van Diggelen, O. P., Keulemans, J. L., Winchester, B., Hofman, I. L., Vanhanen, S. L., Santavuori, P., and Voznyi, Y. V. (1999) A rapid fluorogenic palmitoyl-protein thioesterase assay: pre- and postnatal diagnosis of INCL. Mol. Genet. Metab. 66, 240–4

Vartak, N., Papke, B., Grecco, H., Rossmannek, L., Waldmann, H., Hedberg, C., and Bastiaens, P. (2014) The autodepalmitoylating activity of APT maintains the spatial organization of palmitoylated membrane proteins. Biophys J 106, 93–105

Verkruyse, L. A., and Hofmann, S. L. (1996) Lysosomal targeting of palmitoyl-protein thioesterase. J. Biol. Chem. 271, 15831–6

Wallingford, JB, and Development, H.-R. (2005) The developmental biology of Dishevelled: an enigmatic protein governing cell fate and cell polarity. Development 132, 4421-4436

Walter, D., Venancio, O., Buza, E., Tobias, J., Deshpande, C., Gudiel, A., Kim-Kiselak, C., Cicchini, M., Yates, T., and Feldser, D. (2017) Systematic In Vivo Inactivation of Chromatin-Regulating Enzymes Identifies Setd2 as a Potent Tumor Suppressor in Lung Adenocarcinoma. Cancer Res 77, 1719–1729

Walter, S. A., Cutler, R. E., Martinez, R., Gishizky, M., and Hill, R. J. (2003) Stk10, a new member of the polo-like kinase kinase family highly expressed in hematopoietic tissue. J. Biol. Chem. 278, 18221–8

Wan, J., Roth, A., Bailey, A., and Davis, N. (2007) Palmitoylated proteins: purification and identification. Nat Protoc 2, 1573–84

Wang A, Deems RA, Dennis EA. (1997) Cloning, expression, and catalytic mechanism of murine lysophospholipase I. J Biol Chem. 272(19):12723-12729.

Wang A, Loo R, Chen Z, Dennis EA. (1997) Regiospecificity and catalytic triad of lysophospholipase I. J Biol Chem. 272(35):22030- 22036.

Wang, B., Tang, Z., Gong, H., Zhu, L., and Liu, X. (2017) Wnt5a promotes epithelial-to-mesenchymal transition and metastasis in non-small-cell lung cancer. Biosci. Rep. 37

Wang, W., Runkle, K. B., Terkowski, S. M., Ekaireb, R. I., and Witze, E. S. (2015) Protein Depalmitoylation Is Induced by Wnt5a and Promotes Polarized Cell Behavior. J. Biol. Chem. 290, 15707–16

Wang, X., Zhao, X., Yi, Z., Ma, B., Wang, H., Pu, Y., Wang, J., and Wang, S. (2018) WNT5A promotes migration and invasion of human osteosarcoma cells via SRC/ERK/MMP-14 pathway. Cell Biol. Int. 42, 598–607

Wang, Z., and Yan, X. (2013) CD146, a multi-functional molecule beyond adhesion. Cancer Lett 330, 150–162

Weeraratna, A. T., Jiang, Y., Hostetter, G., Rosenblatt, K., Duray, P., Bittner, M., and Trent, J. M. (2002) Wnt5a signaling directly affects cell motility and invasion of metastatic melanoma. Cancer Cell 1, 279–88

Weilenga, V.J., Heider, K., Offerhaus, G.J.A., Adolf, G., van den Berg, F.M., Ponta, H., Herrlich, P., and Pals, S.T. (1993) Expression of CD44 variant proteins in human colorectal cancer is related to tumor progression. Cancer Research. 53, 4754,4756

Willert, K., Brown, J. D., Danenberg, E., Duncan, A. W., Weissman, I. L., Reya, T., Yates, J. R., and Nusse, R. (2003) Wnt proteins are lipid-modified and can act as stem cell growth factors. Nature 423, 448–52

Witze, E., Litman, E., Argast, G., Moon, R., and Ahn, N. (2008) Wnt5a control of cell polarity and directional movement by polarized redistribution of adhesion receptors. Sci New York N Y 320, 365–9

Witze, E. S., Connacher, M. K., Houel, S., Schwartz, M. P., Morphew, M. K., Reid, L., Sacks, D. B., Anseth, K. S., and Ahn, N. G. (2013) Wnt5a Directs Polarized Calcium Gradients by Recruiting Cortical Endoplasmic Reticulum to the Cell Trailing Edge. Dev Cell 26, 645–657

Won, S. J., Davda, D., Labby, K. J., Hwang, S. Y., Pricer, R., Majmudar, J. D., Armacost, K. A., Rodriguez, L. A., Rodriguez, C. L., Chong, F. S., Torossian, K. A., Palakurthi, J., Hur, E. S., Meagher, J. L., Brooks, C. L., Stuckey, J. A., and Martin, B. R. (2016) Molecular Mechanism for Isoform-Selective Inhibition of Acyl Protein Thioesterases 1 and 2 (APT1 and APT2). ACS Chem. Biol. 11, 3374–3382

W.-G. (2012) Dual roles of METCAM in the progression of different cancers. Journal of Oncology.

Yamaguchi, Bradley, McMahon, and Jones (1999) A Wnt5a pathway underlies outgrowth of multiple structures in the vertebrate embryo. Dev Camb Engl 126, 1211–23

Zeidman R, Jackson CS, Magee AI. (2009) Protein acyl thioesterases (Review). Mol Membr Biol. 26(1):32-41.